

54-20-78

NACA TN 3196

0066074

TECH LIBRARY KAFB, NM

# NATIONAL ADVISORY COMMITTEE FOR AERONAUTICS

TECHNICAL NOTE 3196

LIFT AND PITCHING MOMENT AT SUPERSONIC SPEEDS DUE TO  
CONSTANT VERTICAL ACCELERATION FOR THIN SWEPTBACK  
TAPERED WINGS WITH STREAMWISE TIPS

SUPERSONIC LEADING AND TRAILING EDGES

By Isabella J. Cole and Kenneth Margolis

Langley Aeronautical Laboratory  
Langley Field, Va.



Washington  
July 1954

TECHNICAL

AFL 2011



## NATIONAL ADVISORY COMMITTEE FOR AERONAUTICS

## TECHNICAL NOTE 3196

LIFT AND PITCHING MOMENT AT SUPERSONIC SPEEDS DUE TO  
CONSTANT VERTICAL ACCELERATION FOR THIN SWEEPBACK  
TAPERED WINGS WITH STREAMWISE TIPS

## SUPERSONIC LEADING AND TRAILING EDGES

By Isabella J. Cole and Kenneth Margolis

## SUMMARY

On the basis of a solution to the linearized time-dependent wave equation, the nondimensional lift derivative  $C_{L\dot{\alpha}}$  and the corresponding pitching-moment derivative  $C_{m\dot{\alpha}}$  resulting from constant vertical acceleration (that is, linear variation of angle of attack with time) are evaluated for a family of thin sweptback tapered wings with streamwise tips traveling at supersonic speeds.

The analysis is applicable at those speeds for which the wing leading and trailing edges are both supersonic, provided that the Mach lines from the wing apex intersect the trailing edge and that the Mach line from the leading edge of one tip does not intersect the remote half-wing. Use is made of a previous investigation in extending the range of applicability to include cases for which the Mach lines from the wing apex intersect the tips.

Results of the analysis are given in the form of design charts for the stability derivatives  $C_{L\dot{\alpha}}$  and  $C_{m\dot{\alpha}}$  from which fairly rapid estimations of the derivatives can be made for given values of Mach number, aspect ratio, leading-edge sweepback, and taper ratio. For illustrative purposes, some chordwise pressure distributions, spanwise pressure distributions, span load distributions, and variations of the stability derivatives  $C_{L\dot{\alpha}}$  and  $C_{m\dot{\alpha}}$  with several parameters are also included. Some results of the present investigation are combined with previous calculations available for the steady-pitching derivative  $C_{mq}$  to indicate the variations of the total pitching-moment derivative  $C_{mq} + C_{m\dot{\alpha}}$  with wing geometry and Mach number; these calculations are applicable to slowly (first-order frequency) oscillating wings.

## INTRODUCTION

The development of the linearized supersonic-flow theory has allowed the evaluation of most of the important stability derivatives for a variety of isolated wing shapes. Recently, attention has been focused on the thin sweptback tapered wing with side edges parallel to the axis of wing symmetry, that is, streamwise tips. Stability derivatives available for this general plan form for a wide range of supersonic Mach numbers include the lift-curve slope  $C_{L_\alpha}$  (refs. 1 to 3), the damping-in-roll derivative  $C_{l_p}$  (refs. 1, 2, and 4), the lateral-force and yawing-moment derivatives due to rolling  $C_{Y_p}$  and  $C_{n_p}$  (refs. 5 and 6), the static pitching-moment derivative  $C_{m_\alpha}$  (refs. 7 and 8), the lift and pitching-moment derivatives due to steady pitching  $C_{L_q}$  and  $C_{m_q}$  (refs. 7, 8, and 9), and the rolling-moment-due-to-sideslip derivative  $C_{l_\beta}$  (refs. 10 and 11). The aforementioned derivatives, all of which result from "steady state" motions, are available for wings with either subsonic or supersonic leading edges.

Two derivatives resulting from an unsteady state or time-dependent motion are  $C_{L_{\dot{\alpha}}}$  and  $C_{m_{\dot{\alpha}}}$ , the lift and pitching-moment derivatives, respectively, due to a linear angle-of-attack variation with time (the motion is more commonly termed constant vertical acceleration). Inasmuch as the sums  $C_{L_q} + C_{L_{\dot{\alpha}}}$  and  $C_{m_q} + C_{m_{\dot{\alpha}}}$  predict the total lift and pitching-moment derivatives generated by a slowly (first-order frequency) oscillating surface, calculation of the  $\dot{\alpha}$  derivatives corresponding to those already available for steady pitching velocity  $q$  are in order. A previous investigation (ref. 12) treats the subsonic-leading-edge condition; the present paper extends the range of Mach number to include the supersonic-leading-edge condition.

Computational results are presented in the form of design charts covering the practical range of wing-geometry parameters and Mach number from which fairly rapid estimates of the derivatives may be obtained. For illustrative purposes, several chordwise and spanwise pressure distributions, span load distributions, and variations of the derivatives  $C_{L_{\dot{\alpha}}}$ ,  $C_{m_{\dot{\alpha}}}$ , and the sum  $C_{m_q} + C_{m_{\dot{\alpha}}}$  with several parameters are also presented.

## SYMBOLS

$x, y, z$	Cartesian coordinates; x-axis parallel to free-stream direction (see fig. 2)
$V$	free-stream velocity
$\rho$	density of air
$M$	free-stream Mach number
$B$	cotangent of Mach angle, $\sqrt{M^2 - 1}$
$\mu$	Mach angle, $\cot^{-1} B$
$b$	wing span
$c_r$	root chord
$\bar{c}$	mean aerodynamic chord, $\frac{2c_r(\lambda^2 + \lambda + 1)}{3(\lambda + 1)}$
$\lambda$	taper ratio, Tip chord/Root chord
$A$	aspect ratio, $\frac{2b}{c_r(1 + \lambda)} = \frac{b^2}{S}$
$S$	wing area
$\Lambda$	angle of sweep (see fig. 1)
$m = \cot \Lambda_{LE}$	
$k = \frac{\cot \Lambda_{TE}}{\cot \Lambda_{LE}} = \frac{AB(1 + \lambda)}{AB(1 + \lambda) - 4mB(1 - \lambda)}$	
$d$	distance between wing apex and center of gravity; positive when center of gravity is rearward of the wing apex
$\alpha$	angle of attack
$t$	time

$\dot{\alpha}$	rate of change of angle of attack with time, $d\alpha/dt$ ; positive $\dot{\alpha}$ indicates downward acceleration
$q$	steady pitching velocity about y-axis; positive as shown in figure 2
$\Delta P$	difference in pressure due to constant vertical acceleration between upper and lower surfaces; positive upward
$(\Delta P)_{\alpha=1}$	difference in pressure due to unit angle of attack between upper and lower surfaces; positive upward
$(\Delta P)_{q=1}$	difference in pressure due to unit pitching velocity about the y-axis between upper and lower surfaces; positive upward
$\Delta C_p$	pressure-difference coefficient due to constant vertical acceleration, $\frac{\Delta P}{\frac{1}{2}\rho V^2}$
$\phi$	perturbation velocity potential due to constant vertical acceleration, evaluated on upper surface of wing
$\phi_{\alpha=1}$	perturbation velocity potential due to unit angle of attack, evaluated on upper surface of wing
$\phi_{q=1}$	perturbation velocity potential due to unit pitching velocity about y-axis, evaluated on upper surface of wing
$\Gamma$	spanwise distribution of circulation due to constant vertical acceleration
$L$	lift
$M'$	pitching moment; positive as indicated in figure 2
$C_L$	lift coefficient, $\frac{L}{\frac{1}{2}\rho V^2 S}$
$C_m$	pitching-moment coefficient, $\frac{M'}{\frac{1}{2}\rho V^2 S \bar{c}}$

$$C_{L\alpha} = \left( \frac{\partial C_L}{\partial \alpha} \right)_{\alpha \rightarrow 0}$$

$$C_{m\alpha} = \left( \frac{\partial C_m}{\partial \alpha} \right)_{\alpha \rightarrow 0}$$

$$C_{Lq} = \left( \frac{\partial C_L}{\partial \frac{q\bar{c}}{2V}} \right)_{q \rightarrow 0}$$

$$C_{mq} = \left( \frac{\partial C_m}{\partial \frac{q\bar{c}}{2V}} \right)_{q \rightarrow 0}$$

$$C_{L\dot{\alpha}} = \left( \frac{\partial C_L}{\partial \frac{\dot{\alpha}\bar{c}}{2V}} \right)_{\dot{\alpha} \rightarrow 0}$$

$$C_{m\dot{\alpha}} = \left( \frac{\partial C_m}{\partial \frac{\dot{\alpha}\bar{c}}{2V}} \right)_{\dot{\alpha} \rightarrow 0}$$

Subscripts:

TE            trailing edge

LE            leading edge

1,2           components used in breakdown of results

All angles are measured in radians unless otherwise indicated.

## ANALYSIS

### Scope

The types of wings analyzed in the present paper are sketched in figure 1. These wings have vanishingly small thickness, are uncambered, and have arbitrary taper ratio (0 to 1) with tips parallel to the axis

of wing symmetry (streamwise tips). The leading edge is swept back, although the trailing edge may be swept back or swept forward. Actually, certain results ( $C_{L\dot{\alpha}}$ ) of the present investigation are directly applicable to wings with sweptforward leading edges in view of the reversibility theorem (see, for example, ref. 13).

The analysis is carried out within the framework of the linearized theory and the results are thus subject to the usual restrictions and limitations imposed by such simplification. The mathematical derivations are applicable for combinations of wing plan form and Mach number that satisfy the following conditions: (1) the Mach lines from the wing apex intersect the trailing edge, (2) the trailing edge is supersonic, and (3) the Mach line originating at the leading edge of one wing tip does not intersect the remote half-wing. Use is made of the sonic-leading-edge results given in reference 12 and of the span load distributions presented in reference 14 to enable the calculation of the derivatives  $C_{L\dot{\alpha}}$  and  $C_{m\dot{\alpha}}$  for cases where the Mach lines from the wing apex intersect the tips. Inasmuch as the third restriction is a minor one that is applicable in the current investigation to wings of very low aspect ratio only, the computational results presented herein apply, in general, at speeds for which the wing leading and trailing edges are both supersonic.

Orientation of the wing with respect to a system of body axes used in the analysis is shown in figure 2(a); all derivations are carried out with respect to this reference system unless otherwise noted. Design curves for the derivatives are presented relative to a system of principal body axes with the center-of-gravity position assumed to be at the wing apex as shown in figure 2(b). These results are also valid in a system of stability axes (fig. 2(c)) for small angles of attack (see, for example, table I of ref. 12). A formula is included which permits transfer of the given results to those applicable for an arbitrary center-of-gravity location (fig. 2(d)).

In addition to calculations for the derivatives  $C_{L\dot{\alpha}}$  and  $C_{m\dot{\alpha}}$ , tabulations of the velocity-potential and pressure-distribution formulas are included in the present paper. For illustrative purposes several chordwise and spanwise pressure distributions, span load distributions, and variations of the derivatives with wing-geometry parameters and Mach number are presented. The results of the present paper are also combined with those available for steady pitching motion to indicate the variation of the sum  $C_{m\dot{q}} + C_{m\dot{\alpha}}$  with several parameters for a given static-margin condition.

## Derivation of Equations

On the basis of a first-order frequency solution to the linearized time-dependent wave equation for supersonic flow, expressions for the time-dependent perturbation velocity potential and the lifting pressure (evaluated at time  $t = 0$ ) for a wing accelerating downward at a positive angle of attack  $\dot{\alpha}$  may be written as follows (see ref. 15 and eqs. (12) and (13) of ref. 16):

$$\phi = \dot{\alpha} \left[ \frac{M^2}{B^2} \phi_{q=1} + \left( t - \frac{M^2 x}{B^2 V} \right) \phi_{\alpha=1} \right] \quad (1)$$

$$\Delta P = \frac{\dot{\alpha}}{B^2} \left[ M^2 (\Delta P)_{q=1} - \frac{M^2 x}{V} (\Delta P)_{\alpha=1} - 2\rho \phi_{\alpha=1} \right] \quad (2)$$

where  $\phi_{q=1}$  and  $(\Delta P)_{q=1}$  are the perturbation velocity potential (evaluated on the upper surface) and the lifting pressure, respectively, due to unit (positive) steady pitching velocity about the y-axis and where  $\phi_{\alpha=1}$  and  $(\Delta P)_{\alpha=1}$  are, analogously, the perturbation velocity potential and the lifting pressure, respectively, due to unit (positive) angle of attack.

From the results of previous investigations (ref. 2 for  $\Delta C_p$  and  $\phi$  contributed by  $\alpha$  and ref. 8 for  $\Delta C_p$  and  $\phi$  contributed by  $q$ ) dealing with the plan form and speed range considered herein, expressions for the potentials and lifting pressures appearing on the right-hand sides of equations (1) and (2) are readily obtained. Thus, in accordance with equations (1) and (2) the velocity potential  $\phi$  and lifting pressure  $\Delta P$  for the  $\dot{\alpha}$  motion may be tabulated; these results are presented in tables I and II. (For convenience, the pressures in table II are given in coefficient form.)

Although the forces and moments may be obtained by appropriate straightforward integrations of the formulas presented in tables I and II, an alternate and less time-consuming approach has been utilized. Upon elementary integrations of equation (2), expressions for the lift and pitching moment may be conveniently written in derivative form as follows:

$$C_{L\dot{\alpha}} = \frac{M^2}{B^2} C_{Lq} + 2 \frac{M^2}{B^2} C_{m\alpha} - \frac{8}{B^2 S \bar{c}} \int_{-b/2}^{b/2} \int_{x_{LE}}^{x_{TE}} \frac{\phi_{\alpha=1}}{V} dx dy \quad (3)$$



$$C_{m\dot{\alpha}} = \frac{M^2}{B^2} C_{mq} + \frac{2M^2}{B^2 S \bar{c}^2} \int_{-b/2}^{b/2} \int_{x_{LE}}^{x_{TE}} x^2 \frac{(\Delta P)_{\alpha=1}}{\frac{1}{2} \rho V^2} dx dy +$$

$$\frac{8}{B^2 S \bar{c}^2} \int_{-b/2}^{b/2} \int_{x_{LE}}^{x_{TE}} x \frac{\phi_{\alpha=1}}{V} dx dy \quad (4)$$

All stability derivatives appearing in equations (3) and (4) and elsewhere in the text are measured in a system of principal body axes with the center of gravity located at the wing apex. (See fig. 2(b)). The formulas for  $\phi_{\alpha=1}$ ,  $(\Delta P)_{\alpha=1}$ , and the variable  $x$  are expressed with respect to the system of axes used in the analysis (fig. 2(a)).

Integration by parts of the middle term of equation (4), utilization of the relationship

$$\frac{(\Delta P)_{\alpha=1}}{\frac{1}{2} \rho V^2} = \frac{4}{V} \frac{\partial \phi_{\alpha=1}}{\partial x} \quad (5)$$

and combination of like terms yields the following expression for  $C_{m\dot{\alpha}}$ :

$$C_{m\dot{\alpha}} = \frac{M^2}{B^2} \left( C_{mq} + \frac{8}{S \bar{c}^2} \int_{-b/2}^{b/2} \frac{x^2 \phi_{\alpha=1}}{V} \Big|_{x_{LE}}^{x_{TE}} dy \right) -$$

$$\frac{8}{S \bar{c}^2} \left( \frac{M^2}{B^2} + 1 \right) \int_{-b/2}^{b/2} \int_{x_{LE}}^{x_{TE}} \frac{x \phi_{\alpha=1}}{V} dx dy \quad (6)$$

For convenience, equation (3) may be expressed as follows:

$$C_{L\dot{\alpha}} = \frac{M^2}{B^2} (C_{L\dot{\alpha}})_1 - \frac{1}{B^2} (C_{L\dot{\alpha}})_2 \quad (7)$$

where

$$(C_{L\dot{\alpha}})_1 = C_{Lq} + 2C_{m\dot{\alpha}} \quad (8)$$

and

$$(C_{L\dot{\alpha}})_2 = \frac{8}{S\bar{c}} \int_{-b/2}^{b/2} \int_{x_{LE}}^{x_{TE}} \frac{\phi_{\alpha=1}}{V} dx dy \quad (9)$$

In an analogous manner, equation (6) may be expressed as follows:

$$C_{m\dot{\alpha}} = \frac{M^2}{B^2} (C_{m\dot{\alpha}})_1 + \left( \frac{M^2}{B^2} + 1 \right) (C_{m\dot{\alpha}})_2 \quad (10)$$

where

$$(C_{m\dot{\alpha}})_1 = C_{mq} + \frac{8}{S\bar{c}^2} \int_{-b/2}^{b/2} \frac{x^2 \phi_{\alpha=1}}{V} \Big|_{x_{LE}}^{x_{TE}} dy \quad (11)$$

and

$$(C_{m\dot{\alpha}})_2 = - \frac{8}{S\bar{c}^2} \int_{-b/2}^{b/2} \int_{x_{LE}}^{x_{TE}} \frac{x \phi_{\alpha=1}}{V} dx dy \quad (12)$$

Equations and charts for the stability derivatives  $C_{m\alpha}$ ,  $C_{Lq}$ , and  $C_{mq}$  are presented in reference 8 for the wing plan form and Mach number range considered in the present paper. Thus, only the expressions for  $(C_{L\dot{\alpha}})_2$  (eq. (9)),  $(C_{m\dot{\alpha}})_2$  (eq. (12)), and the integral term of  $(C_{m\dot{\alpha}})_1$  (eq. (11)) require derivation. The results given in reference 2 for the velocity potential due to angle of attack were utilized in carrying out the required integrations. Appropriate combination of components, in accordance with equations (7) and (10), will then yield closed-form formulas for the derivatives  $C_{L\dot{\alpha}}$  and  $C_{m\dot{\alpha}}$ . Computations based on these closed-form analytical expressions have been carried out utilizing, to a great extent, automatic computing facilities. (The final formulas themselves are not reproduced herein because of their rather excessive length. The numerical results are believed to be sufficiently detailed to obviate the need for additional calculations.)

## RESULTS AND DISCUSSION

The type of lifting pressure distribution and of span load distribution obtained over some typical wings for the motion considered is of interest. Some illustrative examples of the chordwise and spanwise lifting pressure distributions, calculated by use of table II, are presented in figures 3 and 4; results for the spanwise loading (expressed in terms of the spanwise distribution of circulation) were obtained from reference 14 and are presented in figure 5.

The results of the detailed computations for  $C_{L\dot{\alpha}}$  are presented in figures 6 to 10 and those for  $C_{m\dot{\alpha}}$  in figures 11 to 15. The data are shown for a range of taper ratio from 0 to 1.0 and for a range of the aspect-ratio parameter AB from 3 to 20 (curves for AB = 2 are included for the  $\lambda = 1.0$  cases). The range of leading-edge sweepback angle is included in values of the parameter  $\cot^{-1}B_m$  from  $0^\circ$  to  $45^\circ$ . For convenience, the relationship and correspondence between the parameters  $\cot^{-1}B_m$  and  $B_m$  are shown in figure 16.

The dashed parts of the design curves (figs. 6 to 15) do not represent actual calculations, because these regions correspond to the condition where the Mach lines from the wing apex intersect the tips. However, calculations were made for the sonic-leading-edge condition (using ref. 12) and the curves were extended by means of dashed lines to these calculated end points. The dashed extensions should yield results that are in very close agreement with the true linearized-theory values for most cases. This agreement may be verified for the derivative  $C_{L\dot{\alpha}}$  by appropriate integration (graphical) of the span-load curves presented in reference 14.

For use in locating the desired design-chart data, an index to figures 6 to 15 is presented in tables III and IV. The derivatives presented in these figures are measured relative to a system of principal body axes with moments taken about a center-of-gravity location assumed to be at the wing apex. For arbitrary center-of-gravity locations, the given results may be directly applied in the following manner:

$$(C_{L\dot{\alpha}})_{\text{arbitrary c.g.}} = (C_{L\dot{\alpha}})_{\text{c.g. at wing apex}} \quad (13)$$

$$(C_{m\dot{\alpha}})_{\text{c.g. at distance } d \text{ from wing apex}} = (C_{m\dot{\alpha}})_{\text{c.g. at wing apex}} + \frac{d}{c} (C_{L\dot{\alpha}})_{\text{c.g. at wing apex}} \quad (14)$$

where  $d$  is positive when the center of gravity is rearward of the wing apex.

It is sometimes convenient to express the distance  $d$  in terms of the static margin, where static margin is defined as the distance, expressed in percent  $\bar{c}$ , between the center of gravity and the center of pressure due to angle of attack (usually termed the aerodynamic center), and is considered positive when the center of gravity is forward of the aerodynamic center. Thus, the parameter  $d$  may be replaced by the equation

$d = \text{Distance between wing apex and aerodynamic center} - \text{Static margin}$

or

$$d = \frac{-C_{m_\alpha} \bar{c}}{C_{L_\alpha}} - \text{Static margin} \quad (15)$$

(Design charts for the derivatives  $C_{m_\alpha}$  and  $C_{L_\alpha}$  for the plan form and Mach number range considered in the present paper are presented in ref. 8.)

The results calculated herein are also directly applicable to a system of stability axes (fig. 2(c)), inasmuch as for small angles of attack there is little change in the derivative  $C_{L_\alpha}$  and no change in the derivative  $C_{m_\alpha}$ . The results for  $C_{L_\alpha}$  may also be applied to plan forms with "reverse" geometry because, as shown in reference 13, the total lift remains unchanged when the flow is reversed. (The distribution of lift, of course, is not invariant with flow direction.)

Some illustrative variations of the stability derivatives with aspect ratio, Mach number, leading-edge sweepback, and taper ratio are presented in figures 17 and 18. Figure 19 presents some variations of the total pitching-moment derivative  $C_{m_q} + C_{m_\alpha}$  with the aforementioned parameters; the results are applicable to slowly (first-order frequency) oscillating wings. The required data for  $C_{m_q}$  were obtained from reference 8.

#### CONCLUDING REMARKS

On the basis of a solution to the linearized time-dependent wave equation, the nondimensional lift derivative  $C_{L_\alpha}$  and the corresponding pitching-moment derivative  $C_{m_\alpha}$  resulting from constant vertical acceleration have been evaluated for a family of thin sweptback tapered wings with streamwise tips traveling at supersonic speeds. The analysis is applicable, in general, at Mach numbers for which the wing leading and trailing edges are both supersonic.

Computational results are presented in the form of generalized design curves which permit fairly rapid estimations of the stability derivatives  $C_{L\dot{\alpha}}$  and  $C_{m\dot{\alpha}}$  for broad ranges of the parameters aspect ratio, taper ratio, and leading-edge sweepback. For illustrative purposes, several chordwise pressure distributions, spanwise pressure distributions, span load distributions, and variations of the derivatives with wing-geometry parameters and Mach number are also shown.

Results presented herein for the  $\dot{\alpha}$  motion may be directly added to those already available for the steady pitching motion to enable the determination of the total lift and pitching-moment derivatives generated by a slowly (first-order frequency) oscillating wing. In order to illustrate this application, some variations of the pitching-moment derivative with wing geometry and Mach number are presented.

Langley Aeronautical Laboratory,  
National Advisory Committee for Aeronautics,  
Langley Field, Va., April 7, 1954.

## REFERENCES

1. Malvestuto, Frank S., Jr., Margolis, Kenneth, and Ribner, Herbert S.: Theoretical Lift and Damping in Roll at Supersonic Speeds of Thin Sweptback Tapered Wings With Streamwise Tips, Subsonic Leading Edges, and Supersonic Trailing Edges. NACA Rep. 970, 1950. (Supersedes NACA TN 1860.)
2. Harmon, Sidney M., and Jeffreys, Isabella: Theoretical Lift and Damping in Roll of Thin Wings With Arbitrary Sweep and Taper at Supersonic Speeds - Supersonic Leading and Trailing Edges. NACA TN 2114, 1950.
3. Cohen, Doris: Formulas for the Supersonic Loading, Lift, and Drag of Flat Swept-Back Wings With Leading Edges Behind the Mach Lines. NACA Rep. 1050, 1951.
4. Walker, Harold J., and Ballantyne, Mary B.: Pressure Distribution and Damping in Steady Roll at Supersonic Mach Numbers of Flat Swept-Back Wings With Subsonic Edges. NACA TN 2047, 1950.
5. Margolis, Kenneth: Theoretical Calculations of the Lateral Force and Yawing Moment Due to Rolling at Supersonic Speeds for Sweptback Tapered Wings With Streamwise Tips. Subsonic Leading Edges. NACA TN 2122, 1950.
6. Harmon, Sidney M., and Martin, John C.: Theoretical Calculations of the Lateral Force and Yawing Moment Due to Rolling at Supersonic Speeds for Sweptback Tapered Wings With Streamwise Tips. Supersonic Leading Edges. NACA TN 2156, 1950.
7. Malvestuto, Frank S., Jr., and Hoover, Dorothy M.: Lift and Pitching Derivatives of Thin Sweptback Tapered Wings With Streamwise Tips and Subsonic Leading Edges at Supersonic Speeds. NACA TN 2294, 1951.
8. Martin, John C., Margolis, Kenneth, and Jeffreys, Isabella: Calculation of Lift and Pitching Moments Due to Angle of Attack and Steady Pitching Velocity at Supersonic Speeds for Thin Sweptback Tapered Wings With Streamwise Tips and Supersonic Leading and Trailing Edges. NACA TN 2699, 1952.
9. Walker, Harold J., and Ballantyne, Mary B.: Pressure Distribution and Damping in Steady Pitch at Supersonic Mach Numbers of Flat Swept-Back Wings Having All Edges Subsonic. NACA TN 2197, 1950.

10. Margolis, Kenneth, Sherman, Windsor L., and Hannah, Margery E.: Theoretical Calculation of the Pressure Distribution, Span Loading, and Rolling Moment Due to Sideslip at Supersonic Speeds for Thin Sweptback Tapered Wings With Supersonic Trailing Edges and Wing Tips Parallel to the Axis of Wing Symmetry. NACA TN 2898, 1953.
11. Sherman, Windsor L., and Margolis, Kenneth: Theoretical Calculations of the Effects of Finite Sideslip at Supersonic Speeds on the Span Loading and Rolling Moment for Families of Thin Sweptback Tapered Wings at an Angle of Attack. NACA TN 3046, 1953.
12. Malvestuto, Frank S., Jr., and Hoover, Dorothy M.: Supersonic Lift and Pitching Moment of Thin Sweptback Tapered Wings Produced by Constant Vertical Acceleration. Subsonic Leading Edges and Supersonic Trailing Edges. NACA TN 2315, 1951.
13. Harmon, Sidney M.: Theoretical Relations Between the Stability Derivatives of a Wing in Direct and in Reverse Supersonic Flow. NACA TN 1943, 1949.
14. Cole, Isabella J., and Margolis, Kenneth: Span Load Distributions Resulting From Constant Vertical Acceleration for Thin Sweptback Tapered Wings With Streamwise Tips. Supersonic Leading and Trailing Edges. NACA TN 3120, 1954.
15. Gardner, C.: Time-Dependent Linearized Supersonic Flow Past Planar Wings. Communications on Pure and Appl. Math., vol. III, no. 1, March 1950, pp. 33-38.
16. Ribner, Herbert S., and Malvestuto, Frank S., Jr.: Stability Derivatives of Triangular Wings at Supersonic Speeds. NACA Rep. 908, 1948. (Supersedes NACA TN 1572.)

TABLE I.- FORMULAS FOR VELOCITY POTENTIAL DISTRIBUTION DUE TO CONSTANT VERTICAL ACCELERATION

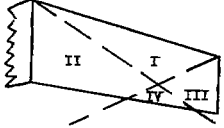

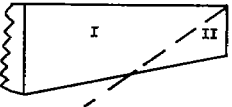
Region (see sketch)	Formula for $\phi$
	Conditions $\begin{cases} Ba > 1 \\  Bak  \geq 1 \\ BA \geq \frac{bBa}{(1+\lambda)(1+Ba)} \\ BA \geq \frac{4\lambda Ba}{(1+\lambda)(Ba-1)} \end{cases}$
I	$\frac{d(mx-y)}{\sqrt{B^2m^2-1}} \left[ tV - \frac{M^2m(mx-y)}{2(B^2m^2-1)} \right]$
II	$\frac{d}{\pi\sqrt{B^2m^2-1}} \left\{ tV \left[ (mx-y) \cos^{-1} \frac{x-B^2my}{B(mx-y)} + (mx+y) \cos^{-1} \frac{x+B^2my}{B(mx+y)} \right] + \right.$ $\left. \frac{M^2m}{2B^2(B^2m^2-1)} \left[ 2x \sqrt{(B^2m^2-1)(x^2-B^2y^2)} - B^2(mx+y)^2 \cos^{-1} \frac{x+B^2my}{B(mx+y)} - B^2(mx-y)^2 \cos^{-1} \frac{x-B^2my}{B(mx-y)} \right] \right\}$
III	$\frac{d}{\pi\sqrt{B^2m^2-1}} \left\{ tV \left[ (mx-y) \cos^{-1} \frac{mx-b(Ba+1)+y(2Ba+1)}{mx-y} + \sqrt{(b-2y)(Ba+1)} \left[ 2m(x+By) - b(Ba+1) \right] \right] + \right.$ $\frac{M^2m}{2(B^2m^2-1)} \left\{ \frac{Bmy(2Ba-1) + b(2-Ba)(Ba+1) - mx(4+Ba)}{3Ba} \sqrt{(b-2y)(Ba+1)} \left[ 2m(x+By) - b(Ba+1) \right] - \right.$ $\left. (mx-y)^2 \cos^{-1} \frac{mx-b(Ba+1)+y(2Ba+1)}{mx-y} \right\} \left. \right\}$
IV	$\sum (II + III - I)$
	Conditions $\begin{cases} Ba = 1 \\  Bak  \geq 1 \\ BA \geq \frac{2}{1+\lambda} \end{cases}$
I	$\frac{2d\sqrt{x^2-B^2y^2}}{Bk} \left( tV - \frac{M^2x}{3B^2} \right)$
II	$\frac{d\sqrt{(b-2y)(By+x)}}{\pi\sqrt{B}} \left[ 2tV + \frac{M^2(By-Bb-x)}{3B^2} \right]$
	Conditions $\begin{cases} Ba = \infty \\  Bak  \geq 1 \\ BA \geq \frac{4}{1+\lambda} \end{cases}$
I	$\frac{dx}{B} \left( tV - \frac{M^2x}{2B^2} \right)$
II	$\frac{d}{\pi\sqrt{B}} \left\{ tV \left[ \frac{x}{\sqrt{B}} \cos^{-1} \frac{x-Bb+2By}{x} + \sqrt{(b-2y)(2x+2By-Bb)} \right] + \right.$ $\left. \frac{M^2}{6B^2} \left[ (2By-Bb-x) \sqrt{(b-2y)(2x+2By-Bb)} - \frac{3x^2}{\sqrt{B}} \cos^{-1} \frac{x-Bb+2By}{x} \right] \right\}$



TABLE II.-- FORMULAS FOR LIFTING PRESSURE DISTRIBUTION DUE TO CONSTANT VERTICAL ACCELERATION

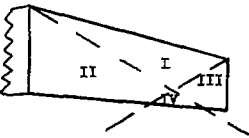
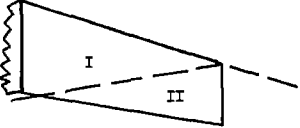
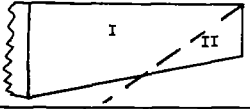
Region (see sketch)	Formula for $\Delta C_p$
	Conditions $\left\{ \begin{array}{l} Bn > 1 \\  Bnk  \geq 1 \\ BA \geq \frac{4Bn}{(1+\lambda)(1+Bn)} \\ BA \geq \frac{4\lambda Bn}{(1+\lambda)(Bn-1)} \end{array} \right.$
I	$-\frac{4d(mx-y)(m^2+1)}{V(B^2m^2-1)^{3/2}}$
II	$\frac{4d}{VB^2x(B^2m^2-1)^{3/2}} \left\{ 2M^2m \sqrt{(x^2-B^2y^2)(B^2m^2-1)} - \right.$ $\left. B^2(m^2+1) \left[ (mx+y) \cos^{-1} \frac{x+B^2my}{B(mx+y)} + (mx-y) \cos^{-1} \frac{x-B^2my}{B(mx-y)} \right] \right\}$
III	$\frac{4d}{VBm(B^2m^2-1)^{3/2}} \left\{ [B(B^2m^2-Bm-1)-m] \sqrt{(b-2y)(Bm+1)[2m(x+By)-b(Bm+1)]} - \right.$ $\left. B(mx-y)(m^2+1) \cos^{-1} \frac{mx-b(Bm+1)+y(2Bm+1)}{mx-y} \right\}$
IV	$\sum (II + III - I)$
	Conditions $\left\{ \begin{array}{l} Bn = 1 \\  Bnk  \geq 1 \\ BA \geq \frac{2}{1+\lambda} \end{array} \right.$
I	$\frac{8d}{3VB^3x \sqrt{x^2-B^2y^2}} [M^2(x^2-2B^2y^2) - 3(x^2-B^2y^2)]$
II	$\frac{2d}{3VB^3x \sqrt{\frac{B(b-2y)}{x+By}}} [M^2(9x-Bb+11By) - 12(By+x)]$
	Conditions $\left\{ \begin{array}{l} Bn = \infty \\  Bnk  \geq 1 \\ BA \geq \frac{4}{1+\lambda} \end{array} \right.$
I	$-\frac{4dx}{VB^3}$
II	$\frac{4d}{VB^3x} \left[ B^{5/2} \sqrt{(b-2y)(2x+2By-Bb)} - x \cos^{-1} \frac{x-Bb+2By}{x} \right]$

TABLE III.- INDEX TO DESIGN CHARTS FOR  $BC_{L\dot{\alpha}}$ 

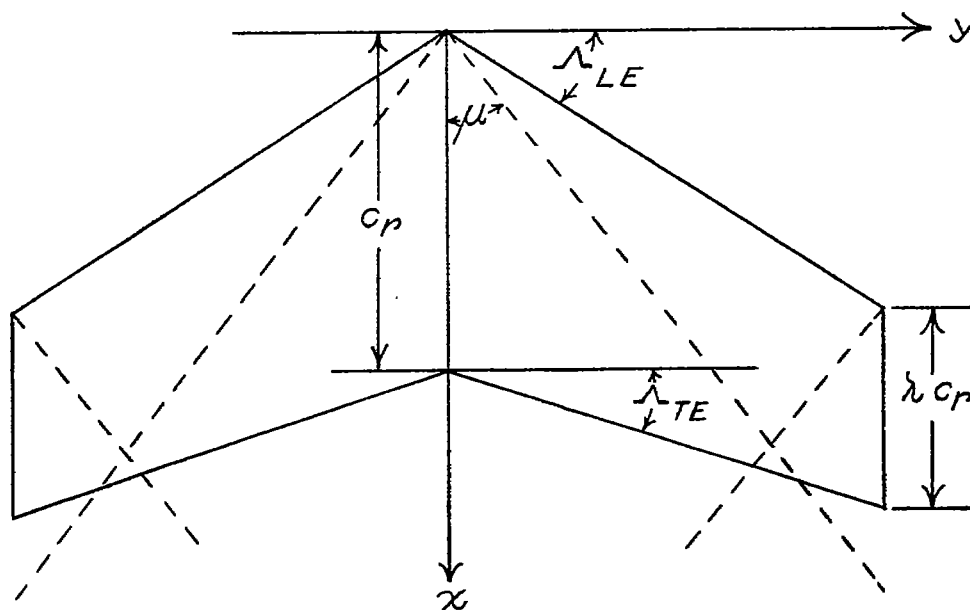
$$\left[ BC_{L\dot{\alpha}} = \frac{M^2}{B^2} B(C_{L\dot{\alpha}})_1 - \frac{1}{B^2} B(C_{L\dot{\alpha}})_2 \right]$$

Component	$\lambda$	AB	$\cot^{-1} B_m$ , deg	$B_m$	Figure	Page	Component	$\lambda$	AB	$\cot^{-1} B_m$ , deg	$B_m$	Figure	Page
$B(C_{L\dot{\alpha}})_1$	0	3 4 5 6 8 8 12 20	18.4 to 45 0 to 45	3 to 1 $\infty$ to 1	6(a) ↓ 6(b) ↓	25 ↓ 26 ↓	$B(C_{L\dot{\alpha}})_1$	0.75	3 4 5 6 6 8 12 20	0 to 45	$\infty$ to 1	9(a) ↓ 9(b) ↓ 9(c) ↓	34 ↓ 35 ↓ 36 ↓
$B(C_{L\dot{\alpha}})_2$	↓	3 4 5 6 8 8 12 20	18.4 to 45 0 to 45	3 to 1 $\infty$ to 1	↓ ↓ ↓ ↓	27 ↓ 27 ↓	$B(C_{L\dot{\alpha}})_2$	↓	3 4 5 6 6 8 12 20	↓	↓	↓ ↓ ↓ ↓	↓ ↓ ↓ ↓
$B(C_{L\dot{\alpha}})_1$	0.25	3 4 5 6 8 8 12 20	3.81 to 45 0 to 45	15 to 1 $\infty$ to 1	7(a) ↓ 7(b) ↓	28 ↓ 29 ↓	$B(C_{L\dot{\alpha}})_1$	1.00	2 3 4 5 6 6 8 12 20	↓	↓	10(a) ↓ 10(b) ↓ 10(c) ↓	37 ↓ 38 ↓ 39 ↓
$B(C_{L\dot{\alpha}})_2$	↓	3 4 5 6 8 8 12 20	3.81 to 45 0 to 45	15 to 1 $\infty$ to 1	↓ ↓ ↓ ↓	30 ↓ 30 ↓	$B(C_{L\dot{\alpha}})_2$	↓	2 3 4 5 6 6 8 12 20	↓	↓	↓ ↓ ↓ ↓	↓ ↓ ↓ ↓
$B(C_{L\dot{\alpha}})_1$	0.50	3 4 5 6 6 8 12 20	0 to 45	$\infty$ to 1	8(a) ↓ 8(b) ↓	31 ↓ 32 ↓	↓	↓	↓	↓	↓	↓ ↓ ↓ ↓	↓ ↓ ↓ ↓
$B(C_{L\dot{\alpha}})_2$	↓	3 4 5 6 6 8 12 20	↓	↓	↓ ↓ ↓ ↓	33 ↓ 33 ↓	↓	↓	↓	↓	↓	↓ ↓ ↓ ↓	↓ ↓ ↓ ↓

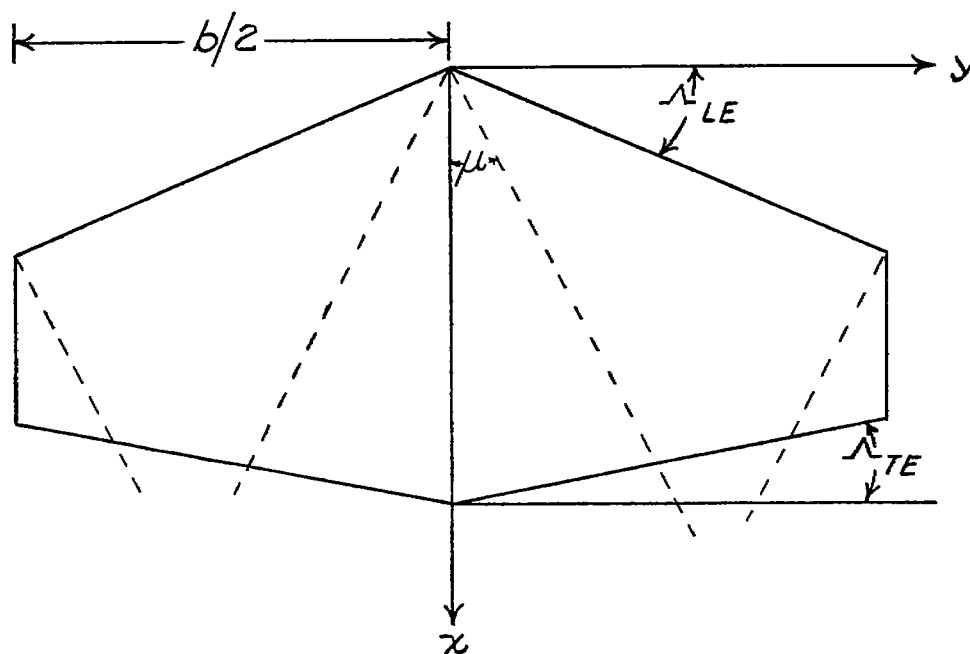
TABLE IV.-- INDEX TO DESIGN CHARTS FOR  $BC_{m_d}$ 

$$BC_{m_d} = \frac{M^2}{B^2} B(C_{m_d})_1 + \left( \frac{M^2}{B^2} + 1 \right) B(C_{m_d})_2$$

Component	$\lambda$	AB	$\cot^{-1} B_m$ , deg	$B_m$	Figure	Page	Component	$\lambda$	AB	$\cot^{-1} B_m$ , deg	$B_m$	Figure	Page
$B(C_{m_d})_1$	0	3 4 5 6 8 12 20	18.4 to 45 0 to 45 ↓ 0 to 42 0 to 35.6 0 to 27.8	3 to 1 ∞ to 1 ↓ ∞ to 1.11 ∞ to 1.4 ∞ to 1.9	11(a)	40	$B(C_{m_d})_2$	0.50	3 4 5 6 8 12 20	0 to 45 ↓ ↓ ↓ ↓ ↓ ↓	∞ to 1 ↓ ↓ ↓ ↓ ↓ ↓	13(c)	48
↓	↓	8 12 20	24 to 45 ↓ ↓	2.25 to 1 ↓ ↓	11(b)	41	$B(C_{m_d})_1$	0.75	3 4 5 6 8 12 20	0 to 45 0 to 42.8 0 to 36 0 to 32.4 0 to 27.4 0 to 21.6 0 to 15.6	∞ to 1 ∞ to 1.08 ∞ to 1.38 ∞ to 1.58 ∞ to 1.93 ∞ to 2.53 ∞ to 3.58	14(a)	49
$B(C_{m_d})_2$	↓	3 4 5 6 8 12 20	0 to 45 ↓ ↓ ↓ ↓ ↓ ↓	∞ to 1 ↓ ↓ ↓ ↓ ↓ ↓	11(c)	42	↓	↓	4 5 6 8 12 20	14 to 45 ↓ ↓ ↓ ↓ ↓ ↓	4.01 to 1 ↓ ↓ ↓ ↓ ↓ ↓	14(b)	50
$B(C_{m_d})_1$	0.25	3 4 5 6 8 12 20	3.81 to 45 0 to 45 ↓ 0 to 40.4 0 to 35.6 0 to 29 0 to 21.6	15 to 1 ∞ to 1 ↓ ∞ to 1.17 ∞ to 1.4 ∞ to 1.8 ∞ to 2.53	12(a)	43	$B(C_{m_d})_2$	↓	3 4 5 6 8 12 20	0 to 45 ↓ ↓ ↓ ↓ ↓ ↓	∞ to 1 ↓ ↓ ↓ ↓ ↓ ↓	14(c)	51
↓	↓	6 8 12 20	18 to 45 ↓ 18 to 43.4 ↓ ↓	3 to 1 ↓ ↓ ↓ ↓	12(b)	44	↓	↓	12 20	↓ ↓ ↓ ↓ ↓ ↓	↓ ↓ ↓ ↓ ↓ ↓	↓ ↓ ↓ ↓ ↓ ↓	↓ ↓ ↓ ↓ ↓ ↓
$B(C_{m_d})_2$	↓	3 4 5 6 8 12 20	3.81 to 45 0 to 45 ↓ ↓ ↓ ↓ ↓	15 to 1 ∞ to 1 ↓ ↓ ↓ ↓ ↓	12(c)	45	$B(C_{m_d})_1$	1.00	2 3 4 5 6 8 12 20	0 to 45 ↓ ↓ ↓ ↓ ↓ ↓ ↓	∞ to 1 ↓ ↓ ↓ ↓ ↓ ↓ ↓	15(a)	52
↓	↓	12 20	↓ ↓ ↓ ↓ ↓ ↓ ↓	↓ ↓ ↓ ↓ ↓ ↓ ↓	↓ ↓ ↓ ↓ ↓ ↓ ↓	↓ ↓ ↓ ↓ ↓ ↓ ↓	$B(C_{m_d})_2$	↓	2 3 4 5 6 8 12 20	↓ ↓ ↓ ↓ ↓ ↓ ↓ ↓	↓ ↓ ↓ ↓ ↓ ↓ ↓ ↓	15(b)	53
$B(C_{m_d})_1$	0.50	3 4 5 6 8 12 20	0 to 45 ↓ 0 to 40.6 0 to 36 0 to 30.6 0 to 25 0 to 17.8	∞ to 1 ↓ ∞ to 1.17 ∞ to 1.38 ∞ to 1.69 ∞ to 2.14 ∞ to 3.11	13(a)	46	↓	↓	5 6 8 12 20	0 to 44.6 0 to 41 0 to 36.6 0 to 29.6 0 to 21.2	∞ to 1.01 ∞ to 1.15 ∞ to 1.35 ∞ to 1.76 ∞ to 2.58	↓ ↓ ↓ ↓ ↓ ↓ ↓	↓ ↓ ↓ ↓ ↓ ↓ ↓
↓	↓	5 6 8 12	16 to 45 ↓ ↓ ↓	3.49 to 1 ↓ ↓ ↓	13(b)	47	↓	↓	5 6 8 12 20	20 to 45 ↓ ↓ ↓ ↓ ↓	2.75 to 1 ↓ ↓ ↓ ↓ ↓	15(c)	54

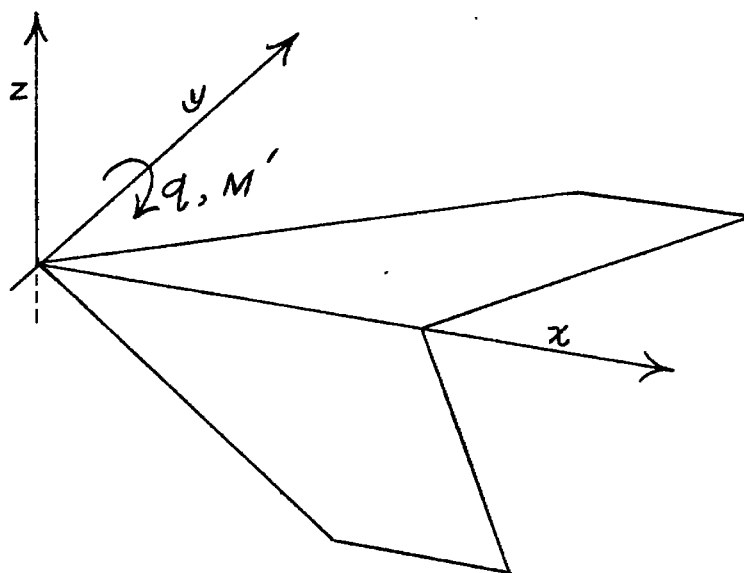


(a) Sweptback trailing edge. Positive  $\Lambda_{TE}$ ; positive  $k$ .

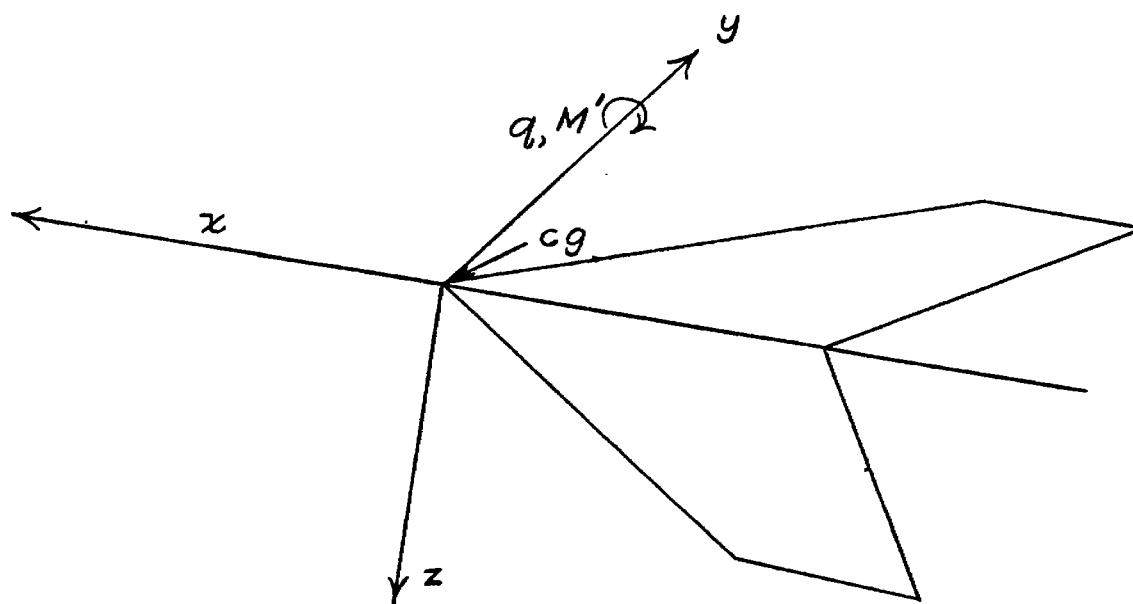


(b) Sweptforward trailing edge. Negative  $\Lambda_{TE}$ ; negative  $k$ .

Figure 1.- Types of wings analyzed.

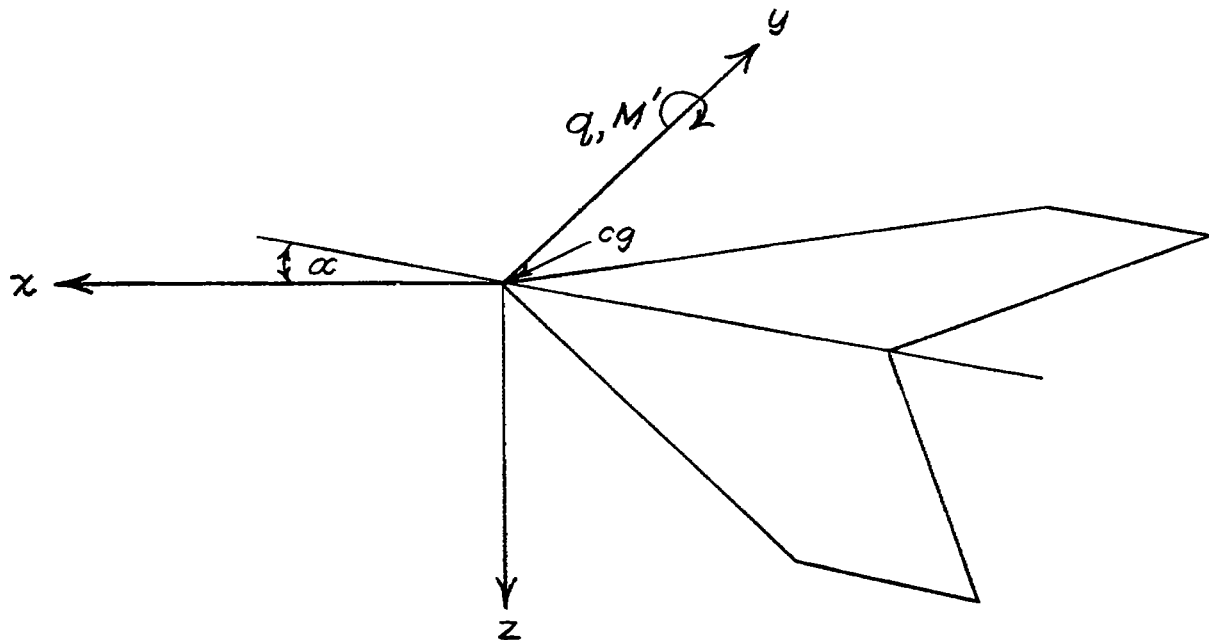


(a) Body axes used in analysis.

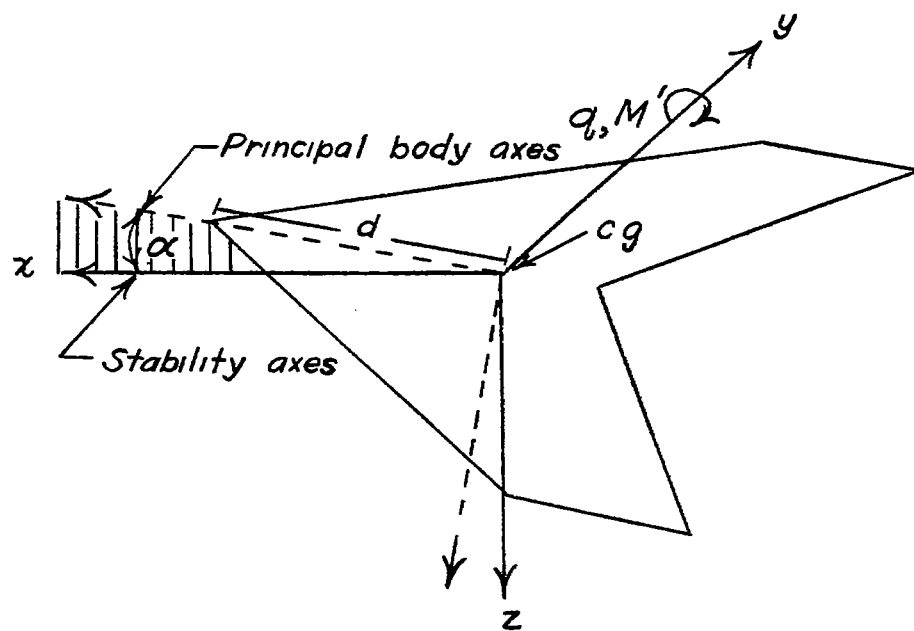


(b) Principal body axes with center of gravity at wing apex.

Figure 2.- Systems of axes and associated data.



(c) Stability axes with center of gravity at wing apex.



(d) Stability and principal body axes with center of gravity located at a distance  $d$  from wing apex.

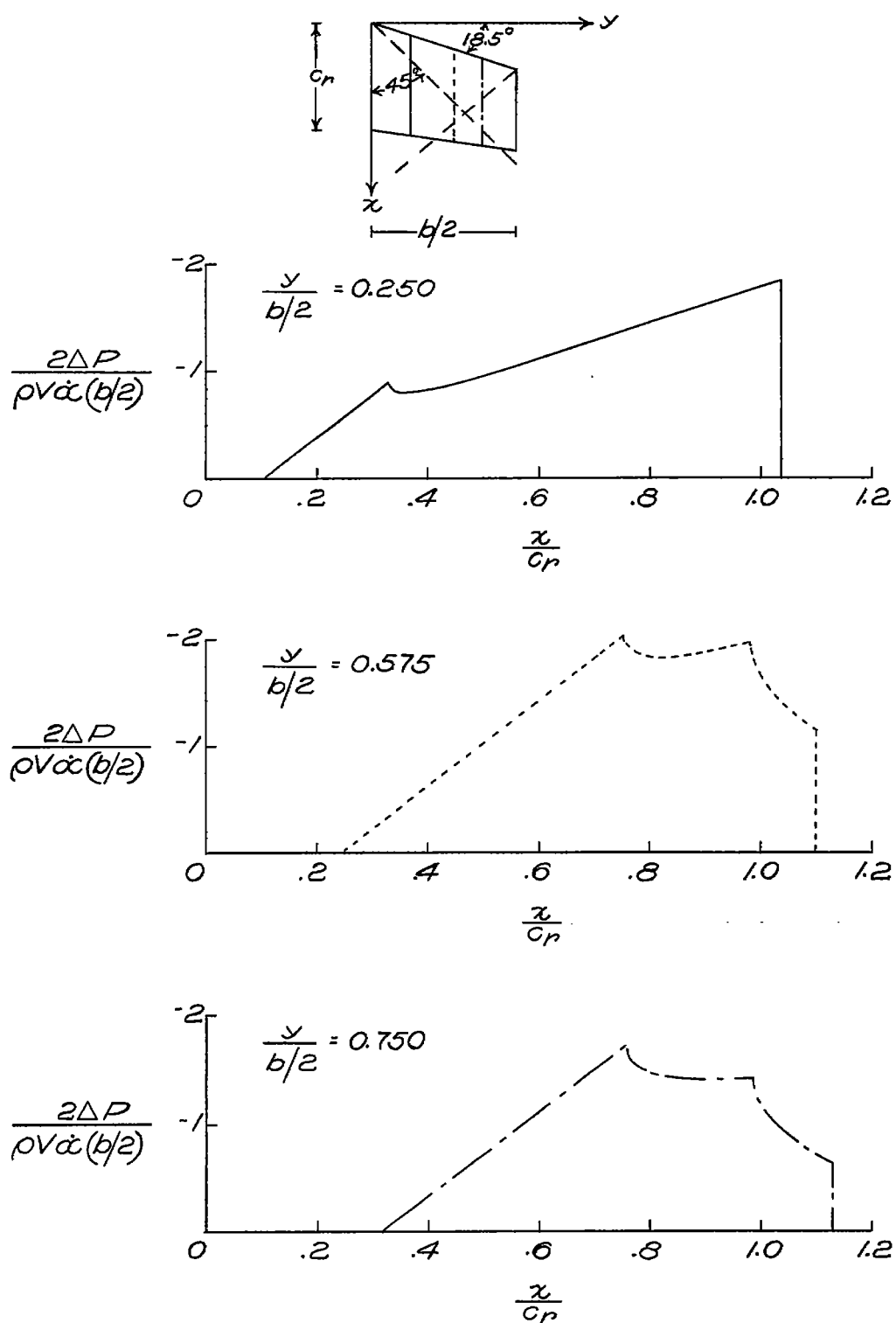


Figure 3.- Some illustrative chordwise pressure distributions.  $A = 3$ ;  
 $\Lambda_{LE} = 18.5^\circ$ ;  $\lambda = 0.75$ ;  $M = \sqrt{2}$ .

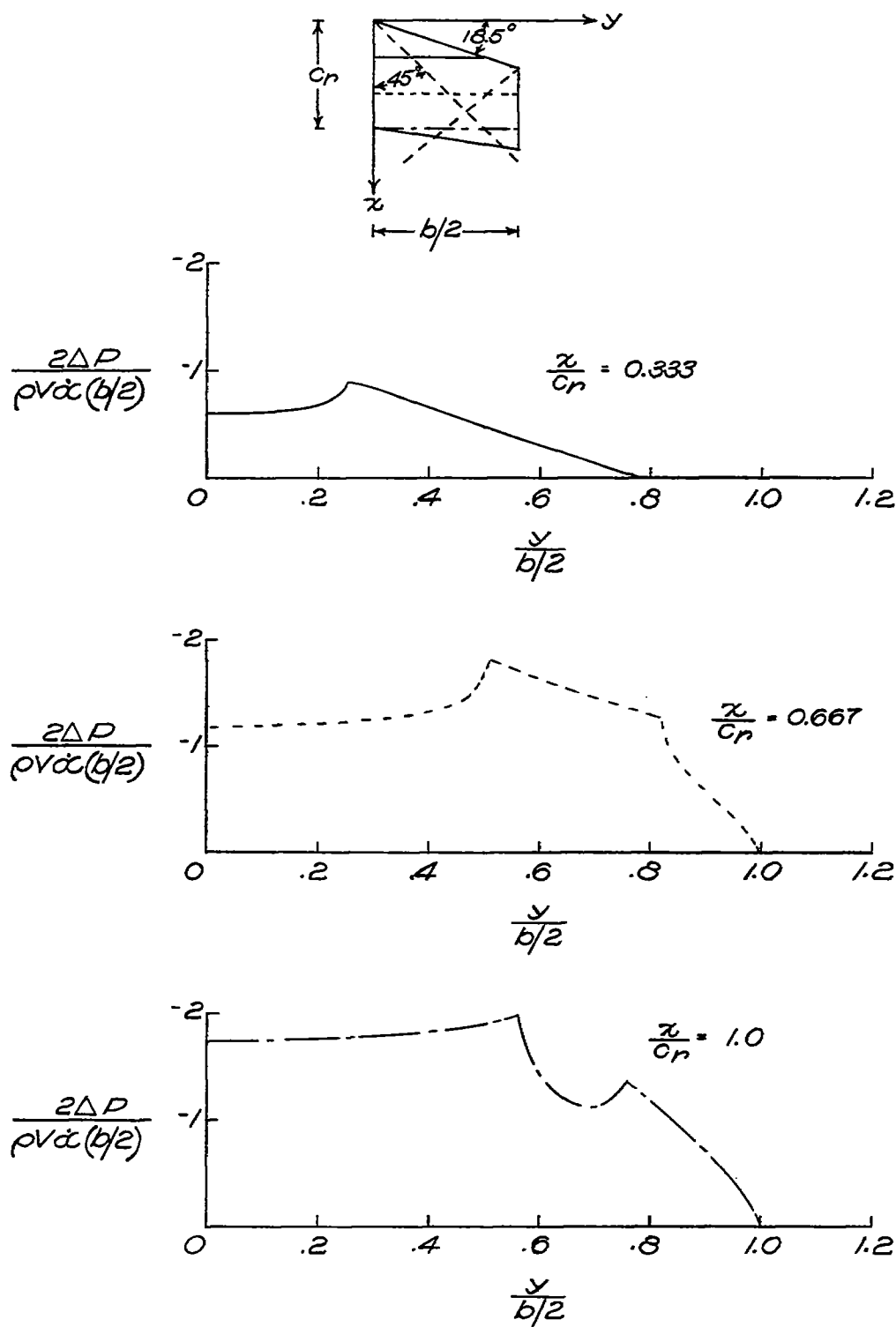


Figure 4.- Some illustrative spanwise pressure distributions.  $A = 3$ ;  
 $\Lambda_{LE} = 18.5^\circ$ ;  $\lambda = 0.75$ ;  $M = \sqrt{2}$ .



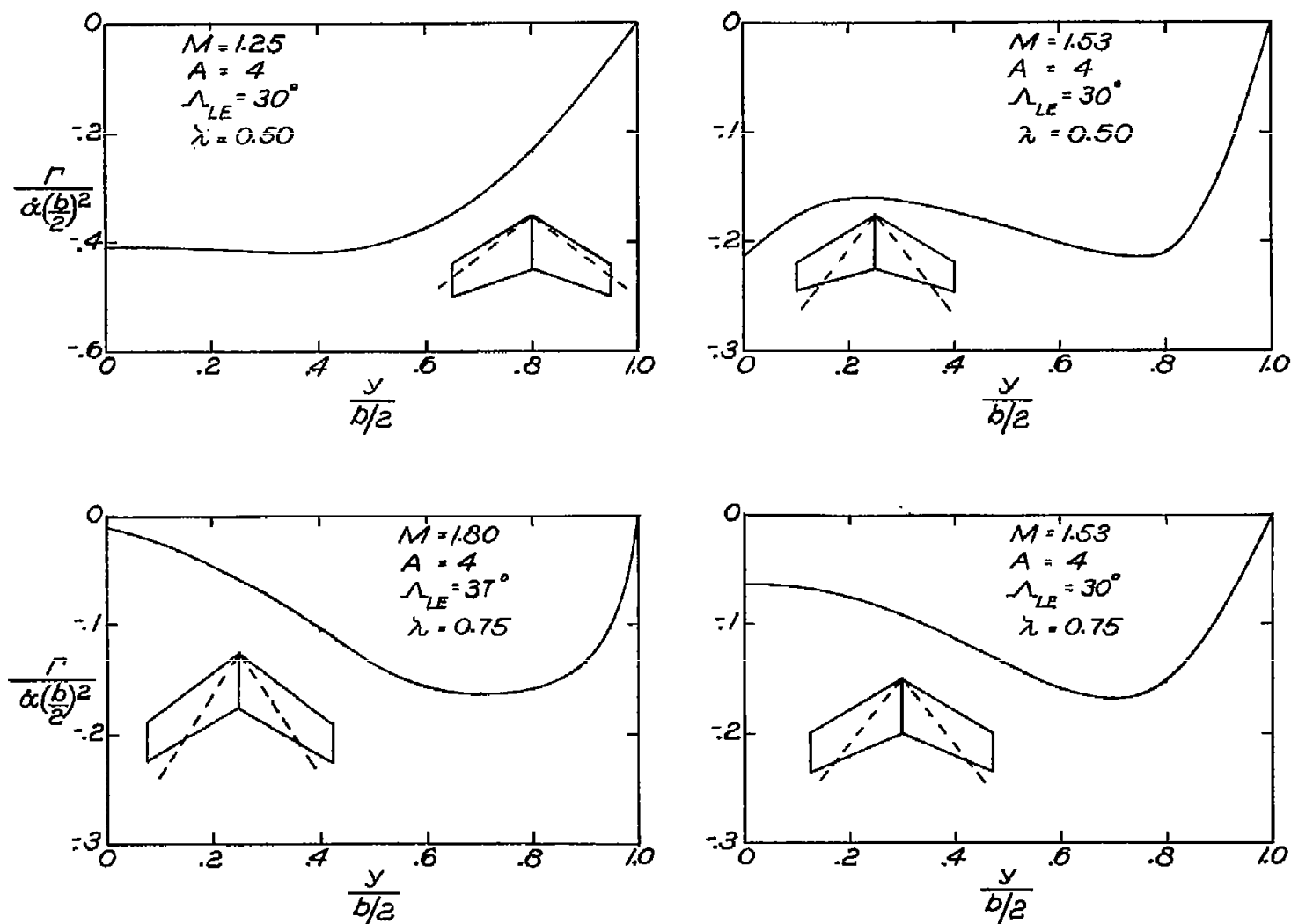
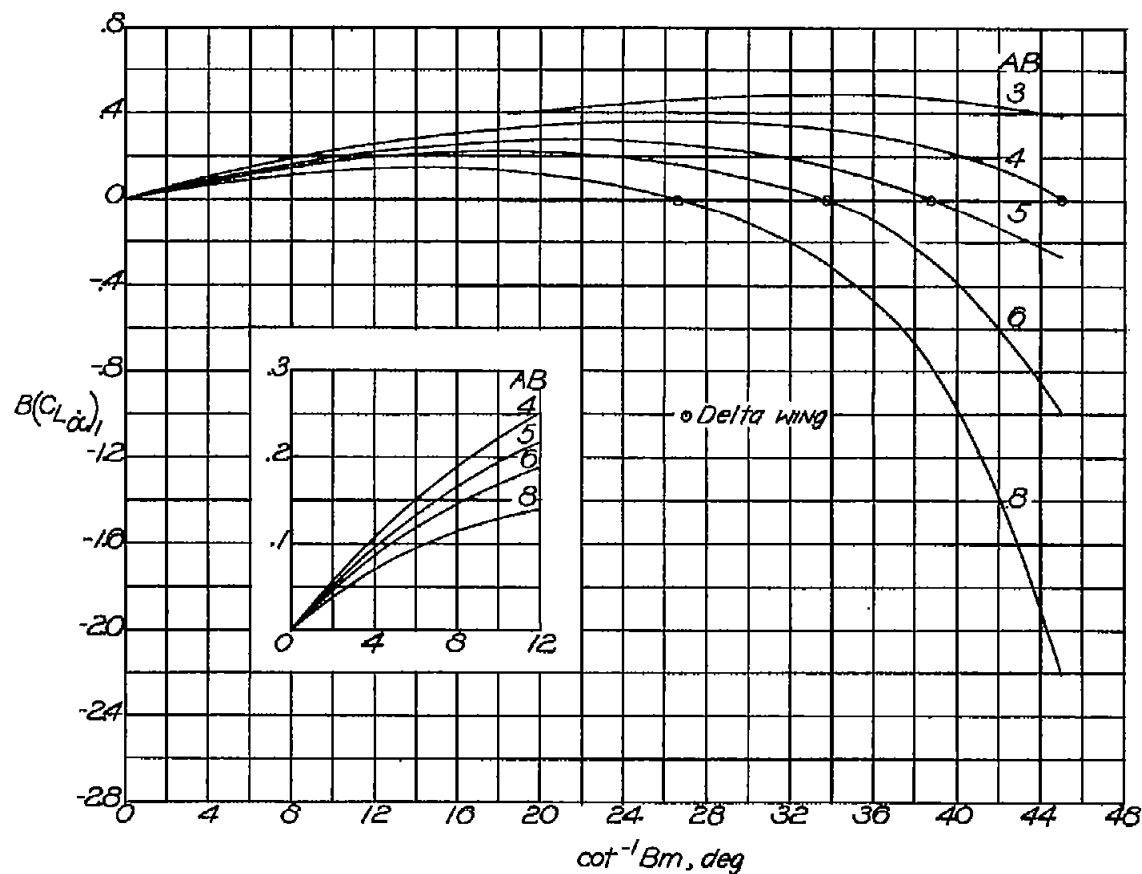


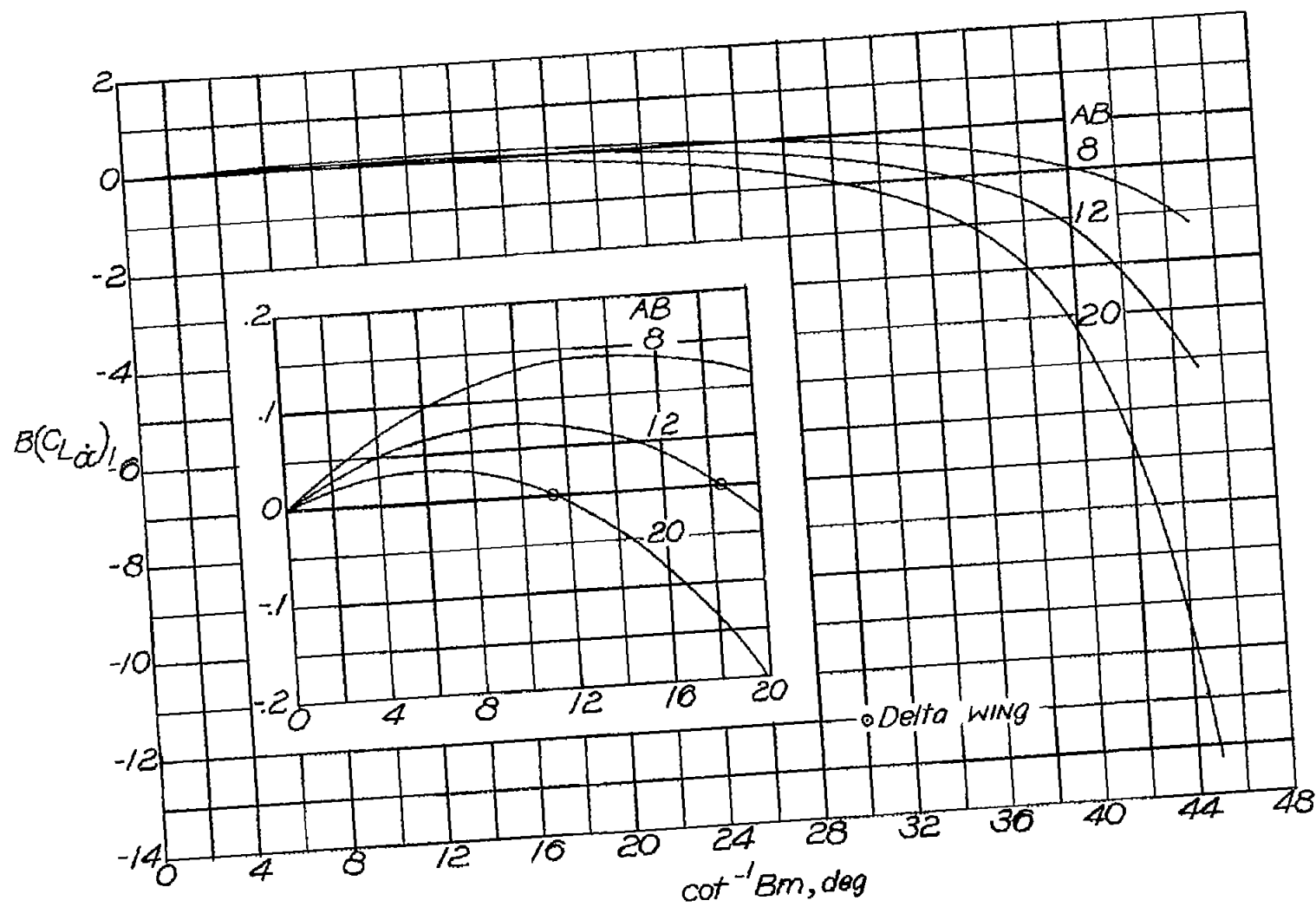
Figure 5.- Some illustrative variations of spanwise distribution of circulation.



(a)  $B(C_L\ddot{\alpha})_1$ .  $\lambda = 0$ ;  $AB = 3$  to  $8$ ;  $\cot^{-1}Bm = 0^\circ$  to  $45^\circ$ .

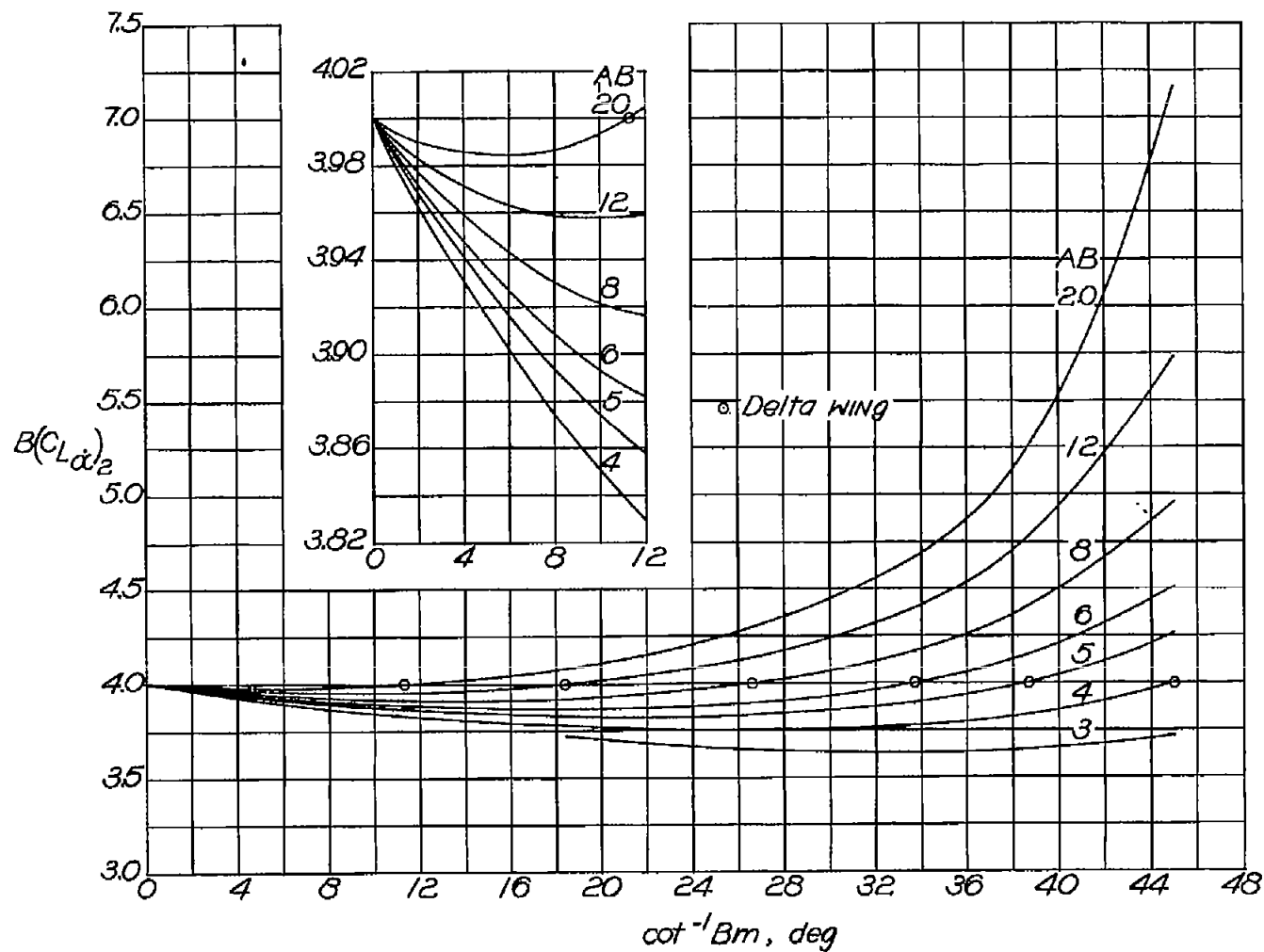
Figure 6.- Variation of  $B(C_L\ddot{\alpha})_1$  and  $B(C_L\ddot{\alpha})_2$  with  $\cot^{-1}Bm$ . Results valid for both principal body and stability systems of axes.

$$BC_{L\ddot{\alpha}} = \frac{M^2}{B^2} B(C_L\ddot{\alpha})_1 - \frac{1}{B^2} B(C_L\ddot{\alpha})_2.$$



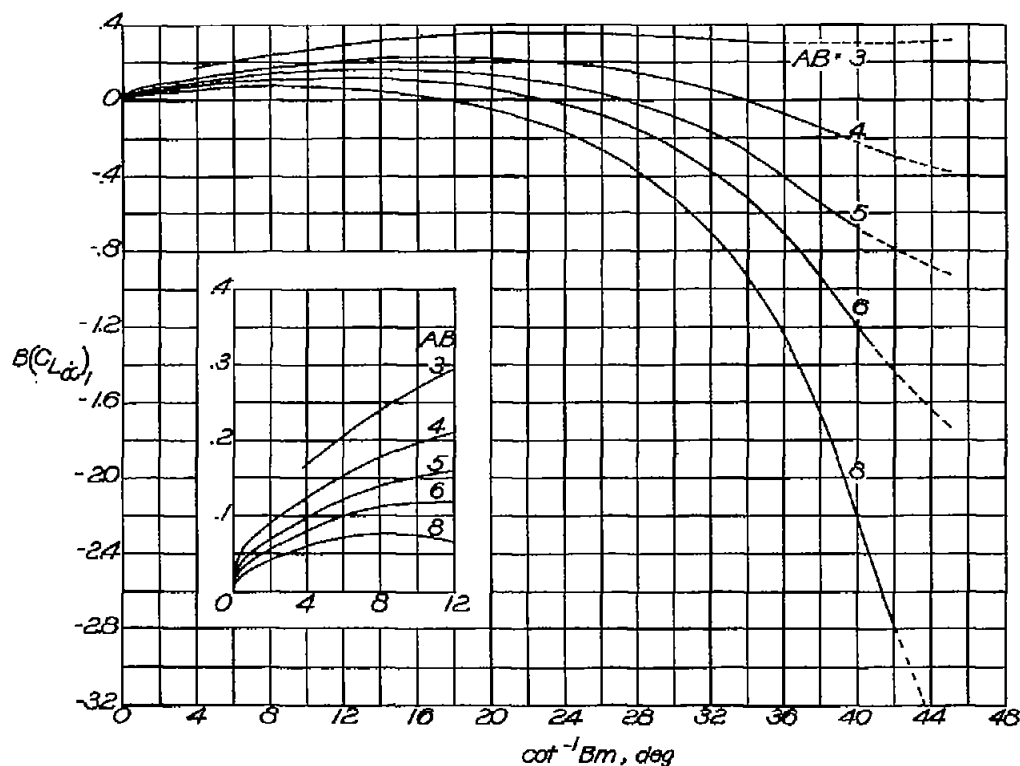
(b)  $B(C_L\alpha)_1$ .  $\lambda = 0$ ;  $AB = 8$  to  $20$ ;  $\cot^{-1} Bm = 0^\circ$  to  $45^\circ$ .

Figure 6.- Continued.



(c)  $B(C_L \alpha_2)$ .  $\lambda = 0$ ;  $AB = 3$  to  $20$ ;  $\cot^{-1} B_m = 0^\circ$  to  $45^\circ$ .

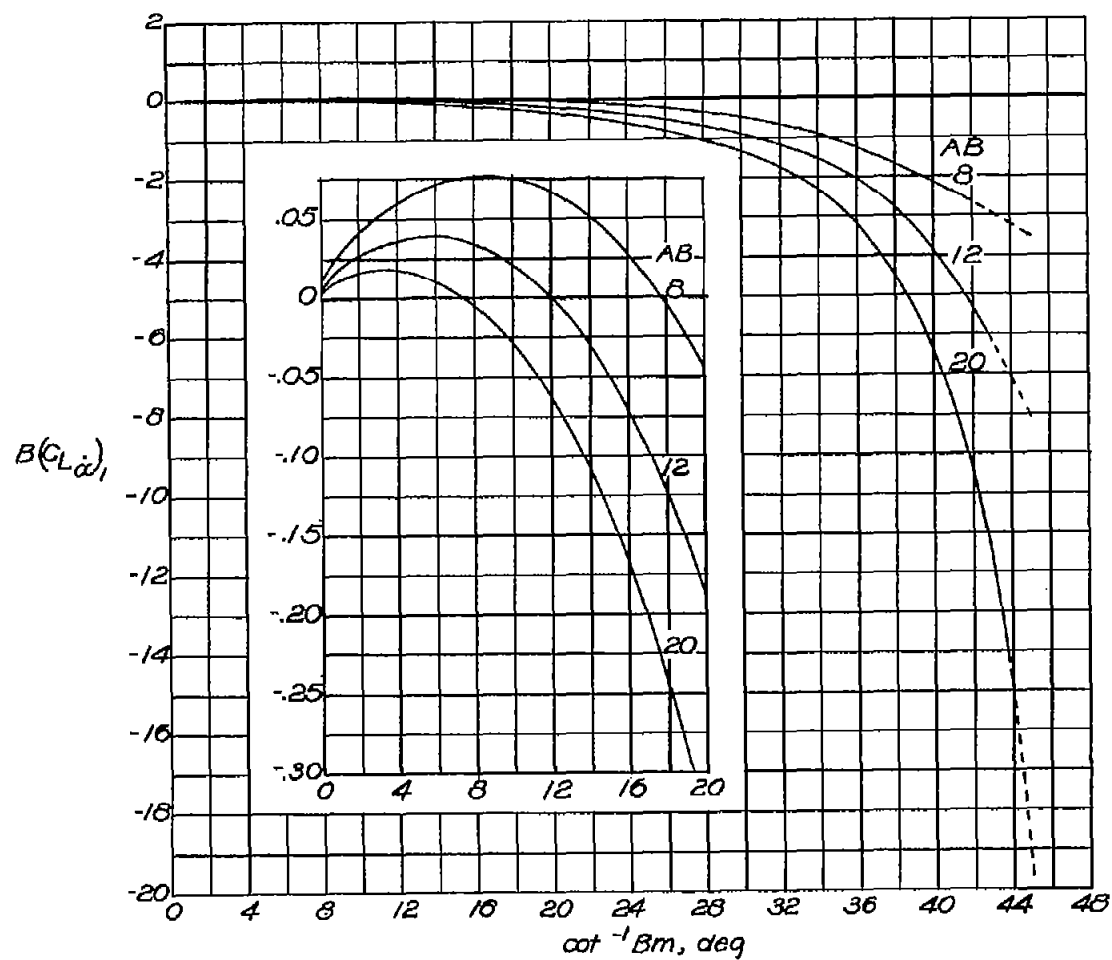
Figure 6.- Concluded.



(a)  $B(C_{L\dot{\alpha}})_1$ .  $\lambda = 0.25$ ;  $AB = 3$  to  $8$ ;  $\cot^{-1} Bm = 0^\circ$  to  $45^\circ$ .

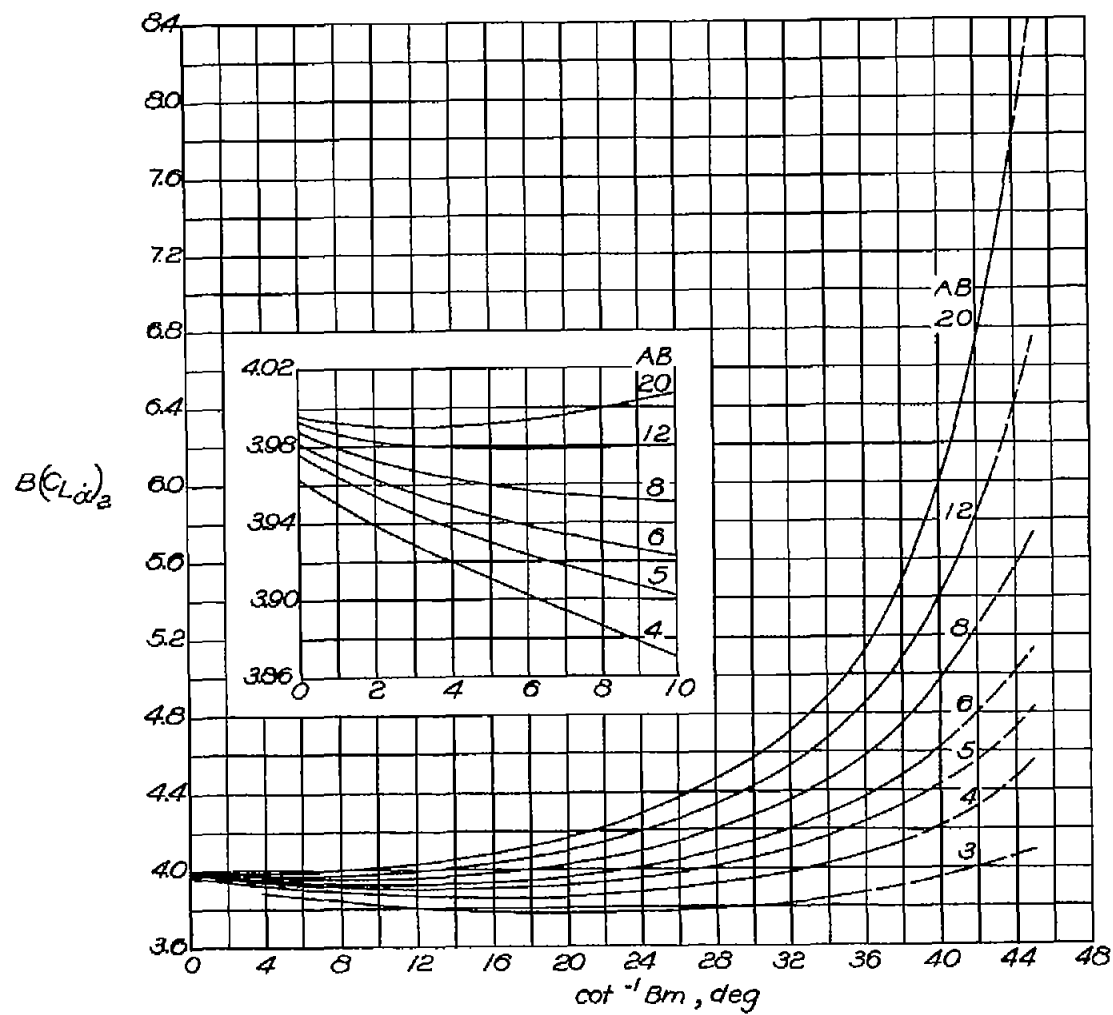
Figure 7.- Variation of  $B(C_{L\dot{\alpha}})_1$  and  $B(C_{L\dot{\alpha}})_2$  with  $\cot^{-1} Bm$ . Results valid for both principal body and stability systems of axes.

$BC_{L\dot{\alpha}} = \frac{M^2}{B^2} B(C_{L\dot{\alpha}})_1 - \frac{1}{B^2} B(C_{L\dot{\alpha}})_2$ . Dashed parts of curves represent extensions of calculated curves (through region which corresponds to condition where Mach lines from wing apex intersect tips) to calculated end points.



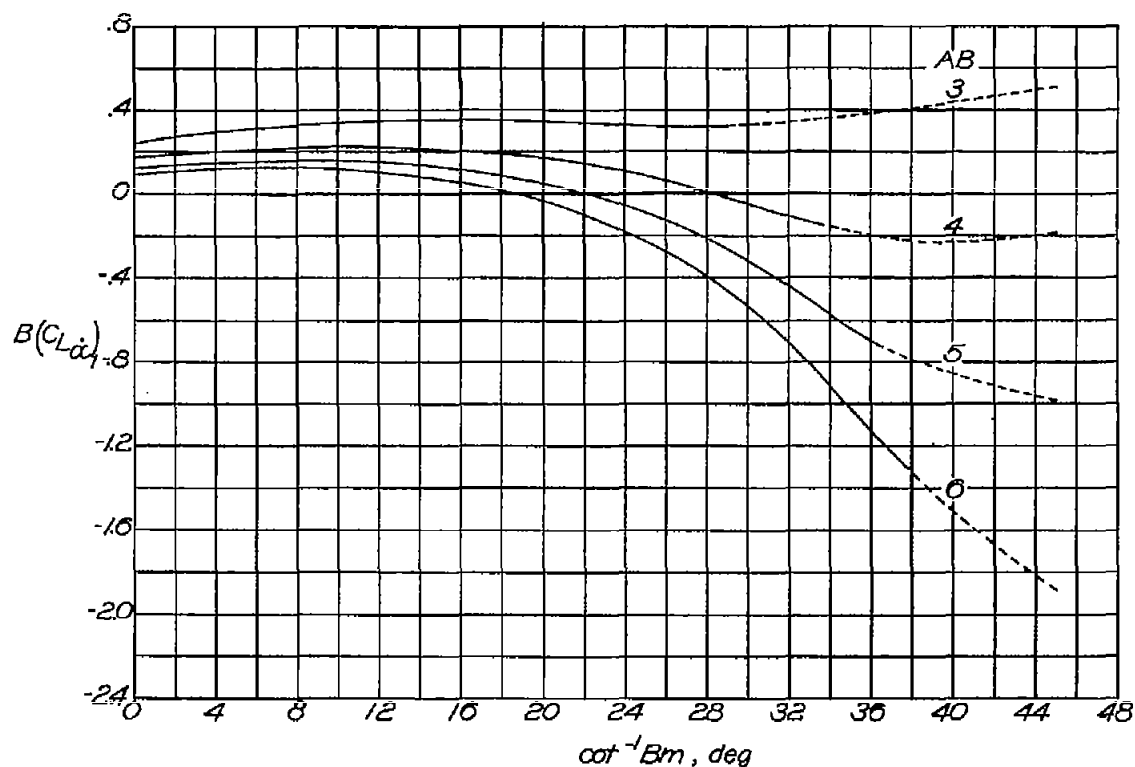
(b)  $B(C_L\dot{\alpha})_1$ .  $\lambda = 0.25$ ;  $AB = 8$  to  $20$ ;  $\cot^{-1}Bm = 0^\circ$  to  $45^\circ$ .

Figure 7.- Continued.



(c)  $B(C_{L\alpha})_2$ .  $\lambda = 0.25$ ;  $AB = 3$  to  $20$ ;  $\cot^{-1} Bm = 0^\circ$  to  $45^\circ$ .

Figure 7.- Concluded.

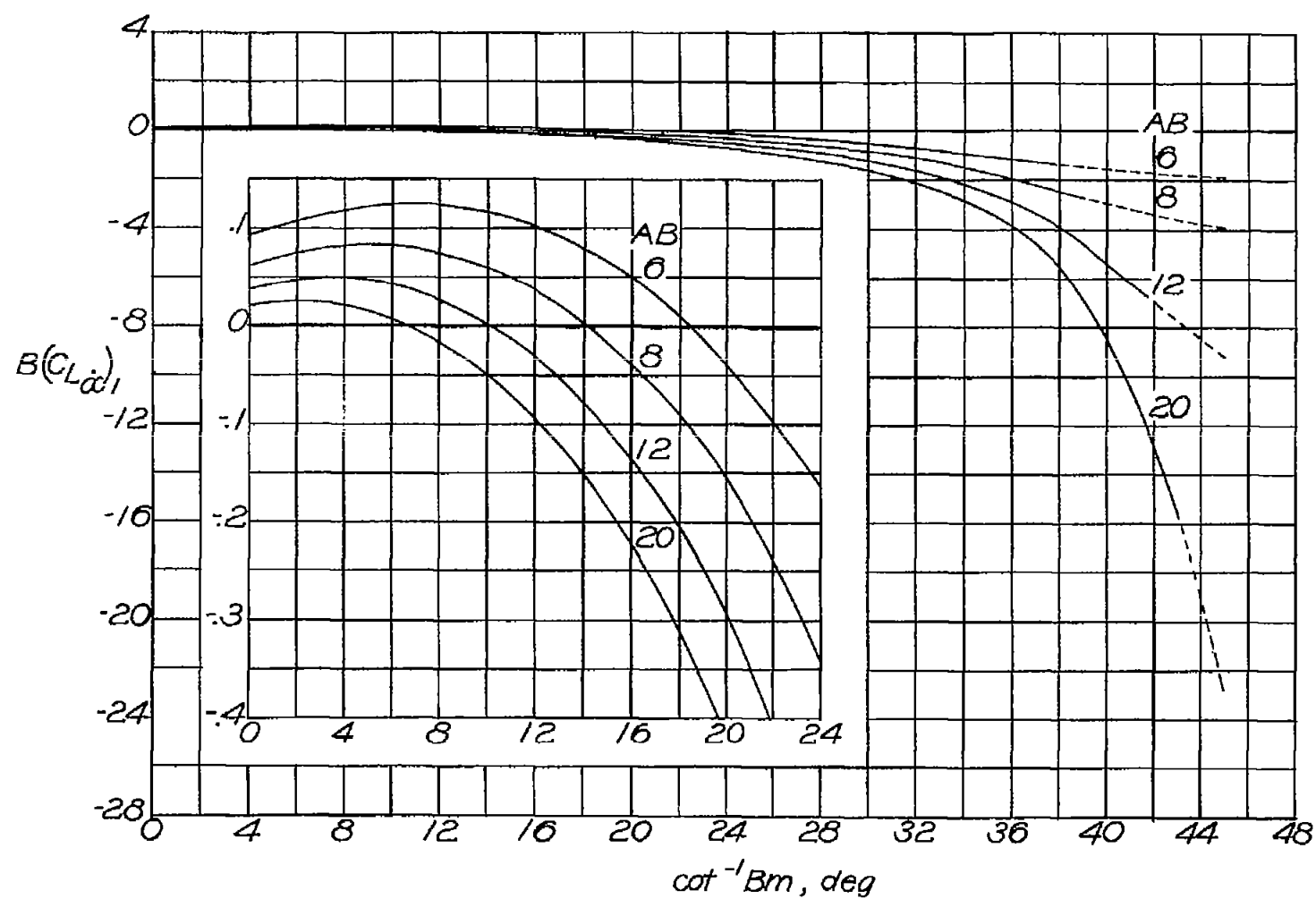


(a)  $B(C_{L\dot{\alpha}})_1$ .  $\lambda = 0.50$ ;  $AB = 3$  to  $6$ ;  $\cot^{-1} Bm = 0^\circ$  to  $45^\circ$ .

Figure 8.- Variation of  $B(C_{L\dot{\alpha}})_1$  and  $B(C_{L\dot{\alpha}})_2$  with  $\cot^{-1} Bm$ . Results valid for both principal body and stability systems of axes.

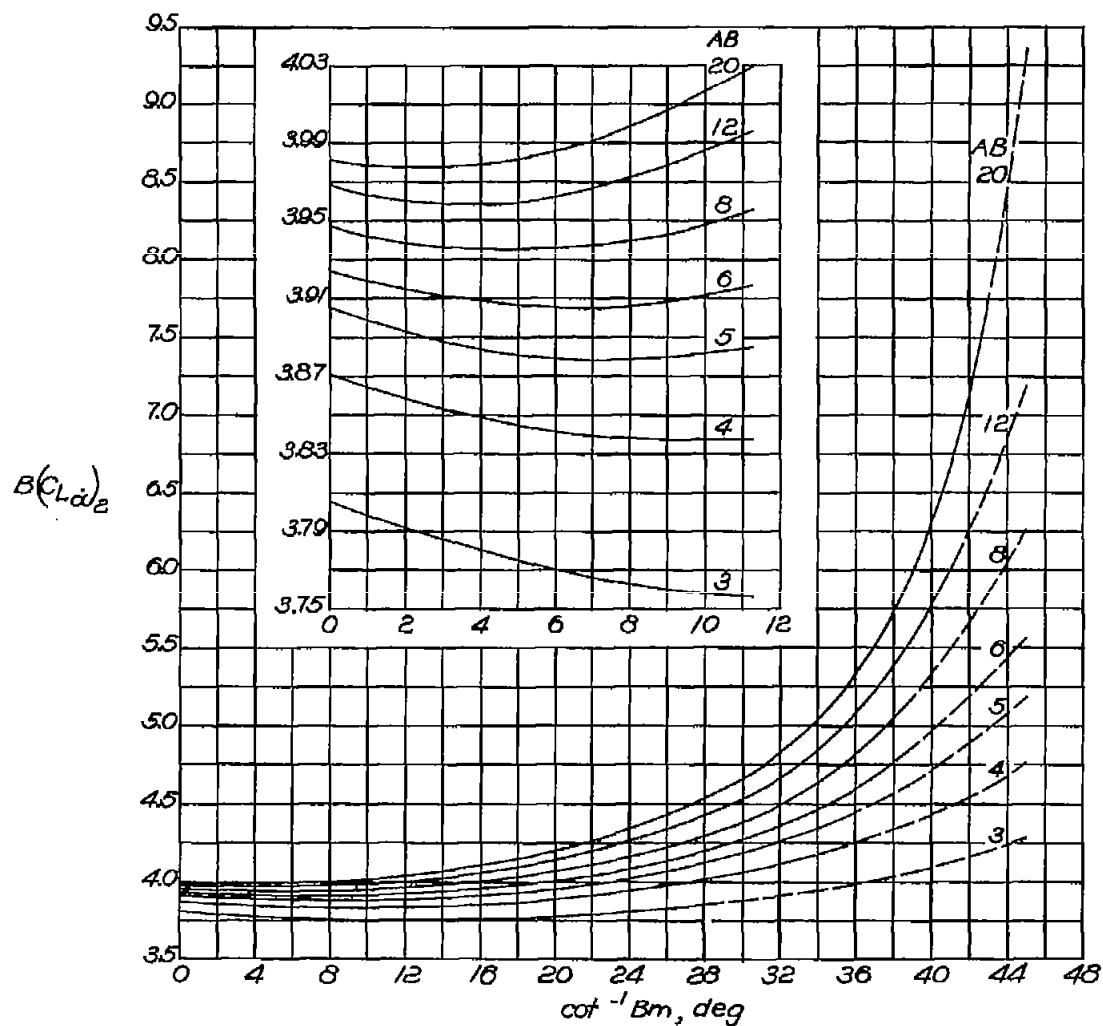
$BC_{L\dot{\alpha}} = \frac{M^2}{B^2} B(C_{L\dot{\alpha}})_1 - \frac{1}{B^2} B(C_{L\dot{\alpha}})_2$ . Dashed parts of curves represent extensions of calculated curves (through region which corresponds to condition where Mach lines from wing apex intersect tips) to calculated end points.





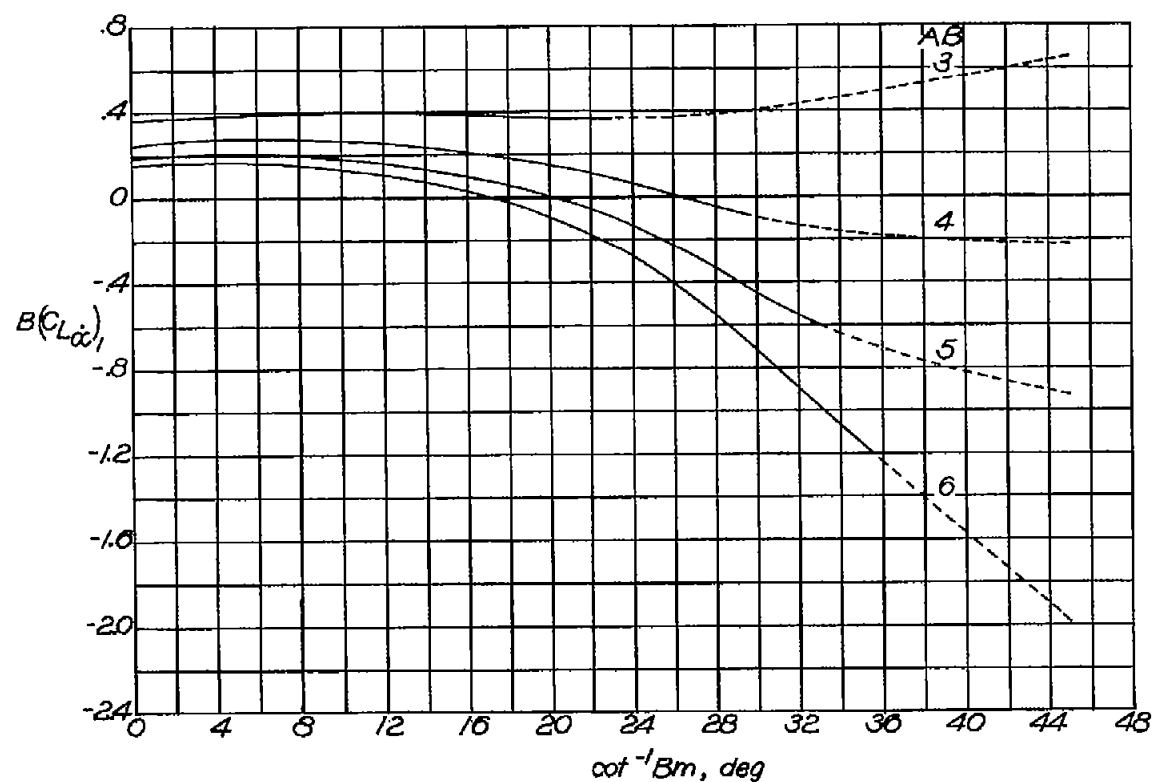
(b)  $B(C_L \ddot{\alpha})_1$ .  $\lambda = 0.50$ ;  $AB = 6$  to  $20$ ;  $\cot^{-1} Bm = 0^\circ$  to  $45^\circ$ .

Figure 8.- Continued.



(c)  $B(C_L\alpha)_2$ .  $\lambda = 0.50$ ;  $AB = 3$  to  $20$ ;  $\cot^{-1} Bm = 0^\circ$  to  $45^\circ$ .

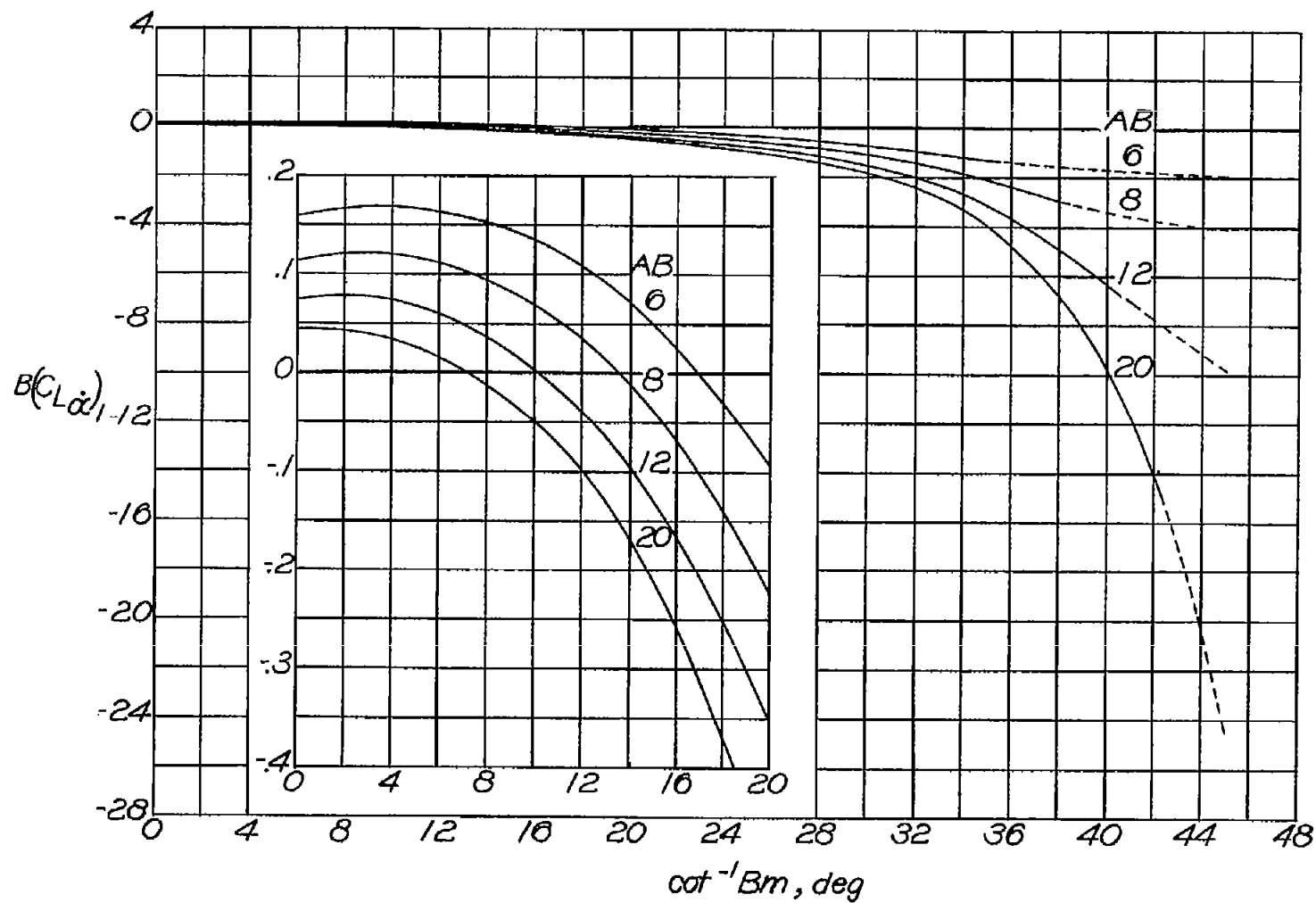
Figure 8.- Concluded.



(a)  $B(C_{L\dot{\alpha}})_1$ .  $\lambda = 0.75$ ;  $AB = 3$  to  $6$ ;  $\cot^{-1}Bm = 0^\circ$  to  $45^\circ$ .

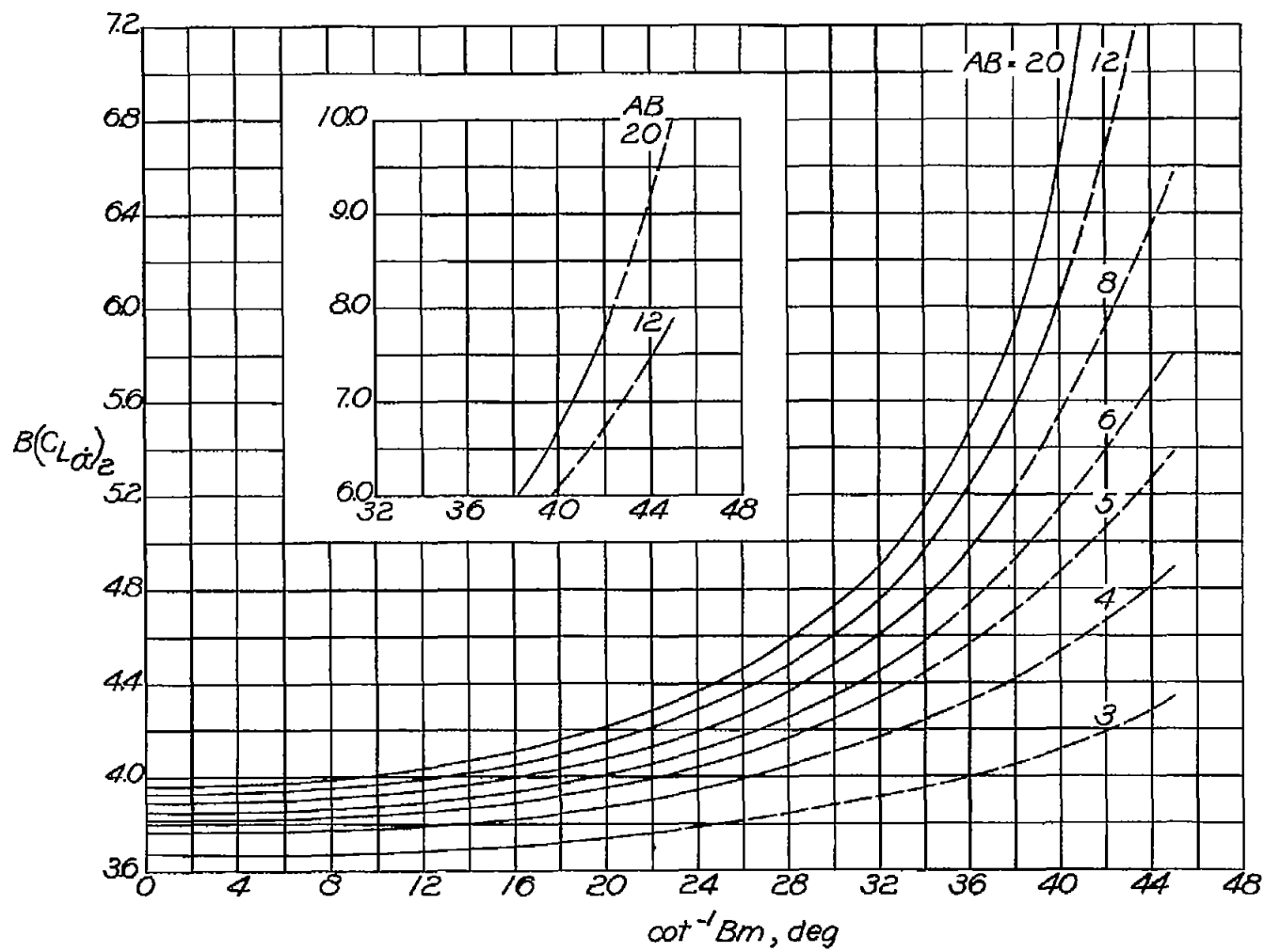
Figure 9.- Variation of  $B(C_{L\dot{\alpha}})_1$  and  $B(C_{L\dot{\alpha}})_2$  with  $\cot^{-1}Bm$ . Results valid for both principal body and stability systems of axes.

$BC_{L\dot{\alpha}} = \frac{M^2}{B^2} B(C_{L\dot{\alpha}})_1 - \frac{1}{B^2} B(C_{L\dot{\alpha}})_2$ . Dashed parts of curves represent extensions of calculated curves (through region which corresponds to condition where Mach lines from wing apex intersect tips) to calculated end points.



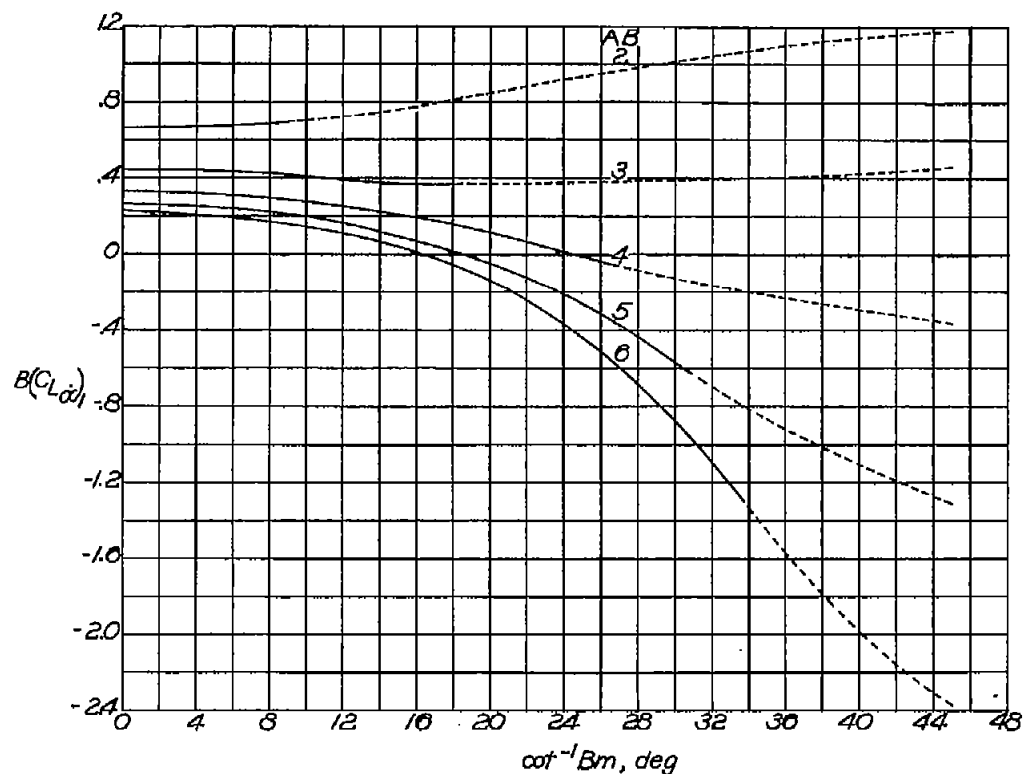
(b)  $B(C_L\alpha)_1$ .  $\lambda = 0.75$ ;  $AB = 6$  to  $20$ ;  $\cot^{-1} B_m = 0^\circ$  to  $45^\circ$ .

Figure 9.- Continued.



(c)  $B(CLa)_2$ .  $\lambda = 0.75$ ;  $AB = 3$  to  $20$ ;  $\cot^{-1} B_m = 0^\circ$  to  $45^\circ$ .

Figure 9.- Concluded.



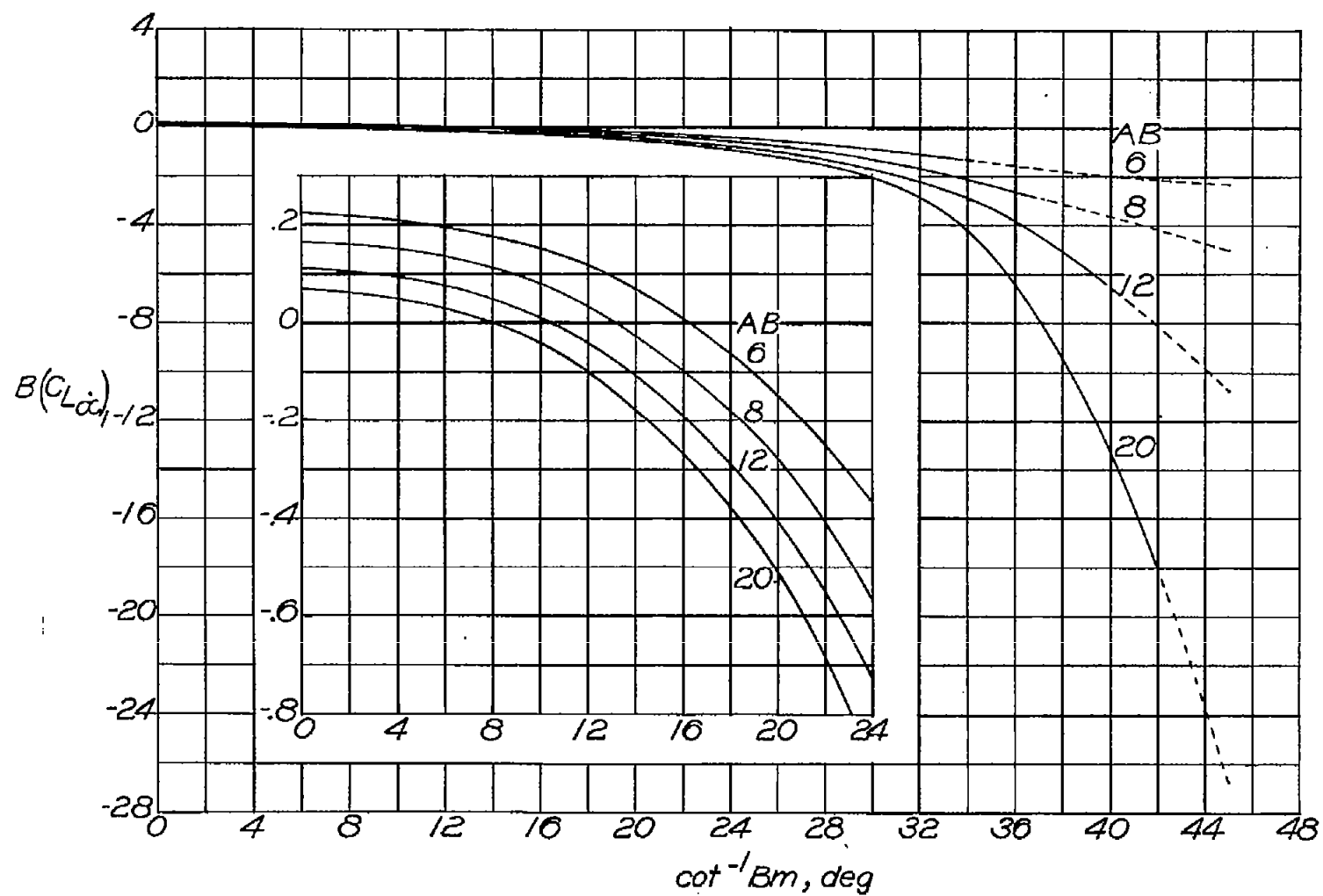
(a)  $B(C_{L\dot{\alpha}})_1$ .  $\lambda = 1.0$ ;  $AB = 2$  to  $6$ ;  $\cot^{-1}Bm = 0^\circ$  to  $45^\circ$ .

Figure 10.- Variation of  $B(C_{L\dot{\alpha}})_1$  and  $B(C_{L\dot{\alpha}})_2$  with  $\cot^{-1}Bm$ . Results

valid for both principal body and stability systems of axes.

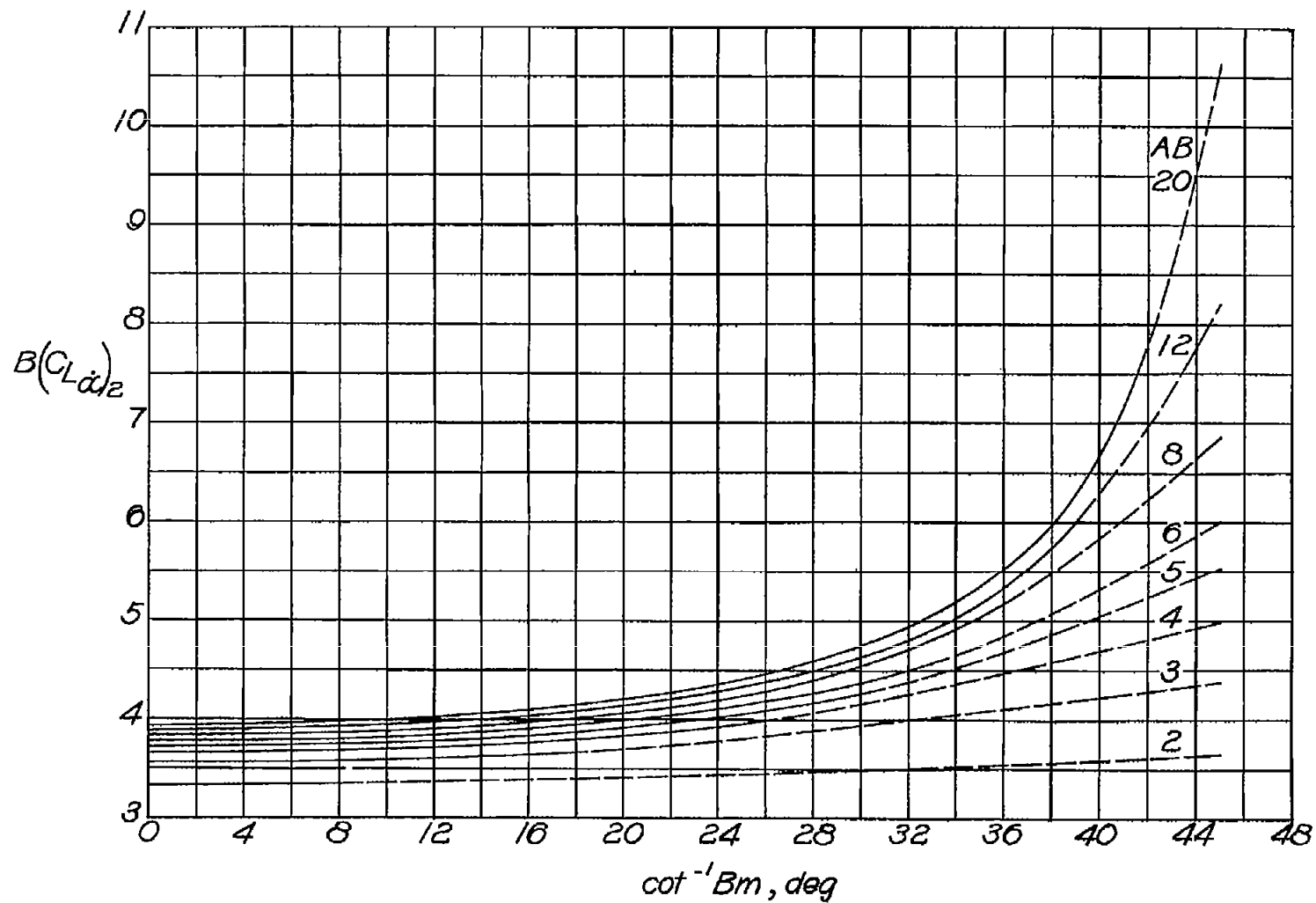
$$BC_{L\dot{\alpha}} = \frac{M^2}{B^2} B(C_{L\dot{\alpha}})_1 - \frac{1}{B^2} B(C_{L\dot{\alpha}})_2. \text{ Dashed parts of curves represent}$$

extensions of calculated curves (through region which corresponds to condition where Mach lines from wing apex intersect tips) to calculated end points.



(b)  $B(C_L \ddot{\alpha})_1$ .  $\lambda = 1.0$ ;  $AB = 6$  to  $20$ ;  $\cot^{-1} Bm = 0^\circ$  to  $45^\circ$ .

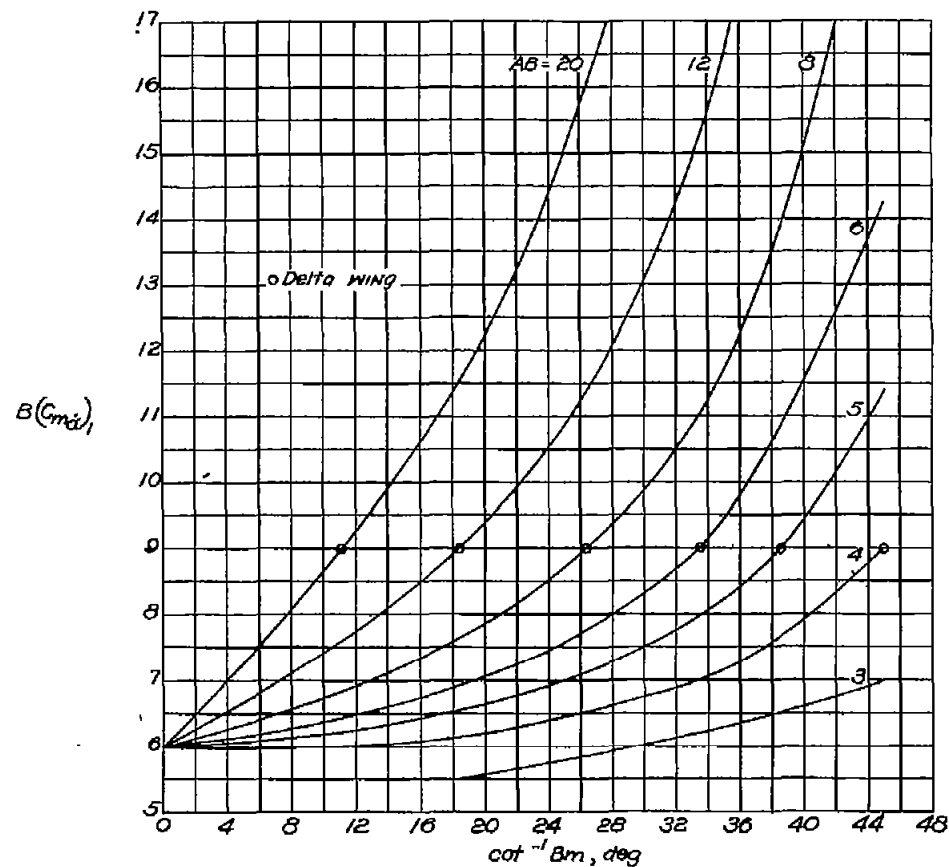
Figure 10.- Continued.



(c)  $B(C_L \dot{\alpha})_2$ .  $\lambda = 1.0$ ;  $AB = 2$  to  $20$ ;  $\cot^{-1} Bm = 0^\circ$  to  $45^\circ$ .

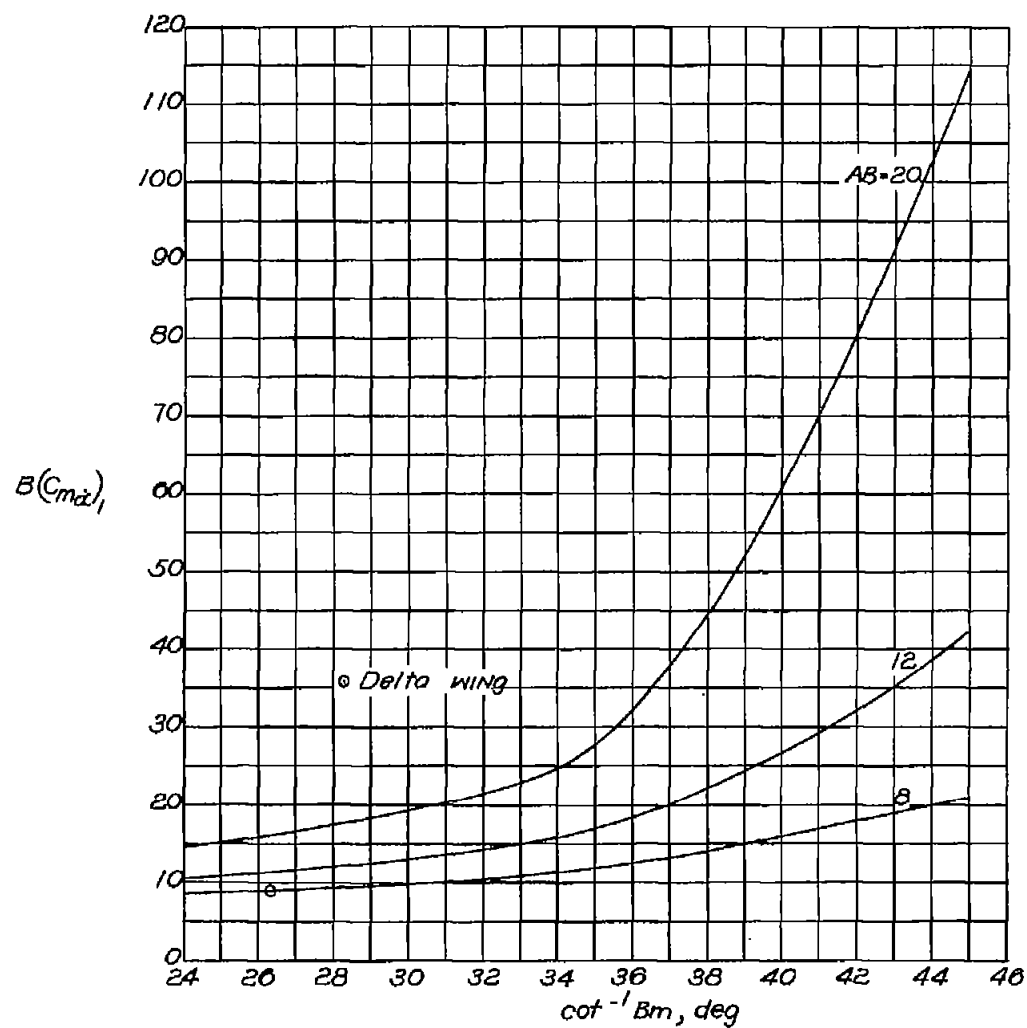
Figure 10.- Concluded.





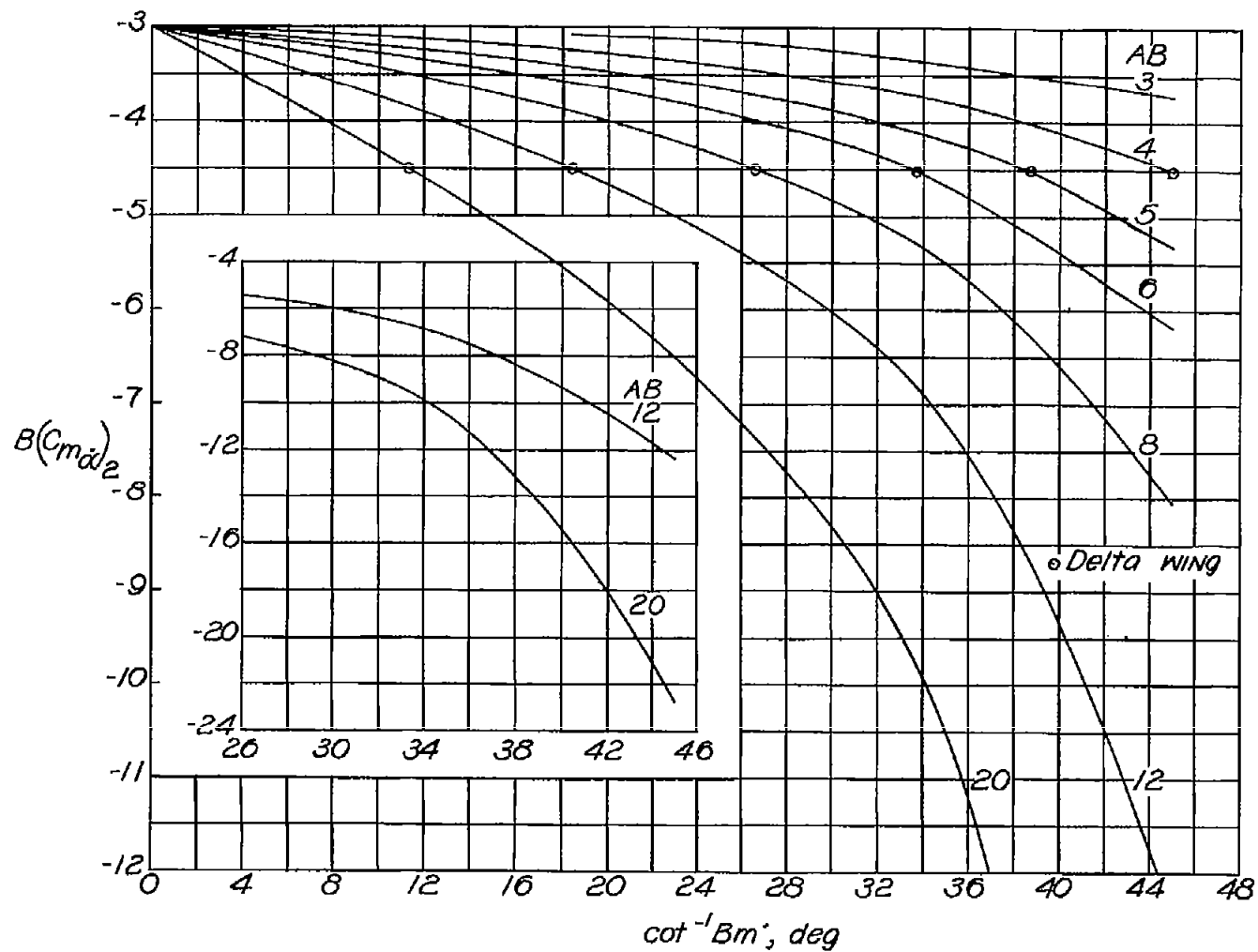
(a)  $B(C_{m\dot{\alpha}})_1$ .  $\lambda = 0$ ;  $AB = 3$  to  $20$ ;  $\cot^{-1} Bm = 0^\circ$  to  $45^\circ$ .

Figure 11.- Variation of  $B(C_{m\dot{\alpha}})_1$  and  $B(C_{m\dot{\alpha}})_2$  with  $\cot^{-1} Bm$ . Results valid for both principal body and stability systems of axes with origin at wing apex.  $BC_{m\dot{\alpha}} = \frac{M^2}{B^2} B(C_{m\dot{\alpha}})_1 + \left(\frac{M^2}{B^2} + 1\right) B(C_{m\dot{\alpha}})_2$ .



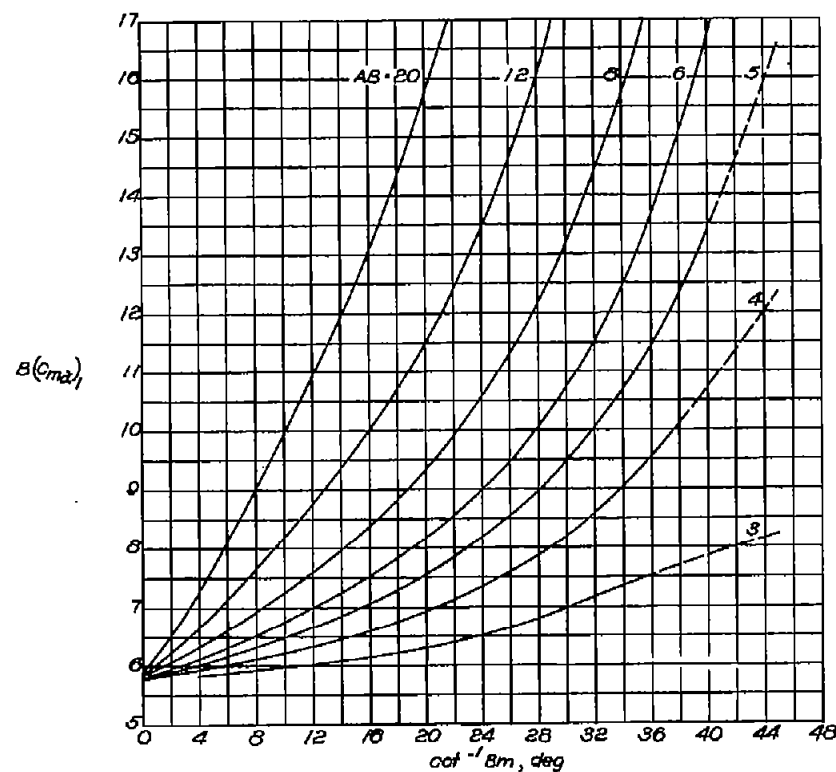
(b)  $B(C_{m\alpha})_1$ .  $\lambda = 0$ ;  $AB = 8$  to  $20$ ;  $\cot^{-1} B_m = 24^\circ$  to  $45^\circ$ .

Figure 11.- Continued.



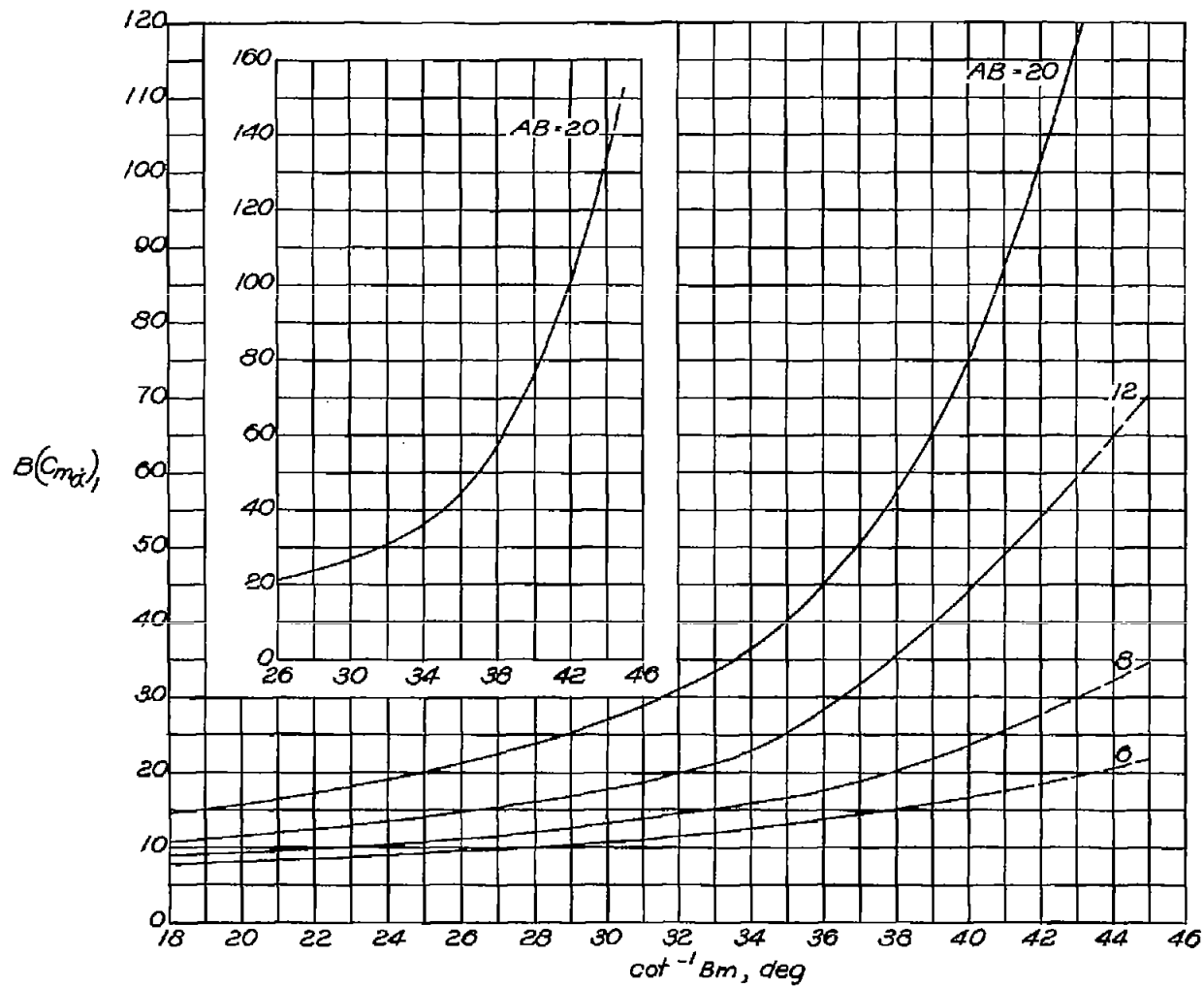
(c)  $B(C_{m\alpha})_2$ .  $\lambda = 0$ ;  $AB = 3$  to  $20$ ;  $\cot^{-1} B_m = 0^\circ$  to  $45^\circ$ .

Figure 11.- Concluded.



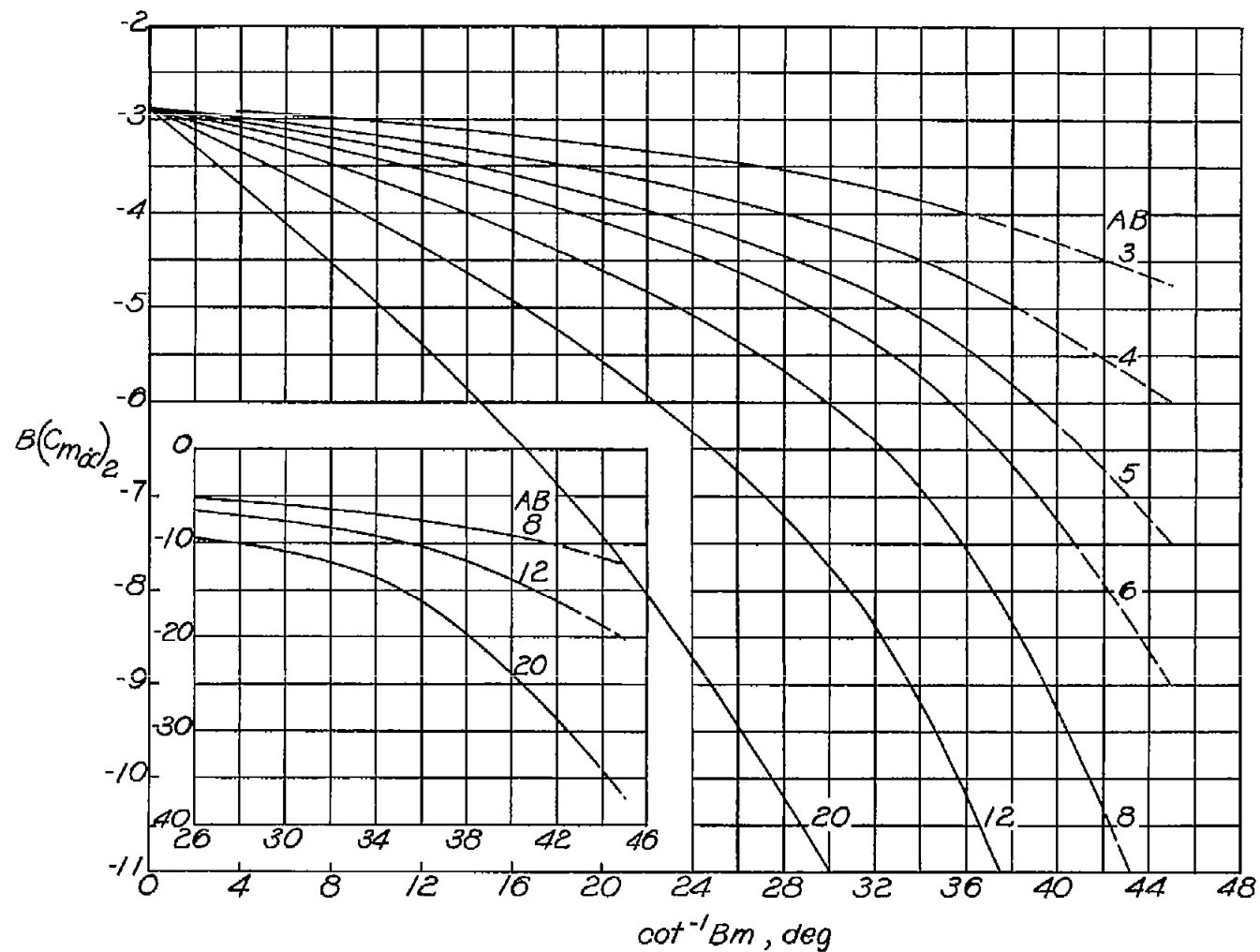
(a)  $B(C_{m_{\alpha}})_1$ .  $\lambda = 0.25$ ;  $AB = 3$  to  $20$ ;  $\cot^{-1} Bm = 0^\circ$  to  $45^\circ$ .

Figure 12.- Variation of  $B(C_{m_{\alpha}})_1$  and  $B(C_{m_{\alpha}})_2$  with  $\cot^{-1} Bm$ . Results valid for both principal body and stability systems of axes with origin at wing apex.  $BC_{m_{\alpha}} = \frac{M^2}{B^2} B(C_{m_{\alpha}})_1 + \left(\frac{M^2}{B^2} + 1\right) B(C_{m_{\alpha}})_2$ . Dashed parts of curves represent extensions of calculated curves (through region which corresponds to condition where Mach lines from wing apex intersect tips) to calculated end points.



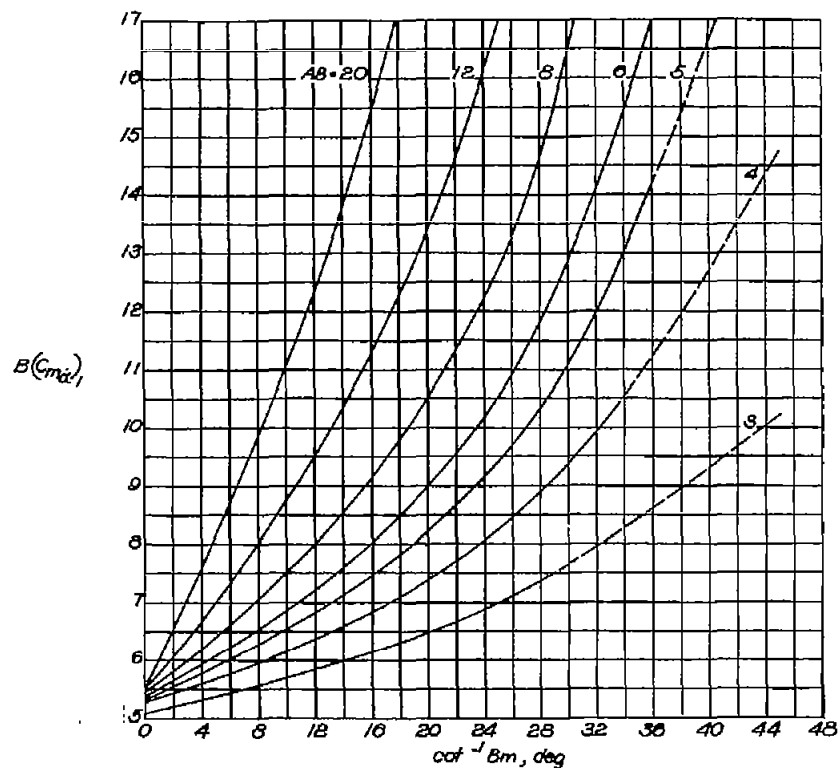
(b)  $B(C_{m\alpha})_1$ .  $\lambda = 0.25$ ;  $AB = 6$  to  $20$ ;  $\cot^{-1} B_m = 18^\circ$  to  $45^\circ$ .

Figure 12.- Continued.



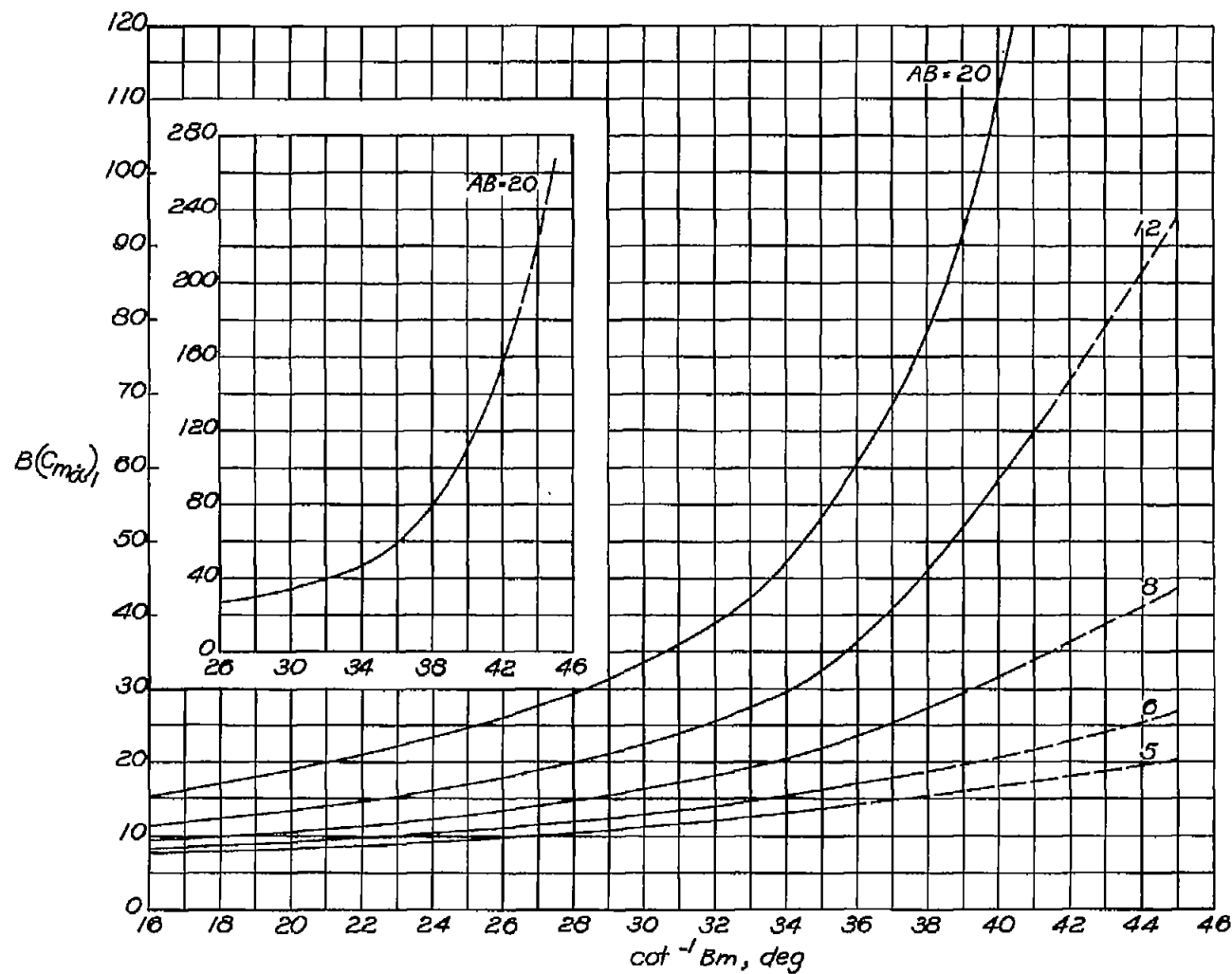
(c)  $B(C_{m\alpha})_2$ .  $\lambda = 0.25$ ;  $AB = 3$  to  $20$ ;  $\cot^{-1} B_m = 0^\circ$  to  $45^\circ$ .

Figure 12.- Concluded.



(a)  $B(C_{m\alpha}^*)_1$ .  $\lambda = 0.50$ ;  $AB = 3$  to  $20$ ;  $\cot^{-1} Bm = 0^\circ$  to  $45^\circ$ .

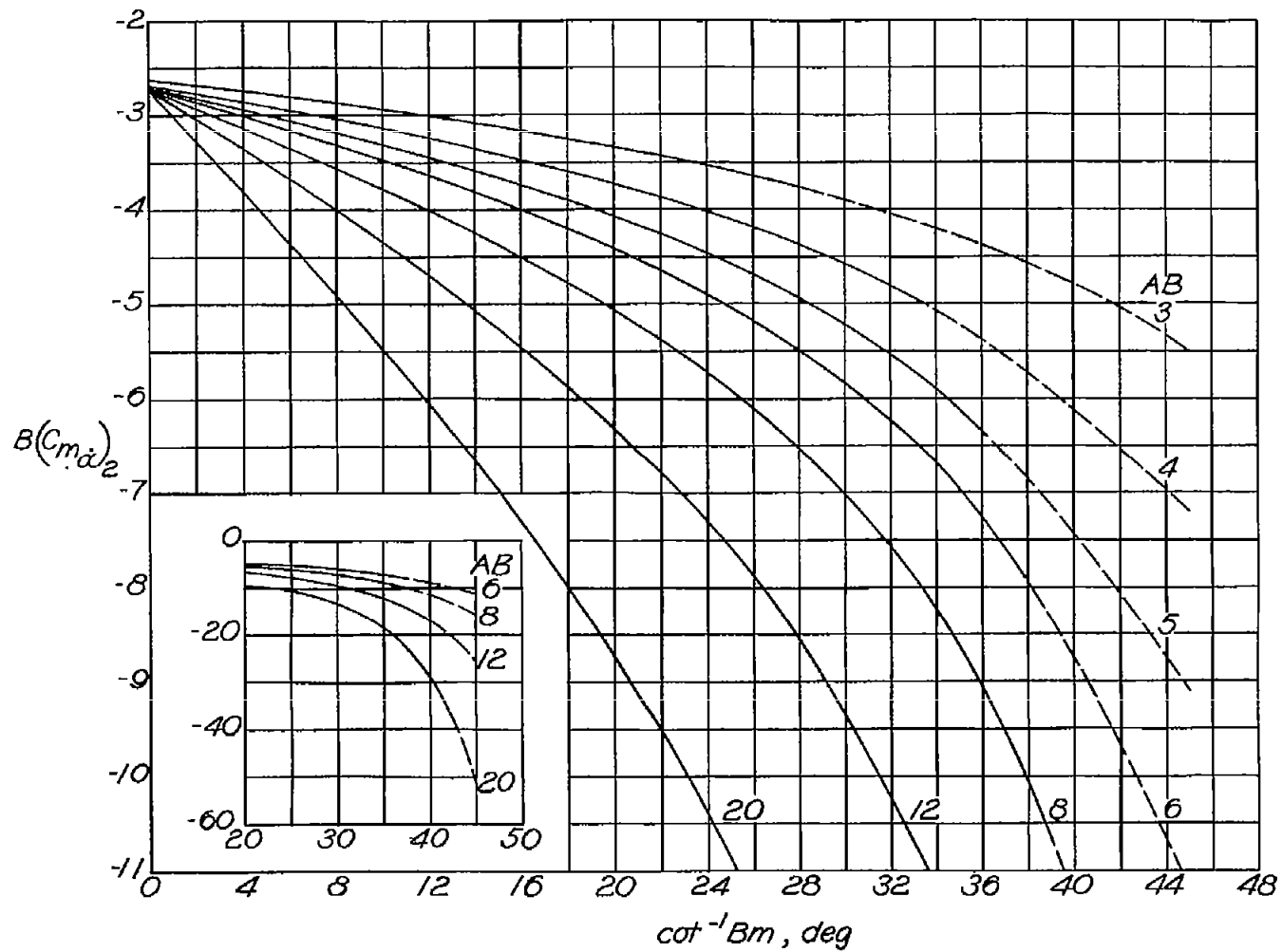
Figure 13.- Variation of  $B(C_{m\alpha}^*)_1$  and  $B(C_{m\alpha}^*)_2$  with  $\cot^{-1} Bm$ . Results valid for both principal body and stability systems of axes with origin at wing apex.  $BC_{m\alpha}^* = \frac{M^2}{B^2} B(C_{m\alpha}^*)_1 + \left(\frac{M^2}{B^2} + 1\right) B(C_{m\alpha}^*)_2$ . Dashed parts of curves represent extensions of calculated curves (through region which corresponds to condition where Mach lines from wing apex intersect tips) to calculated end points.



(b)  $B(C_{m_{\alpha}})_1$ .  $\lambda = 0.50$ ;  $AB = 5$  to  $20$ ;  $\cot^{-1} B_m = 16^\circ$  to  $45^\circ$ .

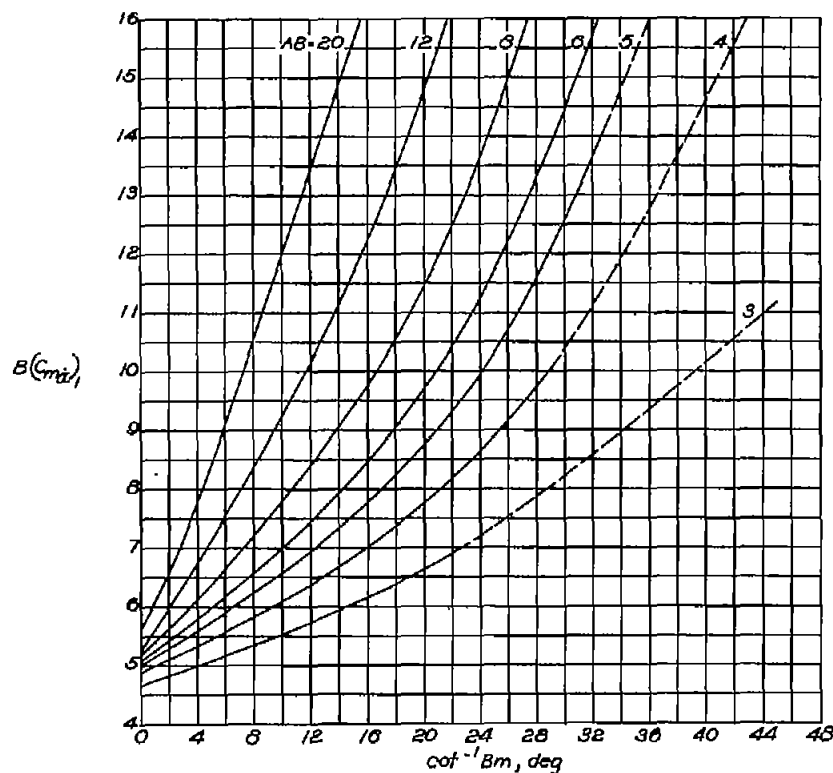
Figure 13.- Continued.





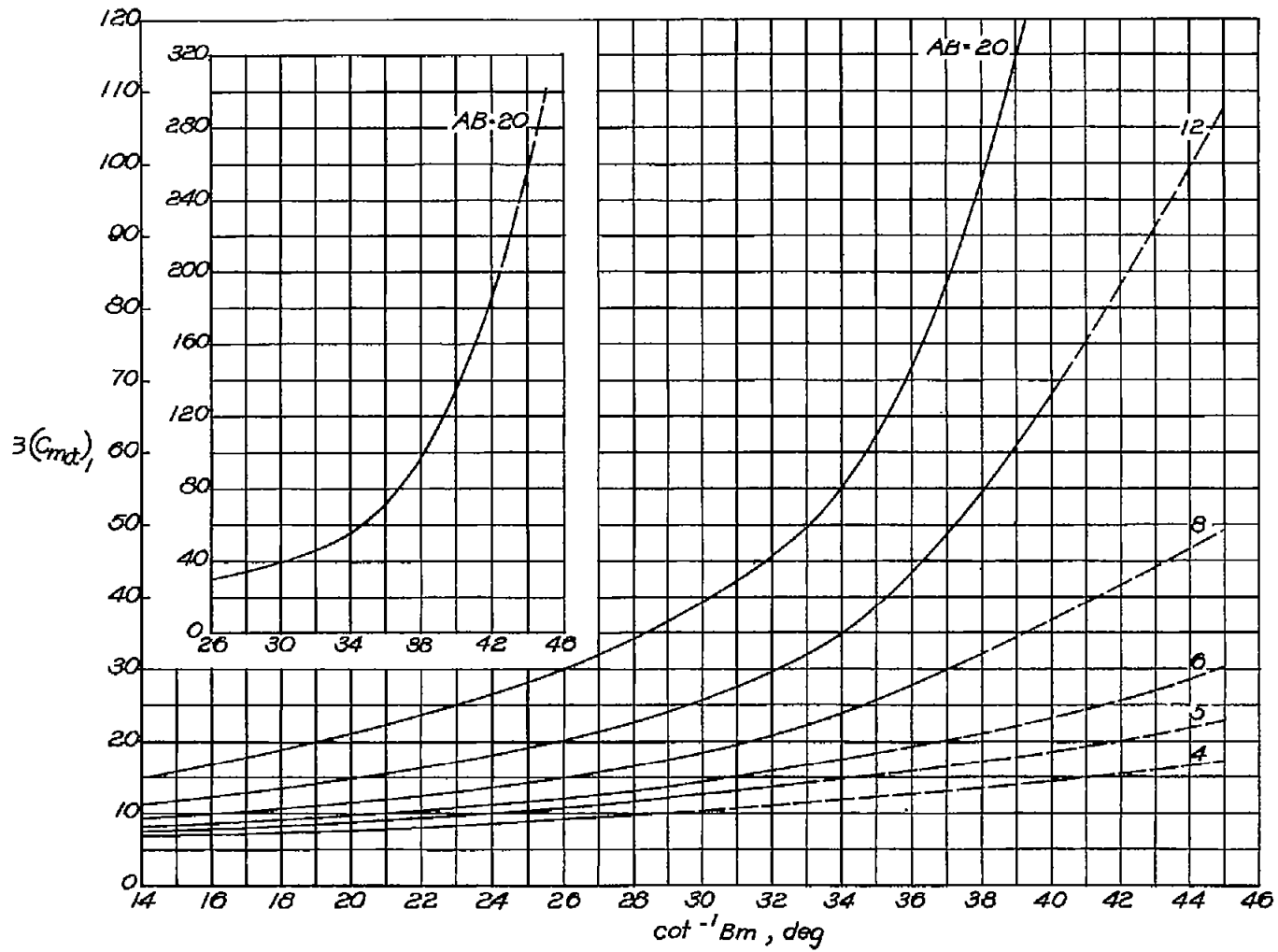
(c)  $B(C_{m\dot{\alpha}})_2$ .  $\lambda = 0.50$ ;  $AB = 3$  to  $20$ ;  $\cot^{-1} Bm = 0^\circ$  to  $45^\circ$ .

Figure 13.- Concluded.



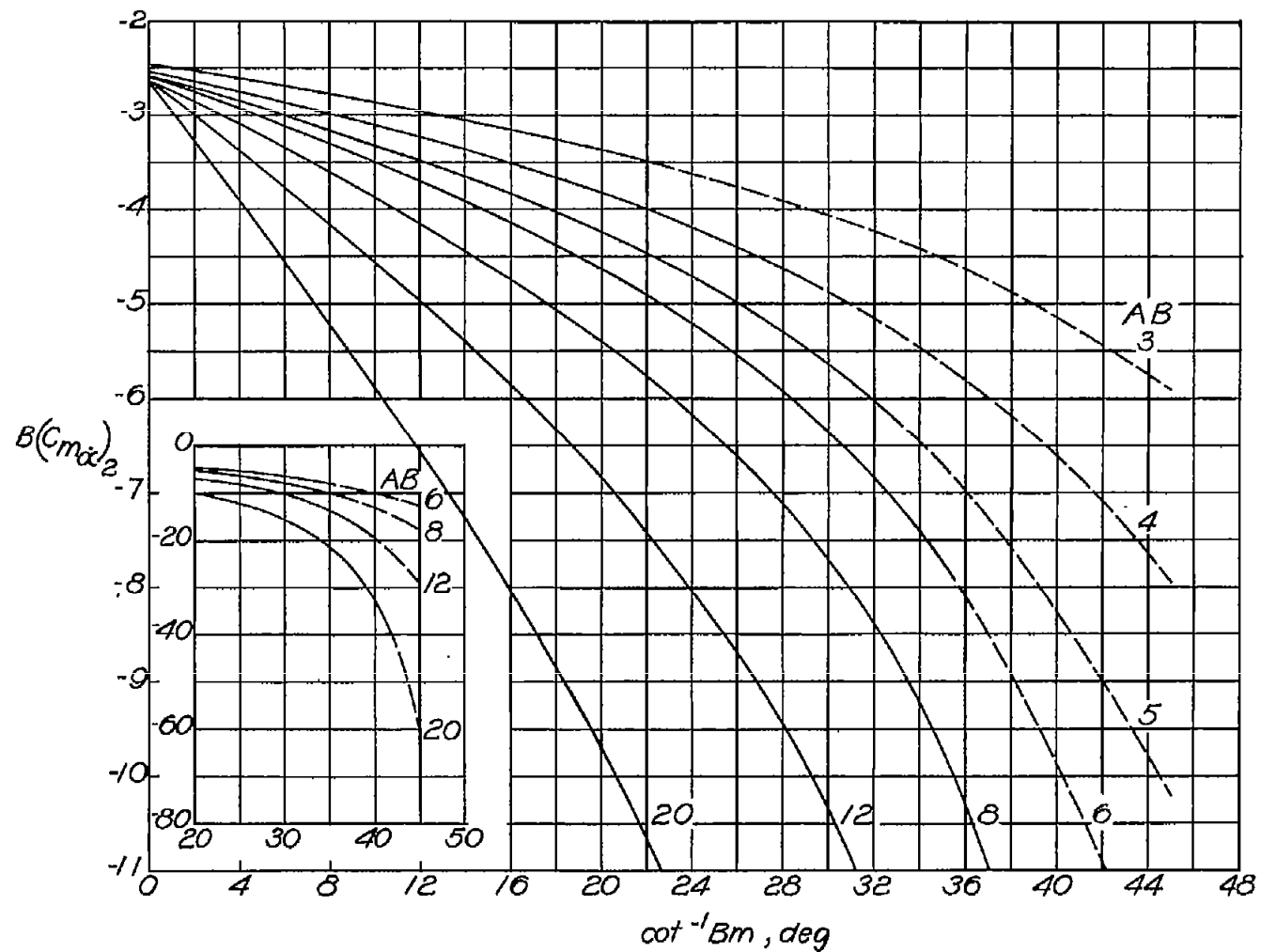
(a)  $B(C_{m_{\alpha}})_1$ .  $\lambda = 0.75$ ;  $AB = 3$  to  $20$ ;  $\cot^{-1} B_m = 0^\circ$  to  $45^\circ$ .

Figure 14.- Variation of  $B(C_{m_{\alpha}})_1$  and  $B(C_{m_{\alpha}})_2$  with  $\cot^{-1} B_m$ . Results valid for both principal body and stability systems of axes with origin at wing apex.  $BC_{m_{\alpha}} = \frac{M^2}{B^2} B(C_{m_{\alpha}})_1 + \left(\frac{M^2}{B^2} + 1\right) B(C_{m_{\alpha}})_2$ . Dashed parts of curves represent extensions of calculated curves (through region which corresponds to condition where Mach lines from wing apex intersect tips) to calculated end points.



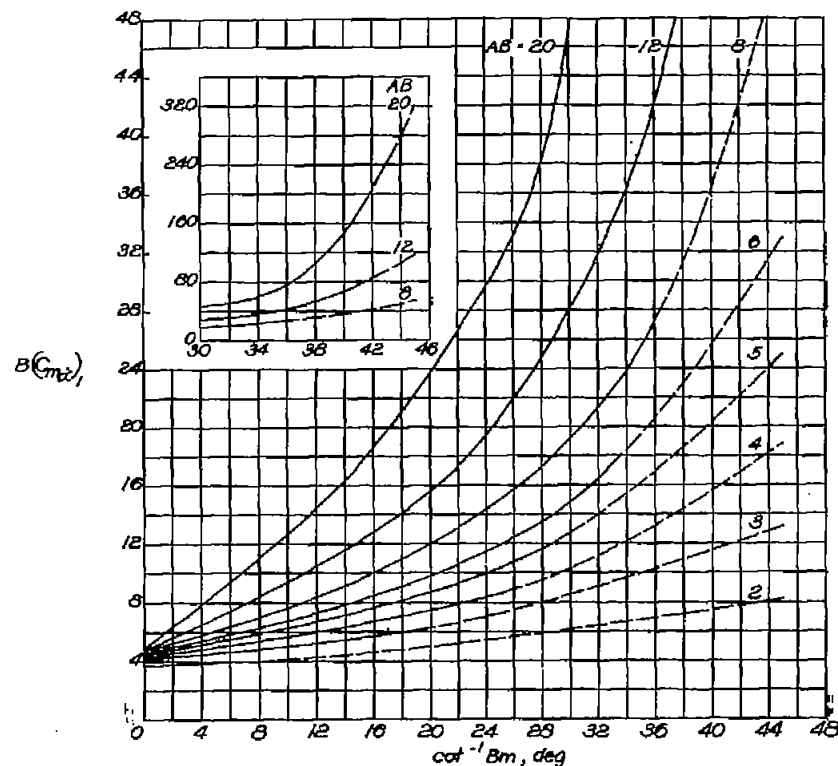
(b)  $B(C_{m\alpha})_1$ .  $\lambda = 0.75$ ;  $AB = 4$  to  $20$ ;  $\cot^{-1} B_m = 14^\circ$  to  $45^\circ$ .

Figure 14.- Continued.



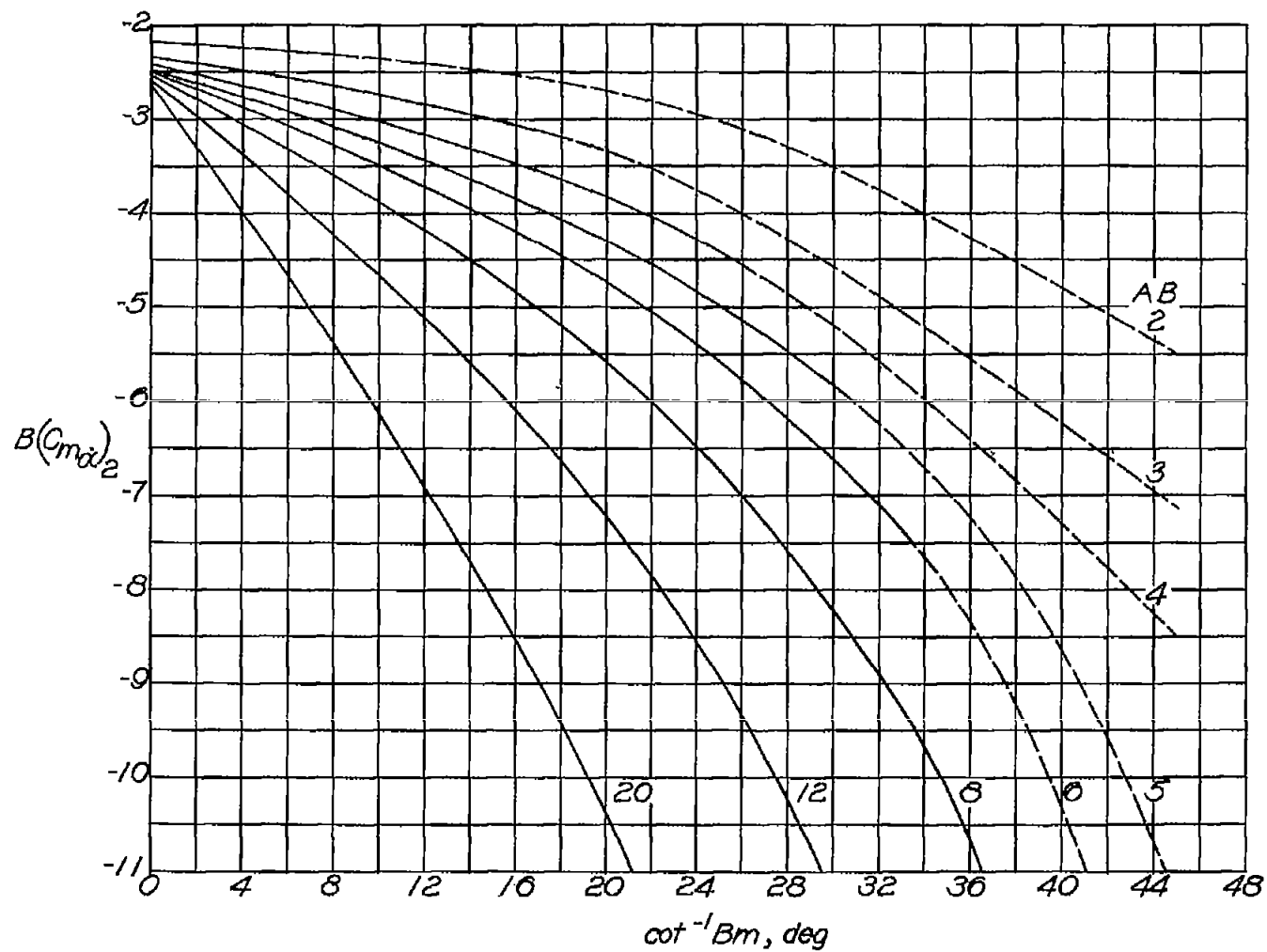
(c)  $B(Cm_{\alpha})_2$ .  $\lambda = 0.75$ ;  $AB = 3$  to  $20$ ;  $\cot^{-1} Bm = 0^\circ$  to  $45^\circ$ .

Figure 14.- Concluded.



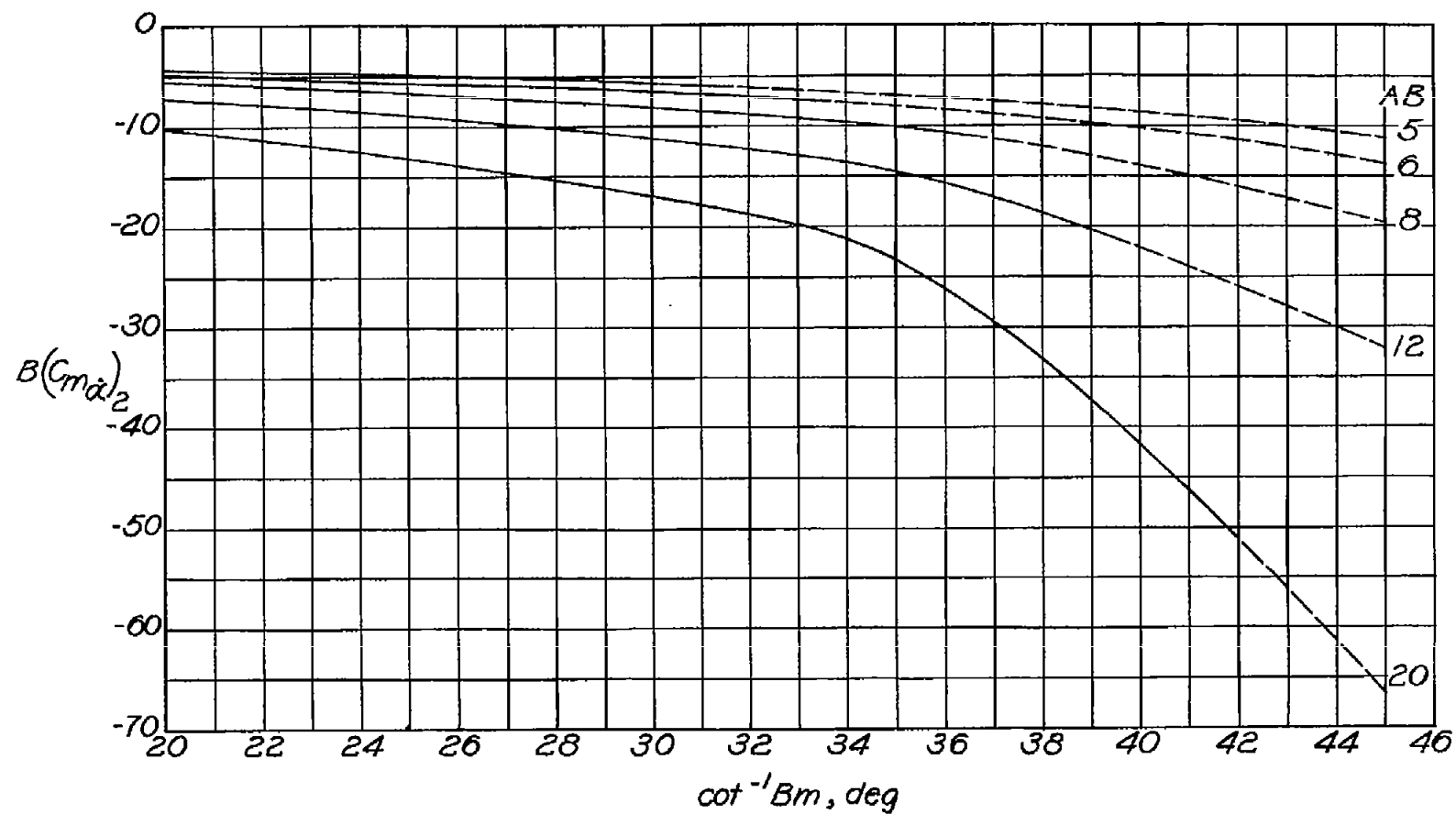
(a)  $B(C_{m\alpha})_1$ .  $\lambda = 1.0$ ;  $AB = 2$  to  $20$ ;  $\cot^{-1} Bm = 0^\circ$  to  $45^\circ$ .

Figure 15.- Variation of  $B(C_{m\alpha})_1$  and  $B(C_{m\alpha})_2$  with  $\cot^{-1} Bm$ . Results valid for both principal body and stability systems of axes with origin at wing apex.  $BC_{m\alpha} = \frac{M^2}{B^2} B(C_{m\alpha})_1 + \left(\frac{M^2}{B^2} + 1\right) B(C_{m\alpha})_2$ . Dashed parts of curves represent extensions of calculated curves (through region which corresponds to condition where Mach lines from wing apex intersect tips) to calculated end points.



(b)  $B(C_{m\alpha})_2$ .  $\lambda = 1.0$ ; AB = 2 to 20;  $\cot^{-1} B_m = 0^\circ$  to  $45^\circ$ .

Figure 15.- Continued.



(c)  $B(C_{m\alpha})_2$ .  $\lambda = 1.0$ ;  $AB = 5$  to  $20$ ;  $\cot^{-1} Bm = 20^\circ$  to  $45^\circ$ .

Figure 15.- Concluded.

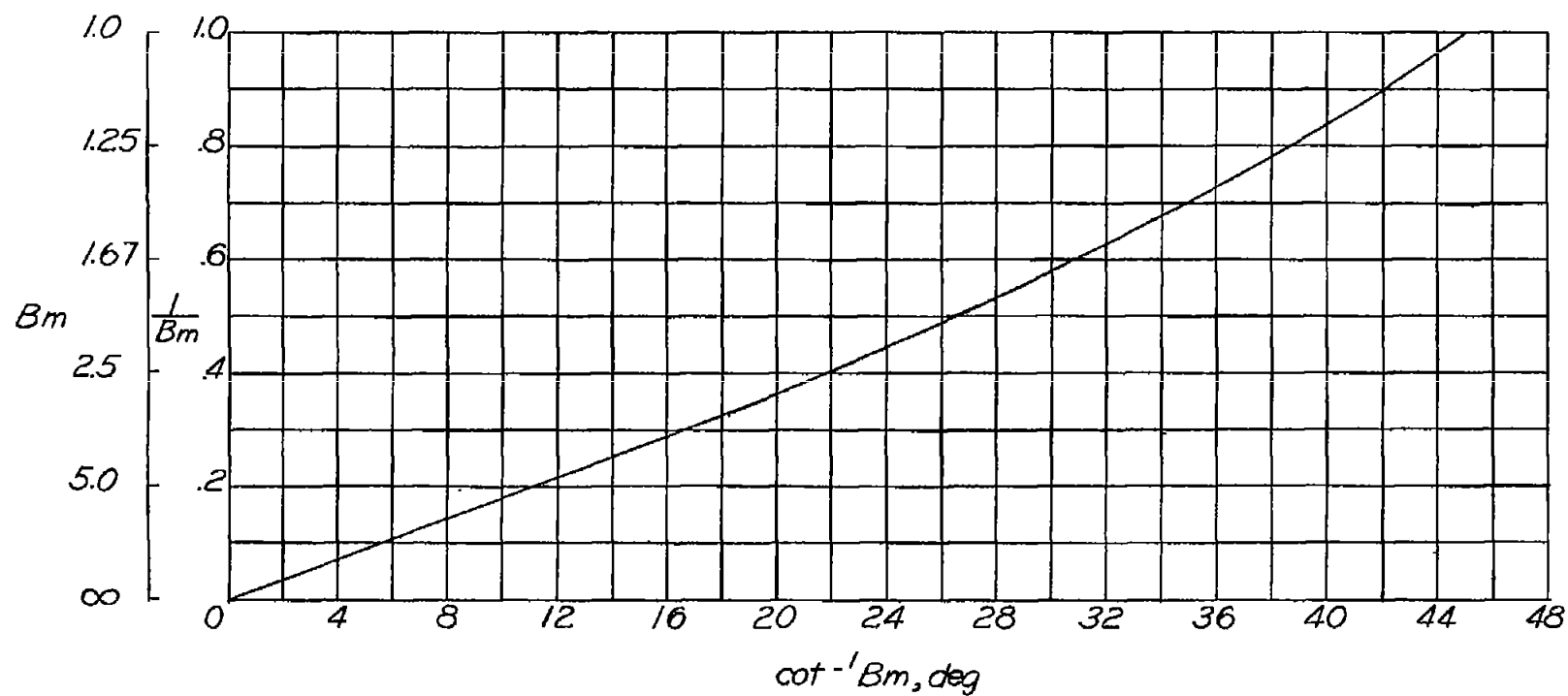
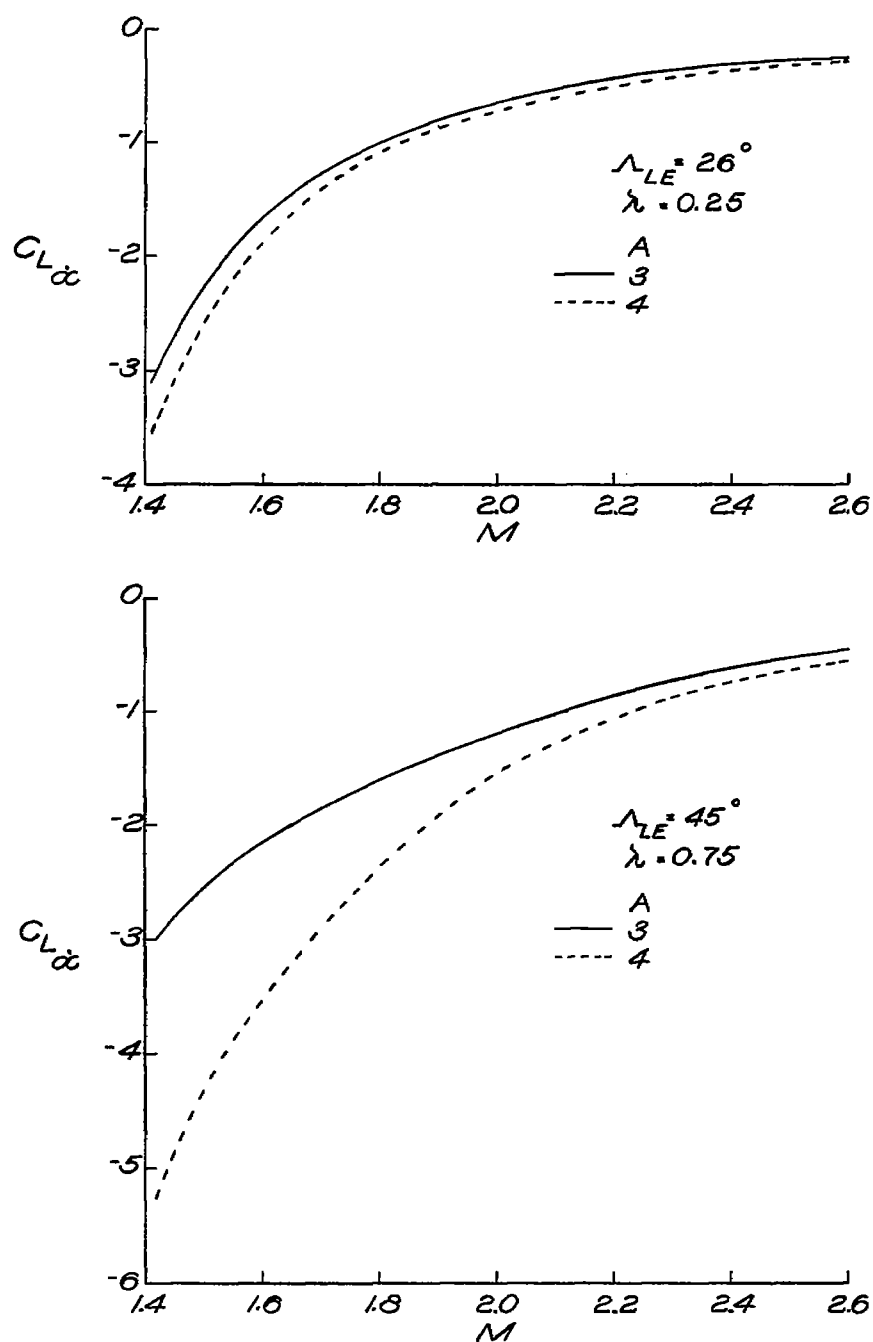


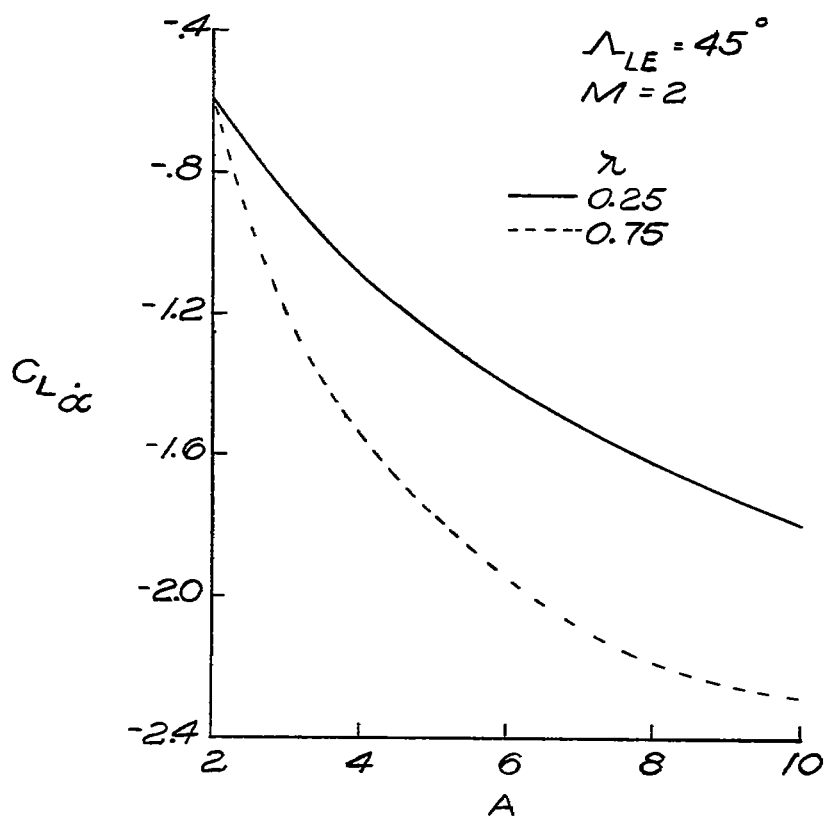
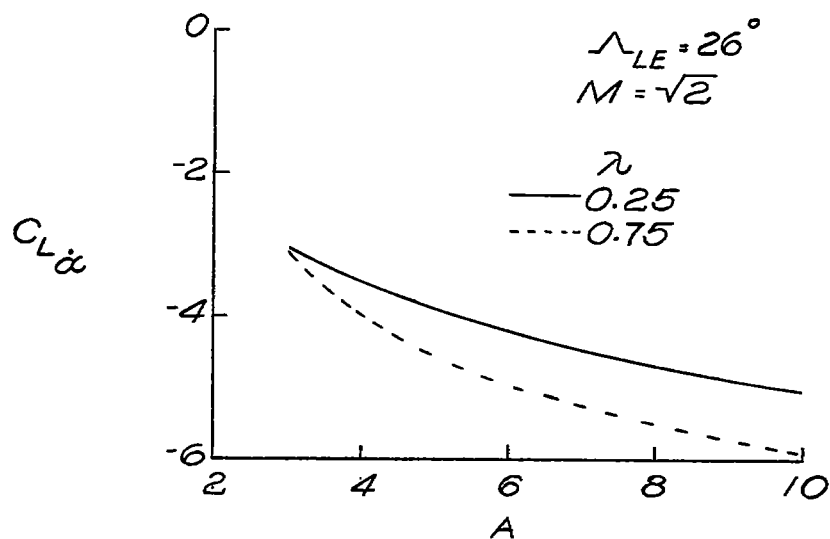
Figure 16.- Relationship of parameters  $B_m$ ,  $1/B_m$ , and  $\cot^{-1} B_m$ .





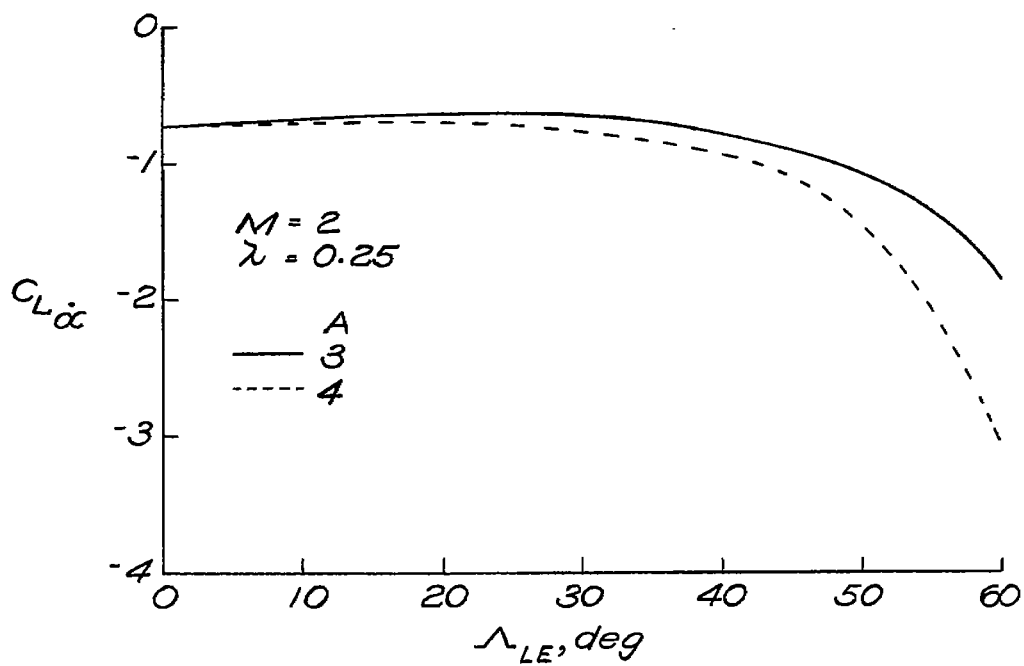
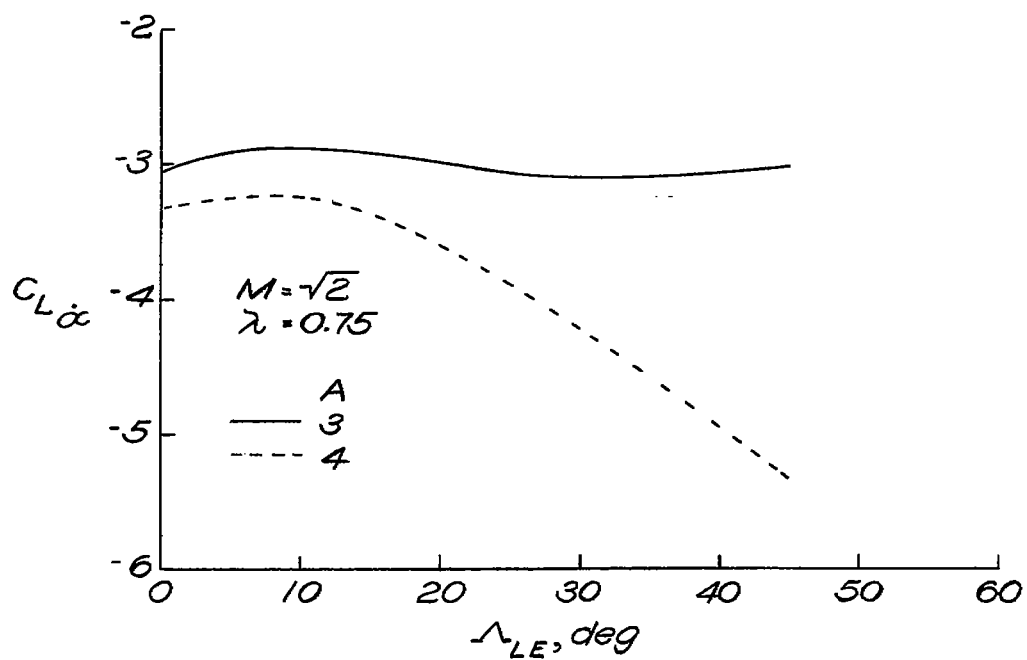
(a) Variation with Mach number.

Figure 17.- Some illustrative variations of stability derivative  $C_{L\alpha}$  with Mach number, aspect ratio, leading-edge sweepback, and taper ratio. Results valid for both principal body and stability systems of axes.



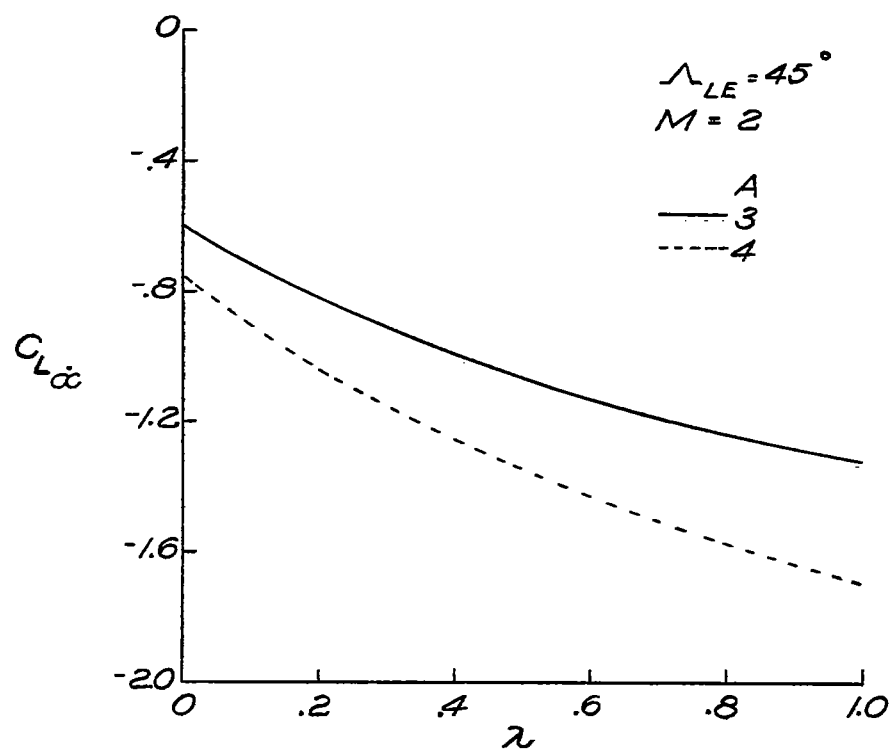
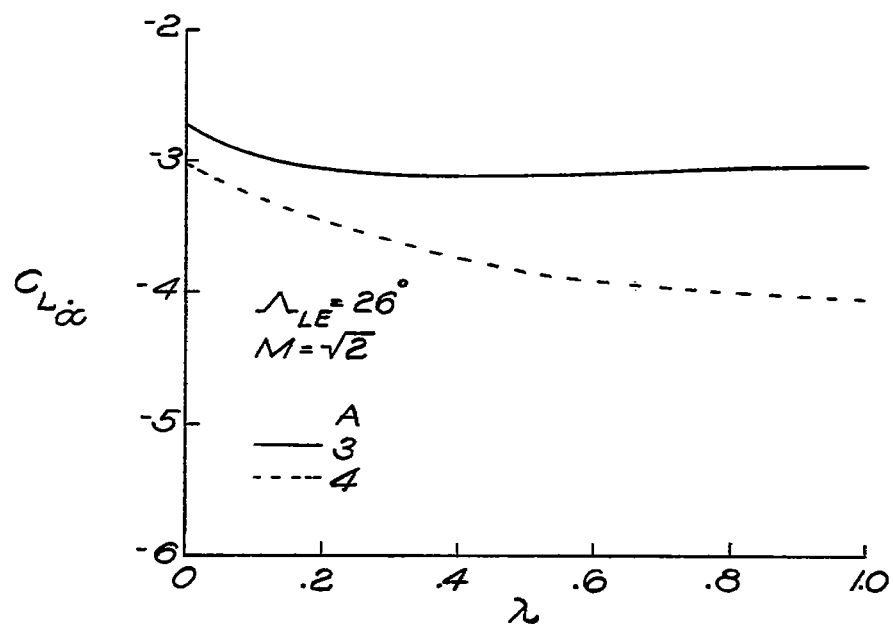
(b) Variation with aspect ratio.

Figure 17.- Continued.



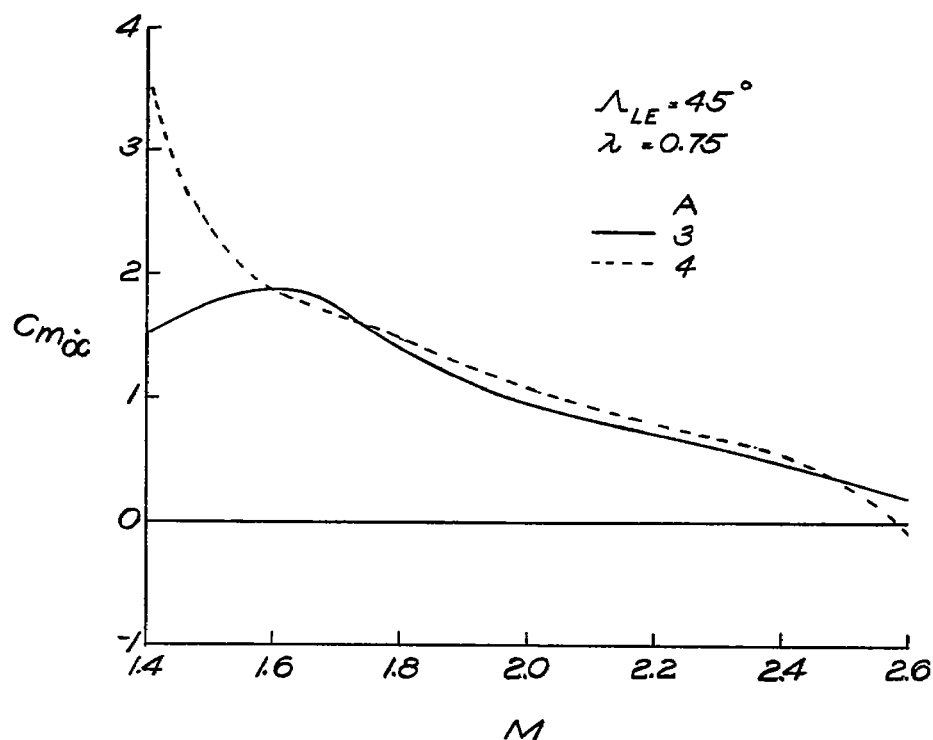
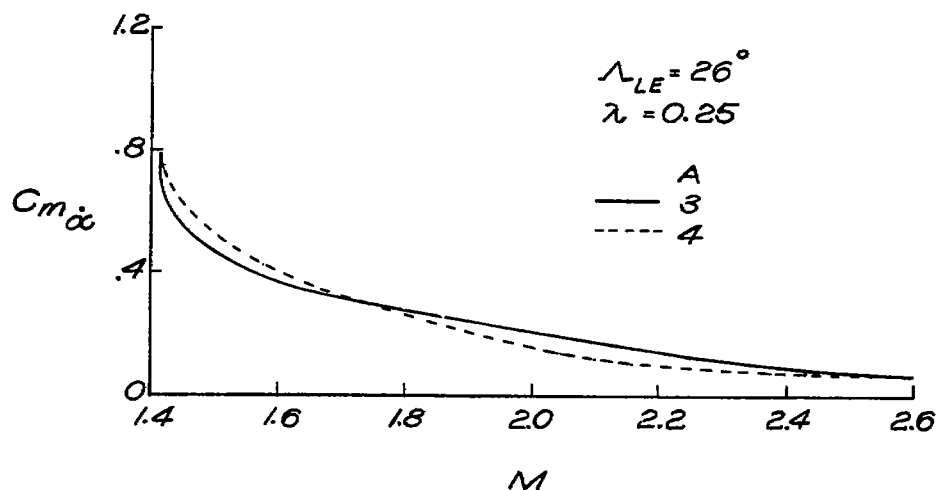
(c) Variation with leading-edge sweepback.

Figure 17.- Continued.



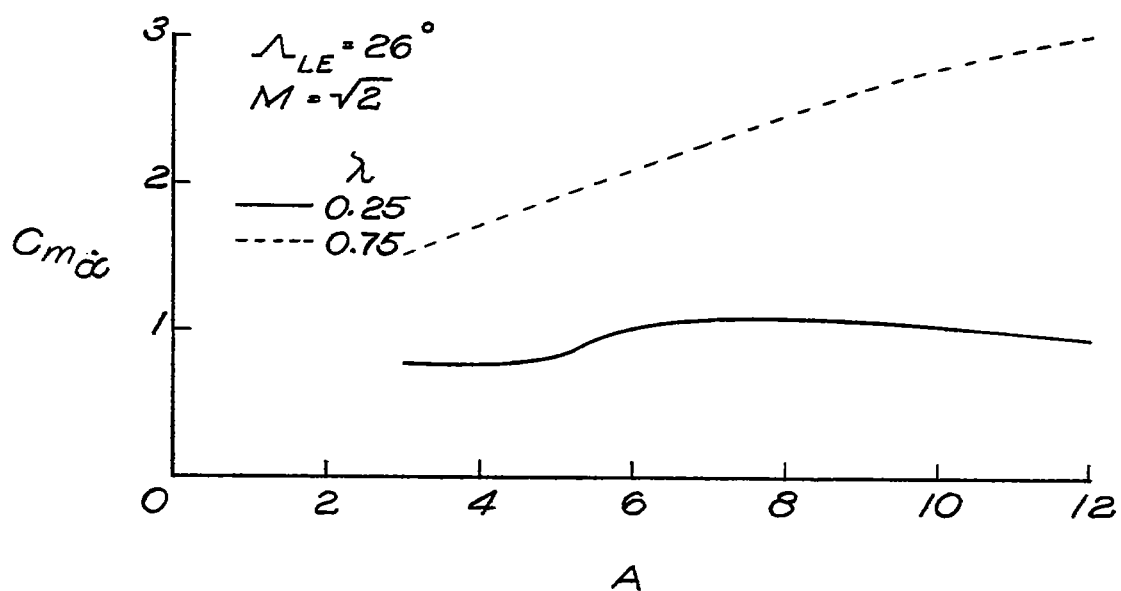
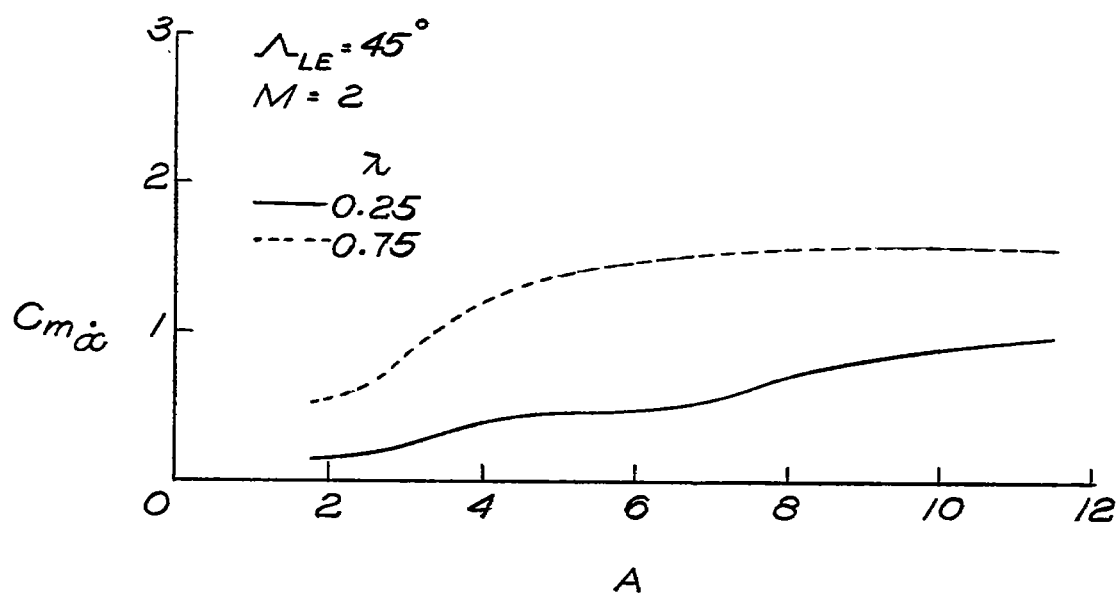
(d) Variation with taper ratio.

Figure 17.- Concluded.



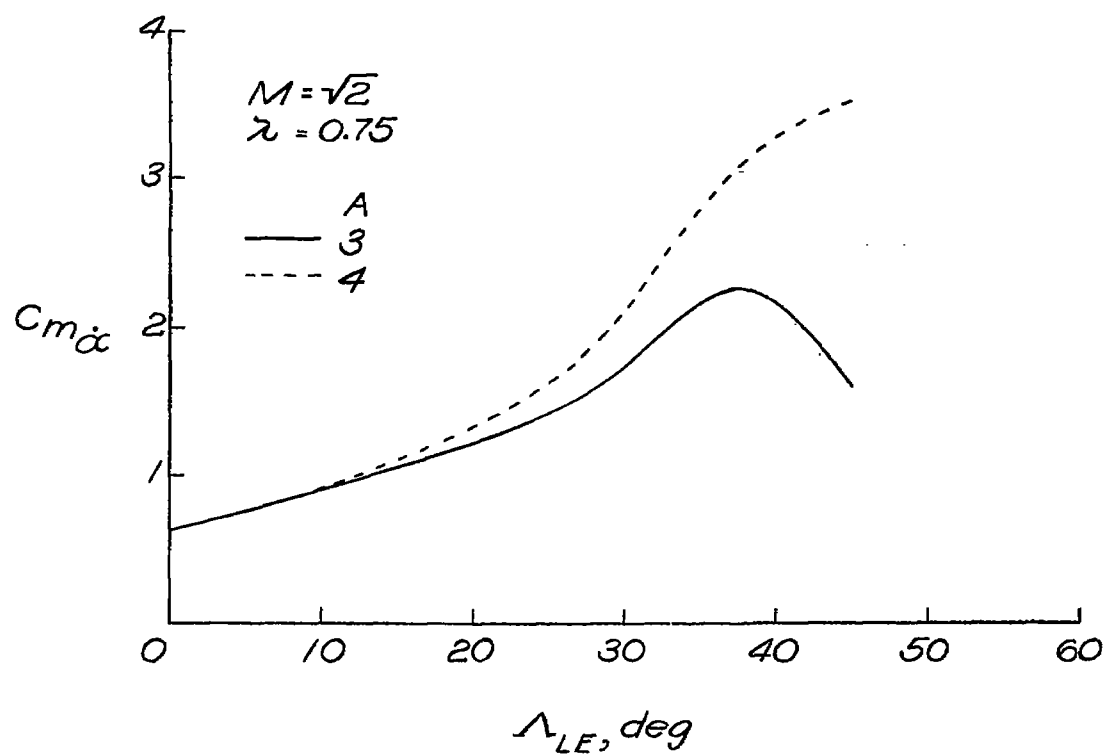
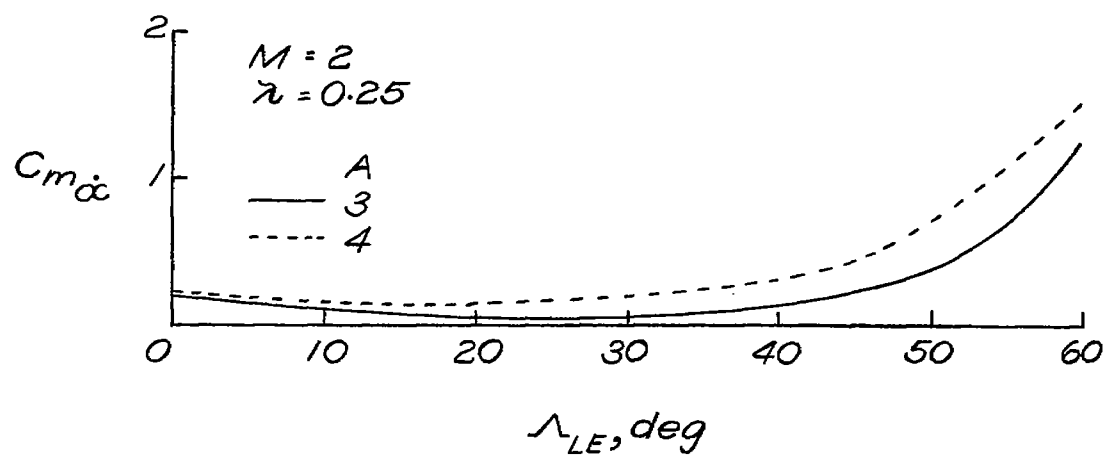
(a) Variation with Mach number.

Figure 18.- Some illustrative variations of stability derivative  $C_{m\ddot{\alpha}}$  with Mach number, aspect ratio, leading-edge sweepback, and taper ratio. Results valid for both principal body and stability systems of axes. Static margin,  $0.05\bar{c}$ .



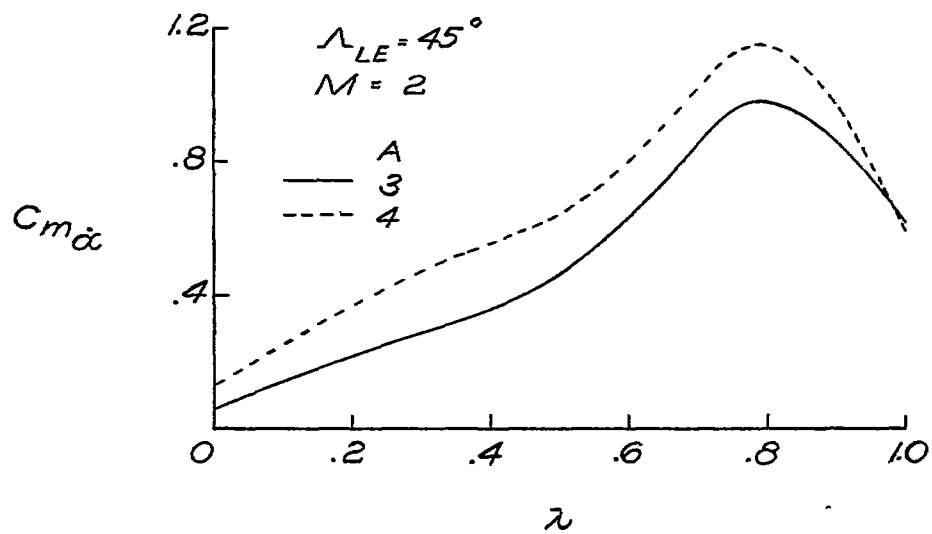
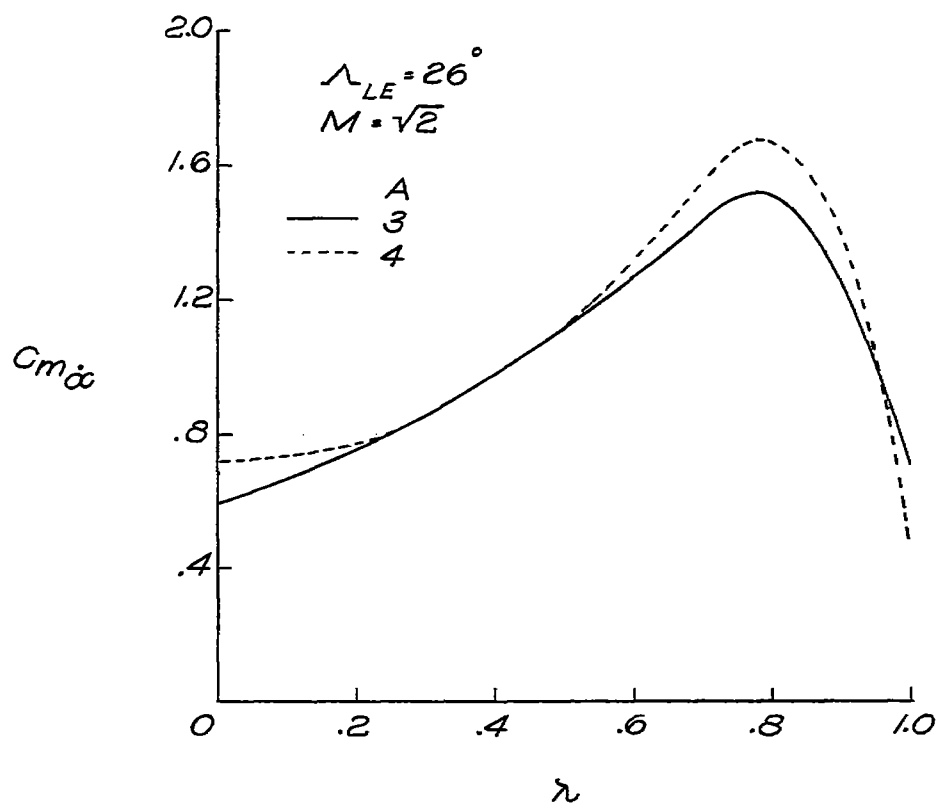
(b) Variation with aspect ratio.

Figure 18.- Continued.



(c) Variation with leading-edge sweepback.

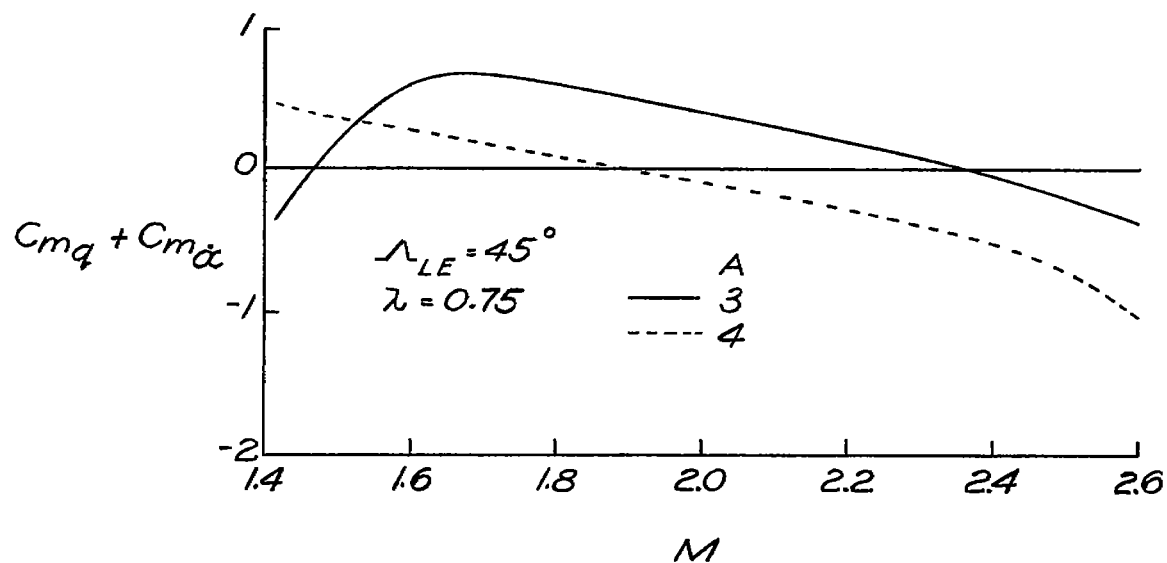
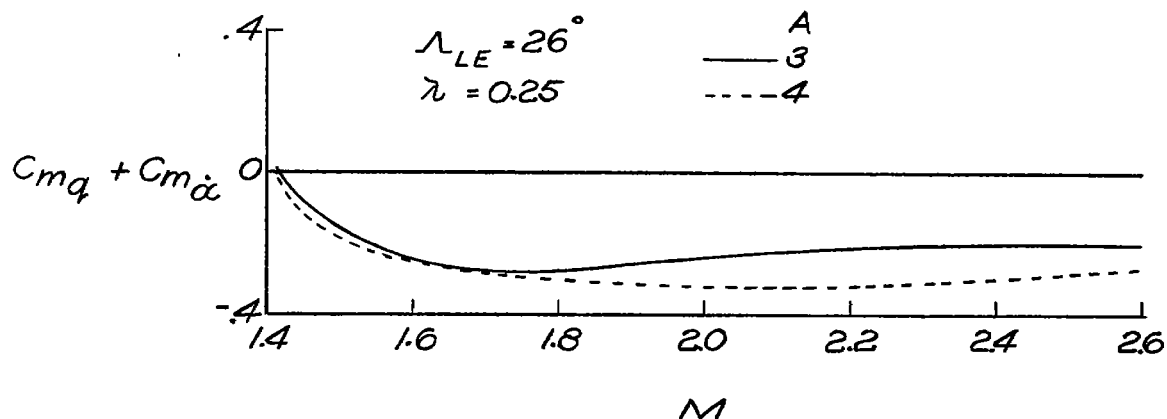
Figure 18.- Continued.



(d) Variation with taper ratio.

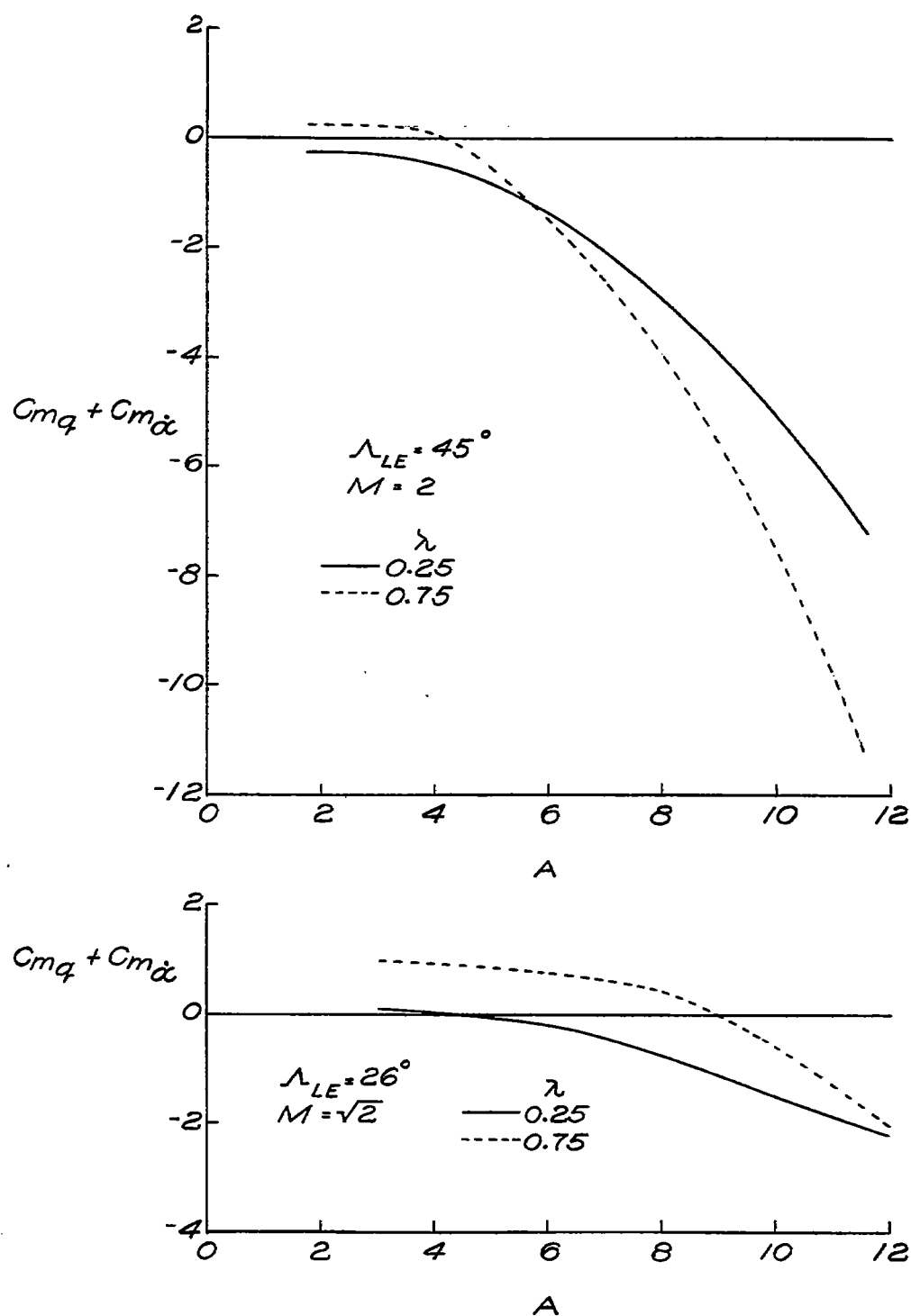
Figure 18.- Concluded.





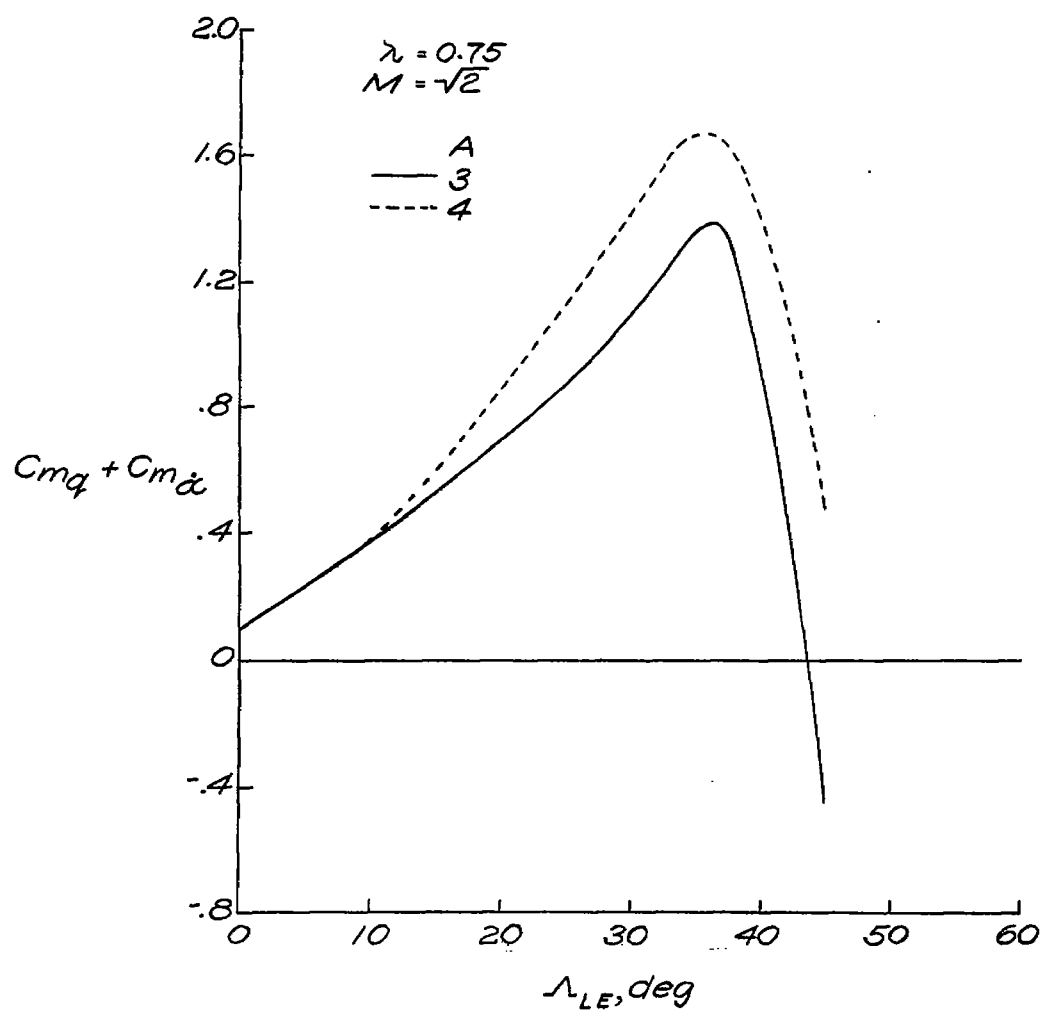
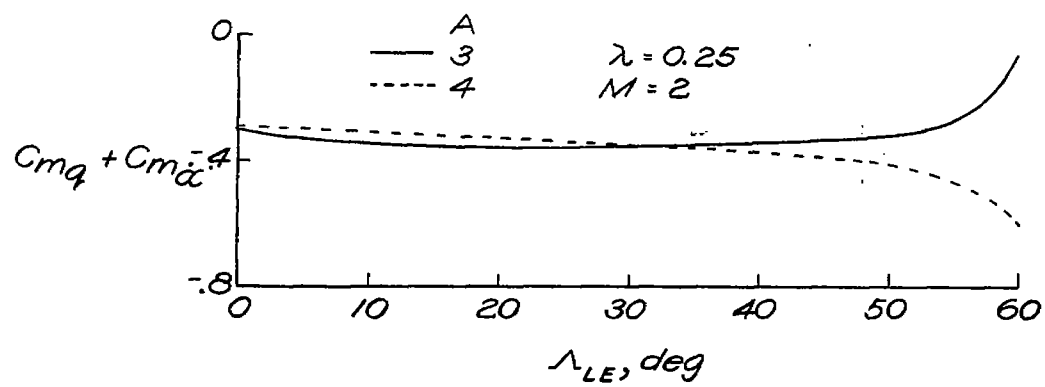
(a) Variation with Mach number.

Figure 19.- Some illustrative variations of total pitching-moment derivative  $C_{mq} + C_{m\dot{\alpha}}$ , generated by a slowly oscillating wing, with Mach number, aspect ratio, leading-edge sweepback, and taper ratio. Results valid for both principal body and stability systems of axes. Static margin, 0.05c.



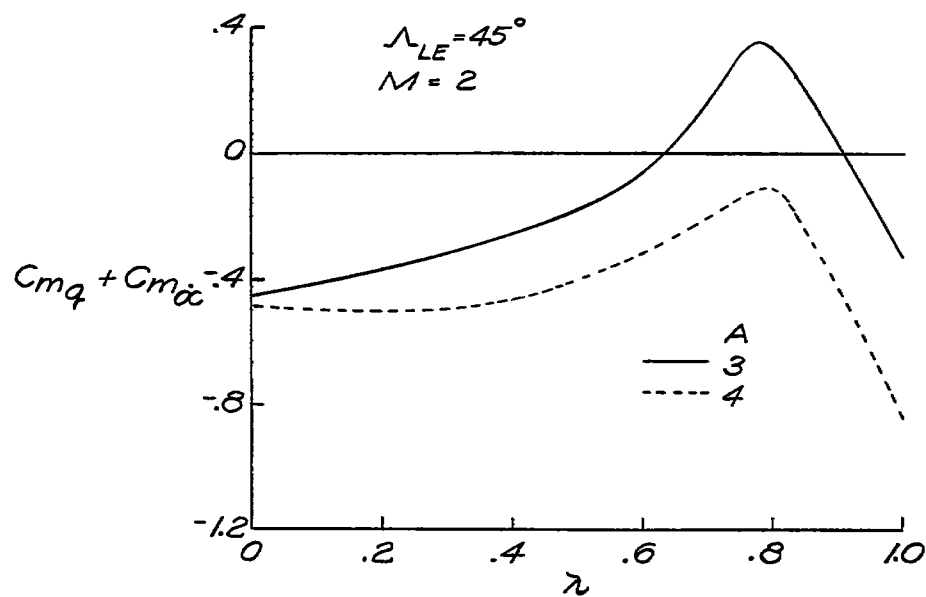
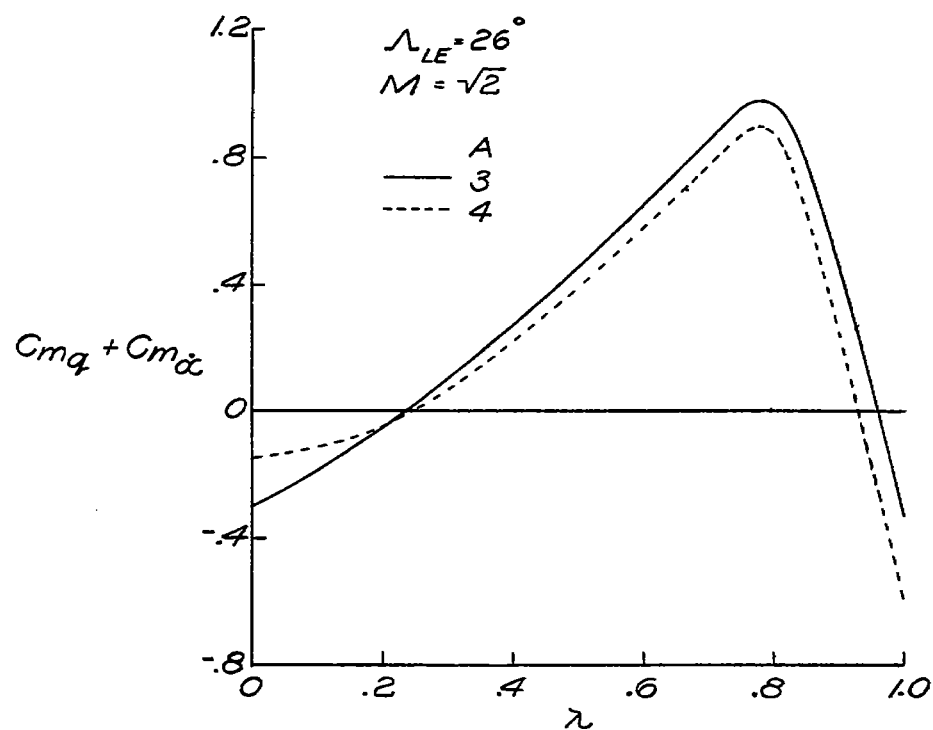
(b) Variation with aspect ratio.

Figure 19.- Continued.



(c) Variation with leading-edge sweepback.

Figure 19.- Continued.



(d) Variation with taper ratio.

Figure 19.- Concluded.